AD-A193 961 ACOUSTIC PRESSURE DISTRIBUTION ON THE BOTTOM OF A WEDGE-SHAPED OCEAN(U) NAVAL POSTGRADUATE SCHOOL MONTEREY CA Y LI DEC 87 1/2

UNCLASSIFIED F/G 20/1 NL

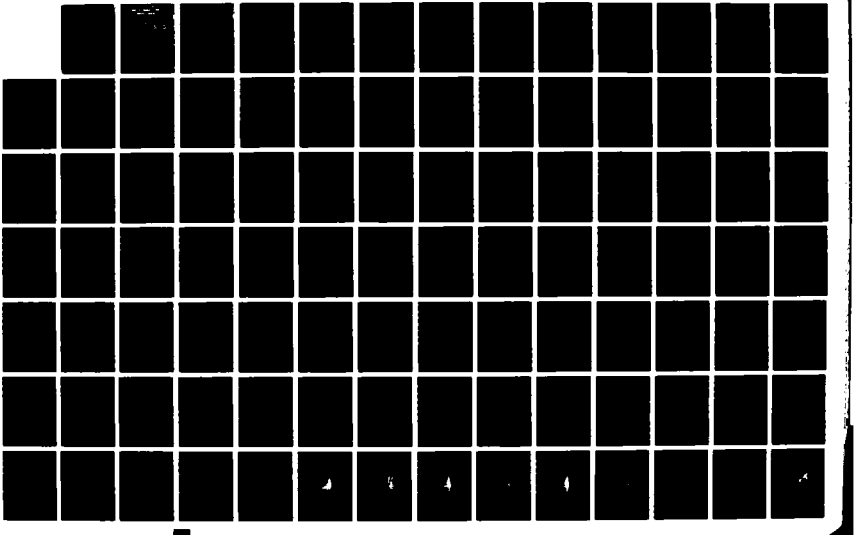

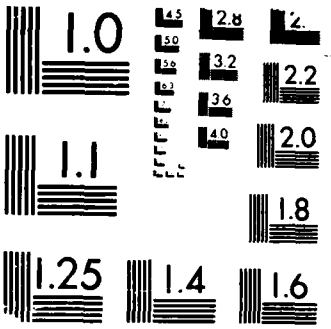

(2)

NAVAL POSTGRADUATE SCHOOL
Monterey, California

THESIS

ACOUSTIC PRESSURE DISTRIBUTION ON THE BOTTOM OF A WEDGE-SHAPED OCEAN

by

Li Yu-Ming

December 1987

Thesis Advisor: A. B. Coppens

Approved for public release; distribution is unlimited.

REPORT DOCUMENTATION PAGE

1a REPORT SECURITY CLASSIFICATION	1b RESTRICTIVE MARKINGS
2a SECURITY CLASSIFICATION AUTHORITY Unlcassified	3 DISTRIBUTION/AVAILABILITY OF REPORT Approved for public release; Distribution unlimited.
2b DECLASSIFICATION/DOWNGRADING SCHEDULE	
4 PERFORMING ORGANIZATION REPORT NUMBER(S)	5 MONITORING ORGANIZATION REPORT NUMBER(S)
6a NAME OF PERFORMING ORGANIZATION Naval Postgraduate School 6b OFFICE SYMBOL (*If applicable*)	7a NAME OF MONITORING ORGANIZATION Naval Postgraduate School
6c ADDRESS (*City, State, and ZIP Code*) Monterey, California 93943-5000	7b ADDRESS (*City, State, and ZIP Code*) Monterey, California 93943-5000
8a NAME OF FUNDING SPONSORING ORGANIZATION 8b OFFICE SYMBOL (*If applicable*)	9 PROCUREMENT INSTRUMENT IDENTIFICATION NUMBER
8c ADDRESS (*City, State, and ZIP Code*)	10 SOURCE OF FUNDING NUMBERS PROGRAM ELEMENT NO / PROJECT NO / TASK NO / WORK UNIT ACCESSION NO

11 TITLE (*Include Security Classification*)
Acoustic Pressure Distribution on the Bottom of Wedge-Shaped Ocean
Unclassified

12 PERSONAL AUTHOR(S)
Li, Yu-Ming

13a TYPE OF REPORT	13b TIME COVERED	14 DATE OF REPORT (*Year, Month, Day*)	15 PAGE COUNT
Master's Thesis	FROM _____ TO _____	1987 Dec 17	101

16 SUPPLEMENTARY NOTATION

17 COSATI CODES			18 SUBJECT TERMS (*Continue on reverse if necessary and identify by block number*)
FIELD	GROUP	SUB-GROUP	Method of Image;FAST Abosrbing; Slow Absorbing Bottom; Dump Distance

19 ABSTRACT (*Continue on reverse if necessary and identify by block number*)

The pressure amplitude distribution along the interface between a wedge-shaped fluid layer overlying fast and slow fluid bottoms were investigated using computer models based on the method of images. The pressure amplitude along the bottom rapidly falls off for distances closer to the apex than that at which adibatic-mode theory predicts cut-off for the lowest mode. This distance is termed the "dump distance" for acoustically fast-bottom condition. In the case of a slow bottom, because the speed of sound ratio is greater than 1, the dump distance does not exist. To facilitate scaling the acoustic fields, a "scaling distance" is introduced: X_o = (wave length)/(4sino$_c$tanB) where $o_c=\cos^{-1}(c_1/c_2)$, B is the angle of the wedge, c_1= speed of sound in water, c_2=speed of sound in bottom, and k_2= w/c_2. X_o appears to have physical meaning as a useful scaling distance.

20 DISTRIBUTION/AVAILABILITY OF ABSTRACT	21 ABSTRACT SECURITY CLASSIFICATION	
☒ UNCLASSIFIED/UNLIMITED ☐ SAME AS RPT ☐ DTIC USERS	Unclassified	
22a NAME OF RESPONSIBLE INDIVIDUAL A. B. Coppens	22b TELEPHONE (*Include Area Code*) 408-646-2941	22c OFFICE SYMBOL 61Cz

☆ U.S. Government Printing Office: 1986—606-24.

Approved for public release; distribution is unlimited.

Acoustic Pressure Distribution on the Bottom of a Wedge-Shaped Ocean

by

Li Yu-Ming
Lieutenant, Republic of China Navy
B.S., R.O.C. Naval Academy, 1981

Submitted in partial fulfillment of the requirements for the degree of

MASTER OF SCIENCE IN ENGINEERING ACOUSTICS

from the

NAVAL POSTGRADUATE SCHOOL
December 1987

Author: _____
Li Yu-Ming

Approved by: _____
A. B. Coppens, Thesis Advisor

_____
J.V. Sanders, Thesis Advisor

_____
S. L. Garrett, Chairman,
Engineering Acoustics Academic Group

_____
Gordon Schacher, Dean,
Engineering and Sciences

ABSTRACT

The pressure amplitude distribution along the interface between a wedge-shaped fluid layer overlying fast and slow fluid bottoms were investigated using computer models based on the method of images. The pressure amplitude along the bottom rapidly falls off for distances closer to the apex than that at which adiabatic-mode theory predicts cut-off for the lowest mode. This distance is termed the "dump distance" for an acoustically fast-bottom condition. In the case of a slow bottom, because the speed of sound ratio is greater than 1, the dump distance does not exist. To facilitate scaling the acoustic fields, a "scaling distance" is introduced: $X_0 = \frac{\lambda}{4 \sin\theta_c \tan\beta}$ where $\theta_C = \cos^{-1}\frac{c_1}{c_2}$, $k_2 = \frac{\omega}{c_2}$, β is the angle of the wedge, c_1 = speed of sound in water, c_2 = speed of sound in bottom, and λ = wavelength in the wedge medium. X_0 appears to have physical meaning as a useful scaling distance.

TABLE OF CONTENTS

I. INTRODUCTION 12

II. DEVELOPMENT 13

A. DESCRIPTION OF THE THEORY 13

1. Image Theory 13

2. Normal Mode with Ray Bundles 16

3. Ray Tracing 16

4. Parabolic Equation 17

5. Buckingham's Approach 17

B. DEVELOPMENT OF THE WEDGE MODEL 18

C. DEVELOPMENT OF THE GRAPHIC PROGRAMS 19

1. Pressure-Amplitude Graphics 20

2. Pressure Contours 21

III. RESULTS FROM THE PLOTS 22

A. DATA PRESENTATION 22

1. The 3-D Plots 22

2. The Contour Plots 22

B. GENERAL PROPERTIES OF THE PLOTS WHICH ARE THE SAME FOR BOTH MODELS 23

C. DIFFERENCE BETWEEN BOTH MODELS 25

IV. EVALUATION 26

A. SPEED-OF-SOUND RATIO, DENSITY RATIO, AND ATTENUATION 26

B. RECEIVER ANGLE 27

C. WEDGE ANGLE 27

D. SOURCE ANGLE 28

E. LLOYD'S MIRROR 28

V. CONCLUSIONS AND RECOMMENDATIONS 29

A. CONCLUSIONS 29

B. RECOMMENDATIONS FOR FURTHER INVESTIGATION 30

APPENDIX A LIST OF 3-D WEDGE PROGRAM AND GRAPHIC PROGRAM 31

APPENDIX B RANGE OF VARIABLE STUDY 38

APPENDIX C FIGURES 39

LIST OF REFERENCES 98

INITIAL DISTRIBUTION LIST 100

LIST OF FIGURES

1	Three-Dimensional Wedge Geometry	39
2	The Geometry of the Image Solution	40
3-A	Pressure on the Bottom of the Wedge as Calculated by the Image Model for the Indicated Values of Parameters	41
3-B	Equal-Pressure Contours on the Bottom of the Wedge for the Indicated Values of Parameters	42
4-A	Pressure on the Bottom of the Wedge as Calculated by the Image Model for the Indicated Values of Parameters	43
4-B	Equal-Pressure Contours on the Bottom of the Wedge for the Indicated Values of Parameters	44
5-A	Pressure on the Bottom of the Wedge as Calculated by the Image Model for the Indicated Values of Parameters	45
5-B	Equal-Pressure Contours on the Bottom of the Wedge for the Indicated Values of Parameters	46
6-A	Pressure on the Bottom of the Wedge as Calculated by the Image Model for the Indicated Values of Parameters	47
6-B	Equal-Pressure Contours on the Bottom of the Wedge for the Indicated Values of Parameters	48
7-A	Pressure on the Bottom of the Wedge as Calculated by the Image Model for the Indicated Values of Parameters	49
7-B	Equal-Pressure Contours on the Bottom of the Wedge for the Indicated Values of Parameters	50
8-A	Pressure on the Bottom of the Wedge as Calculated by the Image Model for the Indicated Values of Parameters	51
8-B	Equal-Pressure Contours on the Bottom of the Wedge for the Indicated Values of Parameters	52
9-A	Pressure on the Bottom of the Wedge as Calculated by the Image Model for the Indicated Values of Parameters	53

9-B Equal-Pressure Contours on the Bottom of the Wedge for the Indicated Values of Parameters 54

10-A Pressure on the Bottom of the Wedge as Calculated by the Image Model for the Indicated Values of Parameters 55

10-B Equal-Pressure Contours on the Bottom of the Wedge for the Indicated Values of Parameters 56

11-A Pressure on the Bottom of the Wedge as Calculated by the Image Model for the Indicated Values of Parameters 57

11-B Equal-Pressure Contours on the Bottom of the Wedge for the Indicated Values of Parameters 58

12 Interference Pattern from a Point Source and an Image Point 59

13-A Pressure on the Bottom of the Wedge as Calculated by the Image Model for the Indicated Values of Parameters 60

13-B Equal-Pressure Contours on the Bottom of the Wedge for the Indicated Values of Parameters 61

13-C Pressure on Axis Response of Wedge 62

14-A Pressure on the Bottom of the Wedge as Calculated by the Image Model for the Indicated Values of Parameters 63

14-B Equal-Pressure Contours on the Bottom of the Wedge for the Indicated Values of Parameters 64

15-A Pressure on the Bottom of the Wedge as Calculated by the Image Model for the Indicated Values of Parameters 65

15-B Equal-Pressure Contours on the Bottom of the Wedge for the Indicated Values of Parameters 66

16-A Pressure on the Bottom of the Wedge as Calculated by the Image Model for the Indicated Values of Parameters 67

16-B Equal-Pressure Contours on the Bottom of the Wedge for the Indicated Values of Parameters 68

17-A Pressure on the Bottom of the Wedge as Calculated by the Image Model for the Indicated Values of Parameters 69

17-B Equal-Pressure Contours on the Bottom of the Wedge for the Indicated Values of Parameters 70

18-A Pressure on the Bottom of the Wedge as Calculated by the Image Model for the Indicated Values of Parameters 71

18-B Equal-Pressure Contours on the Bottom of the Wedge for the Indicated Values of Parameters 72

19-A Pressure on the Bottom of the Wedge as Calculated by the Image Model for the Indicated Values of Parameters 73

19-B Equal-Pressure Contours on the Bottom of the Wedge for the Indicated Values of Parameters 74

20-A Pressure on the Bottom of the Wedge as Calculated by the Image Model for the Indicated Values of Parameters 75

20-B Equal-Pressure Contours on the Bottom of the Wedge for the Indicated Values of Parameters 76

21-A Pressure on the Bottom of the Wedge as Calculated by the Image Model for the Indicated Values of Parameters 77

21-B Equal-Pressure Contours on the Bottom of the Wedge for the Indicated Values of Parameters 78

22-A Pressure on the Bottom of the Wedge as Calculated by the Image Model for the Indicated Values of Parameters 79

22-B Equal-Pressure Contours on the Bottom of the Wedge for the Indicated Values of Parameters 80

23-A Pressure on the Bottom of the Wedge as Calculated by the Image Model for the Indicated Values of Parameters 81

23-B Equal-Pressure Contours on the Bottom of the Wedge for the Indicated Values of Parameters 82

24-A Pressure on the Bottom of the Wedge as Calculated by the Image Model for the Indicated Values of Parameters 83

24-B Equal-Pressure Contours on the Bottom of the Wedge for the Indicated Values of Parameters 84

25-A Pressure on the Bottom of the Wedge as Calculated by the Image Model for the Indicated Values of Parameters 85

25-B Equal-Pressure Contours on the Bottom of the Wedge for the Indicated Values of Parameters 86

26-A Pressure on the Bottom of the Wedge as Calculated by the Image Model for the Indicated Values of Parameters 87

26-B Equal-Pressure Contours on the Bottom of the Wedge for the Indicated Values of Parameters 88

27-A Pressure on the Bottom of the Wedge as Calculated by the Image Model for the Indicated Values of Parameters 89

27-B Equal-Pressure Contours on the Bottom of the Wedge for the Indicated Values of Parameters 90

28-A Pressure on the Bottom of the Wedge as Calculated by the Image Model for the Indicated Values of Parameters 91

28-B Equal-Pressure Contours on the Bottom of the Wedge for the Indicated Values of Parameters 92

29-A Pressure on the Bottom of the Wedge as Calculated by the Image Model for the Indicated Values of Parameters 93

29-B Equal-Pressure Contours on the Bottom of the Wedge for the Indicated Values of Parameters 94

30-A Pressure on the Bottom of the Wedge as Calculated by the Image Model for the Indicated Values of Parameters 95

30-B Equal-Pressure Contours on the Bottom of the Wedge for the Indicated Values of Parameters 96

31 Effective Pressure-Release Bottom 97

LIST OF SYMBOLS

β	=	Wedge angle
G	=	Source angle measured upward from the interface
D	=	Receiver angle measured upward from the interface
R_1	=	Normalized source distance
R_2	=	Normalized receiver distance from the shoreline
Y_0	=	Normalized distance along the shore between the receiver and the source
$\frac{\rho_1}{\rho_2}$	=	Ratio of the medium density to the bottom density (density ratio)
$\frac{c_1}{c_2}$	=	Ratio of the speed of sound in the medium to the speed of sound in the bottom (speed of sound ratio)
$\frac{\alpha}{k_2}$	=	Wave number in the bottom divided into the absorption in the bottom.

ACKNOWLEDGMENT

I wish to thank Professors James V. Sanders and Alan B. Coppens for their support and perseverance in this endeavor.

I. INTRODUCTION

Acoustic propagation in an ocean with a sloping bottom is of growing concern both for theoretical reasons and because of the importance of knowing the performance of acoustic sensors located over the continental slope. This problem has been studied by many scientists [Ref. 1-8], but many have examined only cases of a fluid wedge for which both surfaces are acoustically impenetrable.

In the case of a fluid wedge for which both surfaces are acoustically impenetrable, mathematical examination of the problem has been performed by Bradley and Hudimic [Ref. 1] using both image theory and normal-mode theory.

For practical interest for underwater acoustics, the top boundary may still be approximated as an impenetrable, pressure-release surface, but the bottom surface can no longer be considered to be perfectly reflecting. From a mathematic point of view, this generalization of the boundary conditions has an important repercussion: The wave equation is no longer separable and standard normal-mode theory can no longer be applied.

This research will focus on four tasks:

1. Use the models to reevaluate the fast-bottom case which was done by Lesesne [Ref. 9].
2. Provide output in graphic form for ease of interpretation.
3. Change from the fast bottom model to a slow bottom model and evaluate whether a scaling factor is useful or not.
4. Compare results to others' research.

II. DEVELOPMENT

A. DESCRIPTION OF THE THEORY

1. Image Theory

The approach used in this research is to determine the amplitude and phase of the pressure in the fluid by the method of images [Refs. 8-10]. In 1978, with the aid of a computer model, Coppens, Sanders, Ionnou, and Kawamura [Ref. 11] predicted and measured the pressure amplitude and phase in the up-slope direction along the bottom of a wedge-shaped fluid layer overlying a fast fluid bottom. The geometry is shown in Figure 1.

Baek [Ref. 12] used the same model in 1984 to predict pressure amplitude and phase everywhere within the wedge in the up-slope direction. In the same year, Lesesne [Ref. 9] implemented a model developed by Coppens and Sanders which is not limited to up- or down-slope prediction.

For the wedge-shaped duct, the images which lie on a circle (see Figure 2) are eventually going to appear in the region where the source is located and which, by the established boundary conditions, can contain only the source. However, following Sommerfeld [Ref. 13], the concept of an extended Rieman surface is introduced. The extension of the θ coordinate by introduction of Rieman sheets allows for an infinite (if need be) number of images.

The source and each of the images radiate a spherical wave of the appropriate phase. The phase coherent summation of these waves

yields the total pressure and phase to be found at any field point in the wedge.

The total pressure of all the images and the source along a line of constant x from the apex can be determined by the method of images (see Figure 2).

$$\tilde{P}_N(x) = \sum_{n=1}^{N} (-1)^{INT(N/2)} \left[g_{n-2} \exp[jk_1 x \cos(\theta_n - D)] \right] +$$

$$g_n \exp[jk_1 x \cos(\theta_n + D)] \qquad (1)$$

where

N = $INT(180/\beta)$,

β = the wedge angle,

D = the receiver angle,

G = the source angle.

$\theta_n = (n - 1)\beta + G, \qquad n = 1,3,5,7...$

$\theta_n = n\beta - G, \qquad n = 2,4,6,8...$

$g_n = \prod_{m=1,3,5...}^{n} R(\theta_m) \qquad m \text{ odd}$

$g_n = \prod_{m=2,4,6...}^{n} R(\theta_m) \qquad m \text{ even}$

$g_{-1} = g_0 = +1.0$

The g_{n-2} and g_n are path parameters from the nth image and $R(\theta_n)$ is the reflection coefficient of the bottom with grazing angle θ_n. (For details, see Ref. 12.)

The successive reflection of sound from the surface and bottom is accounted for by multiplying the sound field radiated by each image by the plane wave reflection coefficients corresponding to reflections encountered by the wave as it propagates toward the field point.

For the fast bottom, all distances are normalized to the distance X_0, measured from the apex, at which the lowest mode would attain cut-off in the adiabatic approximation. This distance X_0 is called the dump distance [Ref. 12] (see Figure 2).

$$X_0 = \frac{h}{\tan\beta} = \frac{\lambda}{4 * \sin\theta_c * \tan\beta}$$

λ = wavelength in wedge medium

$\theta_c = \cos^{-1}\frac{c_1}{c_2}$ = critical angle

β = wedge angle

h = water depth at dump distance

For this model, we use wedge angles of the form π/n where n is an integer and consequently no diffraction term exists [Refs. 14-15]. If n is not an integer, then there will be a diffracted wave which will always arrive at a later time than the latest image contribution [Ref. 14].

2. Normal Mode With Ray Bundles

V. K. Kuzentsov's [Ref. 7] normal-mode-with-ray-bundles approach treats the entire domain of the wedge as two zones with respect to the separation at V_m, where V_m is the exit line of the normal mode from the wedge into the half-space. Its position corresponds to the critical wedge thickness for the given normal mode with the non-wave guide zone $r < r_m$. In the wave-guide zone, the normal modes behave as normal modes in an ideal wedge.

3. Ray Tracing

Tien *et al.* [Ref. 16] developed an analysis based on a ray approach. At the depth where the mode would be cut off, it is assumed that a ray reflects from the bottom of the wedge at the critical angle:

> This ray is allowed to reflect from the surface and it reattains the bottom at a grazing angle which is the critical increased by twice the wedge angle. The intervening region of the wedge is filled with a large number of downward-traveling rays whose angles of incidence on the bottom are uniformly increasing between θ and $\theta + 2\beta$. Then, for each ray the transmission into the bottom is calculated. This process is repeated progressively toward the apex of the wedge. There is no attempt to preserve phase information, and the power of the beam in the bottom at each angle of depression is simply the sum of the powers transmitted by the appropriate rays. Calculations performed with the help of a computer again provide good agreement with their experimental observations as far as the angle of depression and beam width of the beam in the bottom were concerned, but this approach predicts that there should be no transmission of sound into the bottom until the cutoff depth is reached. [Ref. 17]

In the ray-tracing method, there is no attempt to preserve phase information, and the power of the beam in the bottom is simply the sum of the power transmitted by the appropriate rays.

4. Parabolic Equation

Jensen and Kuperman [Ref. 4] used the parabolic equation approximation to study up-slope propagation. Their numerical calculations suggested that there is negligible coupling between normal modes. They also obtained some very interesting graphs which show that the energy of a mode passing through cut-off was radiated as a beam into the bottom.

The only significant limitation of this method appears to be that inherent in the approximations necessary for applicability of the parabolic equation itself.

5. Buckingham's Approach

In an A. B. Wood Memorial Lecture, Buckingham [Ref. 2] discussed acoustic propagation in a wedge-shaped ocean. Basically, he follows his previous papers [Ref. 18], modified to include a penetrable bottom. In the original paper [Ref. 18], both forward scattering and backward scattering exists in the acoustic field except when the receiver is located in the vicinity of the source. However, in the penetrable wedge there can be no significant backward-reflected component in the acoustic field [Ref. 2].

Buckingham also used the Rayleigh law of reflection for fast bottom and derived an effective wedge with a pressure-release bottom (see Figure 31): The Rayleigh law of reflection is

$$V = \frac{g \sin \alpha - j(\cos^2\alpha - \cos^2\alpha_c)^{1/2}}{g \sin \alpha + j(\cos^2\alpha - \cos^2\alpha_c)^{1/2}} \qquad (1)$$

where $g = \frac{\rho_2}{\rho_1}$, α is the angle from the normal, and α_c is the critical angle. Here, we are concerned only with grazing angles less than the critical, where total internal reflection occurs. When $\alpha > \alpha_c$, there is a phase change on reflection, 2E, which from equation (1) can be expressed as

$$2E = 2 \tan^{-1}\left[\frac{(\cos^2\alpha - \cos^2\alpha_c)^{1/2}}{g\sin\alpha}\right] \tag{2}$$

Buckingham then points out that similar phase change would occur if the ray had been reflected from a pressure-release surface a distance Δ below the actual interface (Figure 31):

$$\Delta = \left(\frac{\frac{\pi}{2} - E}{k\sin\alpha}\right) \tag{3}$$

where k = wave number in the first fluid. At the critical angle, it is clear from equation (2) that E = 0, in which case,

$$\Delta_0 = \frac{\pi}{2k\sin\alpha_c}$$

B. DEVELOPMENT OF THE WEDGE MODEL

Originally, the fast-bottom model was modified from a computer model by Coppens, which was programmed in FORTRAN by Baek and designed to run on the IBM 3033. The slow-bottom model resulted from a modification of this program. For the slow bottom, the cut-off condition does not exist. However, using the following formula,

$$\theta_0 = \cos^{-1}\left(\frac{1}{c_1/c_2}\right)$$

c_1 = velocity sound in water

c_2 = velocity sound in bottom

a scaling factor is introduced which uses the same idea that was in the fast-bottom model but with the speed of sound ratio inverted.

C. DEVELOPMENT OF THE GRAPHIC PROGRAMS

At this stage, it became necessary to consider alternate forms of data presentation. Because of the large volume of computed values, numerical output had become ineffective for recognizing details. The graphic package Disspla [Ref. 20], available on the IBM 3033 computer, was used in conjunction with these programs.

Graphical plots of the data are essential for a clear understanding of the problem. A purpose of this research was to utilize graphics to better determine the physical concepts necessary to interpret the aspects of sound propagation in a wedge-shaped ocean with a penetrable bottom.

Disspla is an option which uses "function calls" from a FORTRAN program to generate graphs. Disspla's use of FORTRAN allows function calls to be written into a program or to be written as separate programs. The data used to compute the graphs can, therefore, be generated within the FORTRAN program or read in from a data file. The latter method was employed since it offered more versatility.

The size of the data file array or the number of points used did not prove to be a limitation on the graphs that were generated. By holding all but two parameters constant, a plot of pressure amplitude versus

the remaining variable was obtained. The position of the receiver on the bottom was usually varied to map the pressure field for a given source location.

The Disspla package supports this, but several problems had to be overcome. The Pocket Guide of Disspla describing this option was incomplete and very confusing. After comparing the various options available, it was decided to use the mode of graphics in which a matrix is used to define the data.

At the beginning, it was necessary to determine the optimal number of matrix points which would provide smooth and reasonable plots. After running through hundreds of plots, it was decided to use 100 x 100 matrix points.

The other important limitation was that the array containing the data points must be initially dimensionalized to the exact size of the data file array. This information was normally passed from the data file during the programs. This made it necessary to initialize the size of the data file array before the graphics program was run.

1. Pressure-Amplitude Graphics

a. The pressure amplitude was plotted as a function of the two receiver coordinates. This produced a 3-D plot. The clearest presentation was a series of 3-D graphs stacked one after another (see Figures 3-A and 4-A), which contain fast- and slow-bottom complementary cases. (In this context, "complementary case" means the two cases obtained by exchanging the relative values of c_1 and c_2.)

b. When the receiver is close to the source, the spatial variation of the pressure amplitude is smaller than the increment, producing artificial structure to the graph. To allow a truer view of this portion of the pressure amplitude, smaller portions of the field

can be viewed with higher resolution without increasing computer time (see Figures 5 and 6).

c. When a fuller view was necessary, the models were modified to ignore the field close to the source (see Figure 7).

2. Pressure Contours

The second graphic program used was a contour plot. The following should be mentioned here:

a. The poly 3 interpolation method was used to produce the plots.

b. The number of matrix points in this program is the same as as for the pressure-amplitude graphics.

c. The increment in the pressure amplitude between contour lines was controlled either automatically or by the user. (In Figures 3-B and 15-B, one can see the difference between the two methods.)

In an attempt to analyze the pressure distribution near the source, a polar graphic program was developed. Here, the receiver was positioned on circles centered on the source and moved out in radial increments. Although this polar form satisfactorily dispersed the pressure field near the source, it created very serious geometrical distortion (see Figure 8). As a result, it was not very useful.

III. RESULTS FROM THE PLOTS

A. DATA PRESENTATION

1. The 3-D Plots

Generally, the source is fixed and the pressure amplitude is calculated as a function of receiver position. So, for the three axes of the graphs:

1. The R_2 axis is the normalized receiver distance from the shoreline.
2. The Y_0 axis is the normalized distance along the shoreline between the receiver and the source.
3. The vertical axis is the pressure amplitude.

The resolution of the plots is set by specifying a 100 x 100 matrix of pressure calculation, which means:

$$100 = \frac{\text{The range of } R_2 \text{ (or } Y_0)}{\text{The increment of } R_2 \text{ (or } Y_0)}$$

The smaller the range of R_2 (or Y_0), the smaller the increment of R_2 (or Y_0), the higher the resolution of the plots, and the smoother the plots.

2. The Contour Plots

The axes of the contour plot are X and Y, in which X is equal to R_2 and Y is equal to Y_0. The label values on the contour lines are the pressure amplitudes. The increments of the pressure amplitude and the resolution are also controlled by the value of CONMAK [Ref. 20] (see Figure 9-B).

There are many "tear drop" contours, as shown in Figure 4-B. The contours are caused by the limited resolution and disappear at higher resolution (see Figure 9-B).

B. GENERAL PROPERTIES OF THE PLOTS WHICH ARE THE SAME FOR BOTH MODELS

When R_1 is equal to an odd number, the pressure peak is directly under the source, as shown in Figures 10 and 13. When R_1 is equal to an even number, the pressure is a minimum under the source (see Figures 11 and 14). The explanation for this can be found by using only the source, the image character, and the first surface reflected path (see Figure 12).

The time dependence of the signal at a distance d_1 from the source is

$$P_1 = \frac{A}{d_1} e^{-j(\omega t - kd_1)}$$

and the time dependence of the signal arriving at R from the image characterizing the first surface reflected path is

$$P_1^* = \frac{-A}{d_2} e^{-j(\omega t - kd_2)}$$

where d_2 is the distance from the image point to receiver. So,

$$P_T = P_1 + P_1^* = e^{-j\omega t}\left[\frac{A}{d_1} e^{-jkd_1} - \frac{A}{d_2} e^{-jkd_2}\right]$$

$$= e^{-j\omega t}\left[\frac{A}{d_1} - \frac{A}{d_2} e^{-jk(d_2-d_1)}\right]$$

Thus, the phase difference between the signals arriving at R from S and S' is

$$k(d_2 - d_1) = \Delta\phi$$

When constructive interference occurs,

$$\Delta\phi = 2n\pi, \qquad n = 0,1,2,...$$

and when destructive interference occurs,

$$\Delta\phi = (2n + 1)\pi, \quad n = 0,1,2,...$$

The set of points for which $d_2 - d_1$ has a constant value defines a locus along which $\Delta\phi$ is constant. The locus $d_2 - d_1$ = constant is a hyperbola of revolution about the vertical axis connecting the source and the first surface-reflected image. The intersection of this surface and the plane representing the interface between the two media yields elliptical curves close to the source, which evolve into hyperbolic curves far from the source.

These features are observed in the pressure contour plots for the various cases.

The angle of intromission for which the reflection coefficient is zero will exist in the fast-bottom case for $\rho_1 > \rho_2$ or the slow-bottom case for $\rho_1 < \rho_2$. Figures 17 and 18 are for cases possessing angles of intromission; these appear to exhibit no significant pressure changes compared to the non-intromission conditions.

C. DIFFERENCE BETWEEN BOTH MODELS

With the fast bottom, the pressure pattern is much more irregular and the pressure decays with distance from the source less rapidly because, with the fast bottom, more images are totally reflected from the bottom.

IV. EVALUATION

The effects of changing the properties of the wedge and the source position on the prediction of the pressure field were evaluated. As a base-line case, the following parameters were used:

$\beta = 10°$

$G = 5°$

$D = 0°$

$R_1 = 40$

$\frac{\rho_1}{\rho_2} = 0.9$

$c_1/c_2 = 0.9$ (fast bottom)

$c_1/c_2 = 1/0.9$ (slow bottom)

$\alpha/k_2 = 0.0001$

Three-dimensional depictions of the pressure fields for these conditions as functions of R_2 and Y_0 are shown in Figures 3 and 4 for both fast- and slow-bottom cases. The corresponding contour plots are included.

Both models were tested by varying one parameter and holding the others constant. Comparison of pressure-contour plots as well as three-dimensional plots was then used to determine the effect of each parameter.

A. SPEED-OF-SOUND RATIO, DENSITY RATIO, AND ATTENUATION

The base-line case was first examined by changing the speed-of-sound ratio. The positions and number of crests exhibited simple and

clear patterns for the slow-bottom model (see Figure 19) and more complex patterns for the fast-bottom model (see Figure 20) as this ratio was changed from 0.9 (or 1/0.9) to 0.5 (1/0.5). The density ratio was then changed down to a value of 0.5. The positions and number of crests show only minor variation (see Figure 21). This suggests that the major features of the sound field in the wedge are relatively insensitive to minor variations in the characteristics of the bottom.

Finally, the value of α/k_2 was increased from 0.0001 to 0.1. The pressure-pattern did not change significantly but, as expected, the amplitudes of the crests showed sharp decreases as the attenuation increases.

B. RECEIVER ANGLE

The reader should be aware of the fact that the program contained in the appendix was modified as simply as possible, to insure that pressure was calculated infinitesimally above the bottom. If it is desired to calculate the pressure for receiver angles not essentially zero, the leading statements and do loops must be modified.

C. WEDGE ANGLE

As the wedge angle decreases, the dump distance increases, the number of images increases, and therefore the CPU time increases. For example, for $\beta = 10°$, the CPU times for fast-bottom and slow-bottom cases are about 520 seconds and 480 seconds, respectively. If $\beta = 7°$, the CPU time increases to about 900 seconds (see Figures 22 and 23).

D. SOURCE ANGLE

Changing the distance of the source from the apex (but still with $G = \beta/2$) had a great effect on the position of the crests and troughs. However, for the source at large distances from the apex, scaling the receiver position restores the original patterns. For example, if the source is moved outward to twice its original position, a plot with the length scales divided by two produces the same graphic presentation (see Figures 3 and 24 or 4 and 25). This is consistent with Lesesne's observation.

E. *LLOYD'S MIRROR*

Figures 29 and 30 show the field due to the source and the first image point only. The source and the first image are of equal strength. The first image is coherent with the source but π out of phase (see Figure 12). That produces the Lloyd's mirror. The pressure distribution observed is identical for both fast- and slow-bottom programs when they were modified to have the same apparent speed of sound in the wedge. These figures show that major features of the pressure field are due mainly to the source and first image when the receiver is close to the source.

V. CONCLUSIONS AND RECOMMENDATIONS

The theory of 3-D acoustic propagation in a penetrable wedge presented in this research is based on the method of images which includes the fast- and the slow-bottom models. One of the research goals was to test whether the scaling factor method can apply to the slow-bottom case.

A. CONCLUSIONS

For both the fast bottom and the slow bottom, when the receiver is near the source, strong spatial oscillations in pressure are present. These variations are mainly due to interference between the source and the first surface-reflected image.

The primary result of the fast-bottom model is the importance of interference evident in the form of strong spatial oscillation. When the bottom mismatch increases, more interference occurs, because more images contribute to the field.

Generally, investigation of this model showed that the scaling factor worked.

One observation is in violation of physical intuition—when the bottom mismatch increases, more interference should occur. Figures 26, 27, and 28 show the opposite, with less interference as the bottom mismatch increases.

The results for the fast-bottom model are more complex than for the slow-bottom case because the cut-off condition only exists in the

fast-bottom model, which yields more images which correspond to perfect reflections for the bottom.

The method of images does not yield an easy decomposition of the sound field into a form that can be closely associated with normal modes. On the other hand, the method of images provides intrinsically the phase interference effects associated with the superposition of effects that would be more difficult to extract from the adiabatic normal mode. The intrinsic inclusion of absorption in the substrate is an attractive and realistic feature of the image approach. In addition, the image approach appears to avoid the generation of caustics at turning points which are inextricably linked with the results of unmodified ray tracing approaches.

B. RECOMMENDATIONS FOR FURTHER INVESTIGATION

1. For the case of a real fast-bottom, identification of the normal modes of the system and investigation of the possibility of normal mode coupling is worth study.
2. Using the batch system to investigate the small wedge angle is worth study.
3. Changing the position and depth of the receiver is worth study.
4. For the slow bottom, experiments should be undertaken to compare with the theoretical predictions.

APPENDIX A

COMPUTER PROGRAMS

FILE: 3LS4 FORTRAN A1

```
      DEBUG UNIT(6),SUBCHK
      END DEBUG
C     ------------------------------------------------------------------
C     CROSS SLOP TRANSMISSION IN THE WEDGE WITH PENETRABLE LOSSY SLOW
C     BOTTOM ( NO GEOMETRICAL APPROXIMATIONS )
C     ------------------------------------------------------------------
C     DIMENSIONZ(M,M) (21,11), (Y0,R2)--(L,A)
      DIMENSION Z(101,101)
      COMMON WORK(50000)
      INTEGER  A,II,JJ,N1,S1,S2,IE,N,I
      REAL*4  RR1,R2,Y0,Y1,YOSTA,YOINC,R2INC,R2STA,RZ,RZ1,M,J,
     1   B,C(30),CC,C2,D,D1,D2,E(30),E1,E2,F(30),F1,F2,G,H,PI,FI,
     1   P1,P2,P(125,130),PH,Q1,Y2,R3,R8(80),R9(80),
     1   S(30),T,T4,T6,T1(80),TQQ,TQQ1,TQQ2,TQQ3,W,W0,W1,XL,Y,
     1   Z1,Z2,Z3,Z4,Z5,Z6,Z,EL,DIST
      CALL SETIME
      PI = ARCOS(-1.0)
C     ****************************************************************************
C     INPUT PARAMETERS
C     N1 = # OF IMAGINE POINTS
C     B = WEDGE ANGLE (DEG)
C     G = SOURCE ANGLE (DEG)
C     D = RECEIVER ANGLE (DEG)
C     R1 = SOURCE DISTANCE (IN DUMP DISTANCES)
C     R2 = RECEIVER DISTANCE (IN DUMP DISTANCES)
C     Y0 = SHORE DISPLACEMENT (IN DUMP DISTANCES)
C     D1 = RHO1/RHO2
C     CC = C1/C2
C     XL = ALPHA/K2
C     A = # OF RECEIVER POSITIONS IN R2 DIRECTION
C     L = # OF RECEIVER POSITIONS IN Y0 DIRECTION
C     R2INC = INCREMENTAL INCREASE FOR R2
C     Y0INC = INCREMENTAL INCREASE FOR Y0
C     ****************************************************************************
C     ****************************************DATA VALUES*************************
C     CALL TEK618
      CALL COMPRS
C     CALL PAGE(11,8.5)
      B=10.
      G = 1.0*B/4.
```

```
      G = 5
      D = 0.0
      R1 = 10.
      R2 = 5.
      Y0 = 0.
      D1 = .9
C     D1 = 1/.9
C     FOR SLOW-BOTTOM CASE
      CC = 1/0.9
C     FOR FAST-BOTTOM CASE
      CC = 0.9
C     CC = .5
      XL = .0001
      A = 100
      L = 100
      R2INC = .1
      Y0INC = .1
C     ************************************MAIN PROGRAM**********************************************
      Y0STA = Y0
      R2STA = R2
      W = 0.0
      WRITE(6,300) B,G,D
 300  FORMAT (3X,'B = '.F5.2,3X,'G = '.F5.2,3X,'D = ',F5.2,3X)
 310  FORMAT (1X,F5.2,1X,F5.2,1X,F5.2)
      WRITE(6,400) R1
 400  FORMAT (3X,'SOURCE RANGE = ',F8.2)
 410  FORMAT (1X,F6.2)
      WRITE(6,500) D1,CC,XL
 500  FORMAT (3X,'DENSITY RATIO = ',F8.6,3X,'SPEED RATIO = ',F8.6,3X,
     *        'ALPHA/K2 = ',F8,6)
 510  FORMAT (1X,F6.4,1X,F6.4,1X,F6.4)
      WRITE(6,600)
 600  FORMAT (5X,'42',6X,'Y0',10X,'P')
C     WRITE(22,700) R2,Y0
 700  FORMAT (1X,F6.2,1X,F6.2)
      N1 = (180/B + .00001)
      T6 = 180/PI
      B = B/T6
      G = G/T6
      C2 = CC**2
C
      HM=0
      HH=1
          D =HM*B/A
          DD = B/A
          V = 2*B/10
          IF(D.LT.V) GO TO 110
          IF(D.GE.V) GO TO 120
 110      DX = D
C     THIS DO LOOP CALCULATES THE TMETA(N) AND THE IMINAGE SLANT
C     RANGES R8(N) AND R9(N).
C     ------------------------------------------------------------
```

```
C               DO 55 HH = 1.10
                  D = DX+(HH-1)*B/(10*A)
                  DD = B/(10*A)
 120              S1 = 1
C  ------------------------------YEH-----------------------------------------
C               T4 = P1/(2*TAN(ARCOS(1/CC))*TAN(B))
                TQQ = TAN(B)
C       FOR SLOW-BOTTOM CASE
                TQQ1 = ARCOS(1/CC)
C       FOR FAST-BOTTOM CASE
                TQQ1 = ARCOS(CC)
                TQQ2 = TAN(TQQ1)
                TQQ3 = 2.*TQQ2*TQQ
                T4 = PI/TQQ3
                Q1 = 1/SQRT(2.0)
              LP1X=L+1
              IAP1X=A+1
                DO 20 M=1,LP1X
                DO 10 J=1,IAP1X
                D2 = (Y0**2)+(R1**2)+(R2**2)
                R3 = 2*R1*R2
C  ---------------------------------------------------------------------
                DO 30  N = 1,N1
                    IF(S1.GT.0) T1(N)=FLOAT(N-1)*B+G
                    IF(S1.LT.0) T1(N)=FLOAT(N)*B-G
                    S1 = - S1
                    R8(N) = SQRT(D2-R3*COS(T1(N)-D))
                    R9(N) = SQRT(D2-R3*COS(T1(N)+D))
 30             CONTINUE
C  ---------------------------------------------
C  ----------SUM PRESSURE OVER ALL IMINAGES----------------------
C  ---------------------------------------------
                P1 = 0.0
                P2 = 0.0
                DO 40  N = 1,N1
                    S2 = (-1)**(IFIX(N/2+.0001))
                    W1 = 2*C2*XL
C  ---------------------------------------------
C  ----------FEFL COEFFS ALONG WITH UPPER PATH--------------------
C  ---------------------------------------------
                    I1 = IFIX((N-.9999)/2)
                    DO 41  I = 1,I1
                        S(I) = ABS(R1*SIN(T1(N)-2*FLOAT(I)*B)
                              +R2*SIN(2*FLOAT(I)*B-D))/R8(N)
                        C(I) =SQRT(1-(S(I)**2))
                        T = S(I)/D1
                        W0 = (-C2+(C(I)**2))
                        Y = SQRT((W0**2)+(W1**2))
                        Z(M,J) = ABS(W0)
                        IF(Y,LE,Z(M,J)) Y = Z(M,J)
                        Y1 = Q1*SQRT(Y+W0)
```

```
                Y2 = -Q1*SQRT(Y-W0)
                E(I) = (T**2)-(Y2**2)-((Y1**2))/(((T-Y2)**2)+(Y1**2)
                F(I) = (2*Y1*T)/(((T-Y2)**2)+(Y1**2))
 41           CONTINUE
C  ------------------------------------------------------------------------
C  ------------PRODUCT OF REFL COEFFS ALONG NTH UPPER PATH----------------------
C  ------------------------------------------------------------------------
                E1 = 1.0
                F1 = 0.0
                IF(N.LE.2.0) GOTO 422
                DO 42 I = 1, I1
                E2 = E1*E(I)-F1*F(I)
                F2 = F1*E(I)-E1*F(I)
                E1 = E2
                F1 = F2
 42           CONTINUE
C  ***************************************************************
C       FOR SLOW-BOTTOM CASE
 422          T = T4*R8(N)
C       FOR FAST-BOTTOM CASE
 422          T = T4*R8(N)/CC
C  ***************************************************************
                P1 = P1 + S2*(E1*COS(T)+F1*SIN(T))/48(N)
                P2 = P2 + S2*(F1*COS(T)+E1*SIN(T))/48(N)
C  ------------------------------------------------
C  ----------REFL COEFFS ALONG NTH LOWER PATH----------------------
C  ------------------------------------------------
                I1 = I1 +1
                DO 43  I = 1,I1
                S(I) = ABS(R1*SIN(T1(N)-2*FLOAT(I-1)*8)
                        + R2*SIN(2*FLOAT(I-1)*B+D))/R9(N)
                C(I) = SQRT(1-(S(I)**2))
                T = S(I)/D1
                W0 = (-C2+(C(I)**2))
                Y = SQRT((W0**2)+(W1**2))
                Z(M,J) = ABS(W0)
                IF(Y.LE.Z(M,J)) Y = Z(M,J)
                Y1 = Q1*SQRT(Y+W0)
                Y2 = -Q1*SQRT(Y-W0)
                E(I) = ((T**2)-(Y2**2)-(Y1**2))/(((T-YW)**2)_(Y1**2))
                F(I) = (2*Y1*T)/(((T-Y2)**2)+(Y1**2))
C               AN2 = TAN(F(I)/E(I))*T6)
 43           CONTINUE
C  ------------------------------------------------------------------------
C  ------------PRODUCT OF REFL COEFFS ALONG NTH LOWER PATH----------------------
C  ------------------------------------------------------------------------
           E1 = 1.
           F1 = 0.
           DO 44  I = 1,I1
                E2 = E1*E(I)-F1*F(I)
                F2 = F1*E(I)+E1*F(I)
```

```
                E1 = E2
                F1 = F2
 44           CONTINUE
C  ************************************************************
C       FOR SLOW-BOTTOM CASE
              T = T4*R9(N)
C       FOR FAST-BOTTOM CASE
              T = T4*R9(N)/CC   FAST BOTTOM
C  ************************************************************
                P1 = P1 + S2*(E1*COS(T)+F1*SIN(T))/R9(N)
                P2 = P2 + S2*(F1*COS(T)-E1*SIN(T))/R9(N)
 40     CONTINUE
        Z(M,J) = SQRT((P1**2)+D(P2**2))*R1
        IF(W.LT.Z(M,J)) W=Z(M,J)
        WRITE(6,200) R2,Y0,Z(M,J)
 200    FORMAT (3X,F7.3,3X,F7.2,3X,F9.5,3X,F9.5)
C  ************************************************************
C  ************************************************************
        R2 = R2+R2INC
C  ************************************************************
C       DIST = SQRT ((J-41)**2) + (M-1)**2)
C       IF (DIST.LE.20.) Z(M,J) = 0.
C  ************************************************************
 10     CONTINUE
        Y0 = Y0 + Y0INC
        R2 = 5.
 20     CONTINUE
        CALL SURF3D(Z,NX,NY)
        Y0 = 0.
 55      CONTINUE
 33      CONTINUE
        STOP
        END
C  ------------------------------------------------------------
        SUBROUTINE SURF3D(Z,NX,NY)
C  ------------------------------------------------------------
C PLOTS 3D SURFACE OF AN ARRAY Z(NX,NY) OF REGULARLY SPACED POINTS.
C  ------------------------------------------------------------
        DIMENSION Z(101,101)
        DIMENSION RZ(101,L101)
        COMMON WORK(50000)
C  ------------------------------------------------------------
C CHECK DATA STATEMENTS TO ET AXIS LIMITS:
C  ------------------------------------------------------------
        DO 1 I-1,101
        DO 1 J-1,101
 1      RZ(J,I)=Z(I,J)
C  ------------------------------------------------------------
C  ----------PRODUCE CONTOUR PLOT----------
C  ------------------------------------------------------------
        CALL PAGE (11,8.5)
```

```
      CALL SHDCHR(.90,1.,.003,1.)
      CALL AREA2D(9.5,6)
C     CALL NOBRDR
      CALL BLOWUP(.85)
      CALL XNAME ('XXX',1)
      CALL YNAME('YYY',1)
      CALL HEADIN('CONTOUR PLOT$',100,1.,1)
      CALL GRAF(5.,1.,15.,0.,1.,10.)
      CALL FRAME
      CALL BCOMON(50000)
      CALL CONMAK(RZ,101,101,.5)
      CALL CONLIN(0,'SOLID','LABELS',1,1)
      CALL CONANG(90.)
      CALL POLY3
      CALL CONTUR(2,'LABELS','DRAW')
      CALL ENDPL(0)
C     ------------------------------------------------------------------
C     ----------PRODUCE SURFACE PLOT----------
C     ------------------------------------------------------------------
      CALL PAGE(11,8.5)
      CALL AREA2D(9.5,6)
      CALL MX1ALF('STANDARD','*')
      CALL MX2ALF('L/CSTD','+')
C     ------------------------------------------------------------------
C  LABEL AXES:
      CALL X3NAME('R2 A+XIS*$',100)
      CALL Y3NAME('Y0 A+XIS*$',100)
      CALL Z3NAME('PRESSURE A+XIS*$',100)
C     ------------------------------------------------------------------
      CALL VOLM3D(5.,5.,5.)
      CALL YINTAX
      CALL XINTAX
      CALL ZINTAX
      CALL ZAXANG(0.)
      CALL YAXANG(0.)
      CALL XTICKS(5)
      CALL YTICKS(5)
      CALL HEADIN ('SLOW BOTTOM',11,1.5,1)
      CALL HEADIN ('FAST BOTTOM',11,1.5,1)
      CALL MESSAG ('C.P.U. =          SECONDS$',100,6.5,0.)
      CALL MESSAG ('VIEPTS IS 250,350,90$',100.6,6.5)
      CALL MESSAG ('SURMAT IS RZ,1,101,101,101$',100,6,6)
      CALL MESSAG ('SURVIS IS TOP$',10,6,5.5)
      CALL MESSAG ('B(W.A.)-10.,G(S.A)-5.,D(R.A)=0 $',100,6,5)
      CALL MESSAG ('RHO1/RHO2 =.9,ALPHA/K2=.0001 $',100,6.4.5)
      CALL MESSAG ('C1/C2 -1/.9,R1=10.,42=5.,Y0=0.$',100,6,4)
      CALL MESSAG ('R2INC =.1,Y0INC =.1,CMK =.5$',100,6,3.5)
C     ------------------------------------------------------------------
      CALL VUABS(250.,350.,90.)
      CALL SURVIS('TOP')
      CALL GRAF3D (5.,1.,15.,0.,1.,10.,0.,5.,15.)
```

```
      ALL BLSUR
C     CALL SURMAT(RZ,XX,A+1,XX,L+1)
      CALL SURMAT(RZ,1,101,101,101,0)
C     ------------------------------------------------------------------------
      CALL ENDPL(0)
      CALL DONEPL
      CALL GETIME(IET)
      EL = IET * .000026
      WRITE (4,2) EL
 2    FORMAT(20X,'TIME = ',E16.6,'SECONDS.')
      RETURN
      END
```

RANGE OF VARIABLE STUDY

SLOW BOTTOM

FIG	β	$\frac{c_1}{c_2}$	$\frac{\rho_1}{\rho_2}$	G	R_1	D	$R_2\frac{min}{max}$	$Yo\frac{min}{max}$	θ_c	θ_I
3 15	10	$\frac{1}{0.9}$	0.9	5	40	0	$\frac{0}{100}$	$\frac{0}{100}$	X	0°
7	10	$\frac{1}{0.9}$	0.9	5	40	0	$\frac{0}{100}$	$\frac{0}{100}$	X	0°
5	10	$\frac{1}{0.9}$	0.9	5	40	0	$\frac{35}{45}$	$\frac{0}{10}$	X	0°
24	10	$\frac{1}{0.9}$	0.9	5	40	7	$\frac{0}{100}$	$\frac{0}{100}$	X	0°
28	10	$\frac{1}{0.9}$	0.9	5	80	7	$\frac{0}{100}$	$\frac{0}{100}$	X	0°
11	10	$\frac{1}{0.9}$	0.9	5	10	0	$\frac{5}{15}$	$\frac{0}{10}$	X	0°
13	10	$\frac{1}{0.9}$	0.9	5	5	0	$\frac{0}{10}$	$\frac{1}{10}$	X	0°
14	10	$\frac{1}{0.9}$	0.9	5	4	0	$\frac{0}{10}$	$\frac{1}{10}$	X	0°
17	10	$\frac{1}{0.9}$	0.9	5	1	0	$\frac{0}{10}$	$\frac{0}{10}$	X	0°
19	10	$\frac{1}{0.5}$	0.9	5	4	0	$\frac{0}{10}$	$\frac{0}{10}$	X	X
22	10	$\frac{1}{0.5}$	0.5	5	40	0	$\frac{0}{100}$	$\frac{0}{100}$	X	0°
26	10	$\frac{1}{0.9}$	0.9	5	40	0	$\frac{0}{100}$	$\frac{0}{100}$	X	0°

FAST BOTTOM

FIG	β	$\frac{c_1}{c_2}$	$\frac{\rho_1}{\rho_2}$	G	R_1	D	$R_2\frac{min}{max}$	$Yo\frac{min}{max}$	θ_c	θ_I
4 16	10	0.9	0.9	5	40	0	$\frac{0}{100}$	$\frac{0}{100}$	64.16°	X
6	10	0.9	0.9	5	40	0	$\frac{35}{45}$	$\frac{0}{10}$	64.16°	X
9	10	0.9	0.9	5	40	0	$\frac{29.5}{31.5}$	$\frac{86}{88}$	64.16°	X
25	10	0.9	0.9	5	40	7	$\frac{0}{100}$	$\frac{0}{100}$	64.16°	X
29	10	0.9	0.9	5	80	0	$\frac{0}{100}$	$\frac{0}{100}$	64.16°	X
10	10	0.9	0.9	5	1	0	$\frac{0.5}{2}$	$\frac{0}{1.2}$	64.16°	X
21	10	0.9	0.5	5	40	0	$\frac{0}{100}$	$\frac{0}{100}$	64.16°	X
18	10	0.9	$\frac{1}{0.9}$	5	40	0	$\frac{0}{100}$	$\frac{0}{100}$	64.16°	0°
20	10	0.5	0.9	5	40	0	$\frac{0}{100}$	$\frac{0}{100}$	30°	X
23	10	0.5	0.5	5	40	0	$\frac{0}{100}$	$\frac{0}{100}$	30°	X
27	7	0.9	0.9	5	40	0	$\frac{0}{100}$	$\frac{0}{100}$	64.16°	X

X = not exist

APPENDIX C

FIGURES

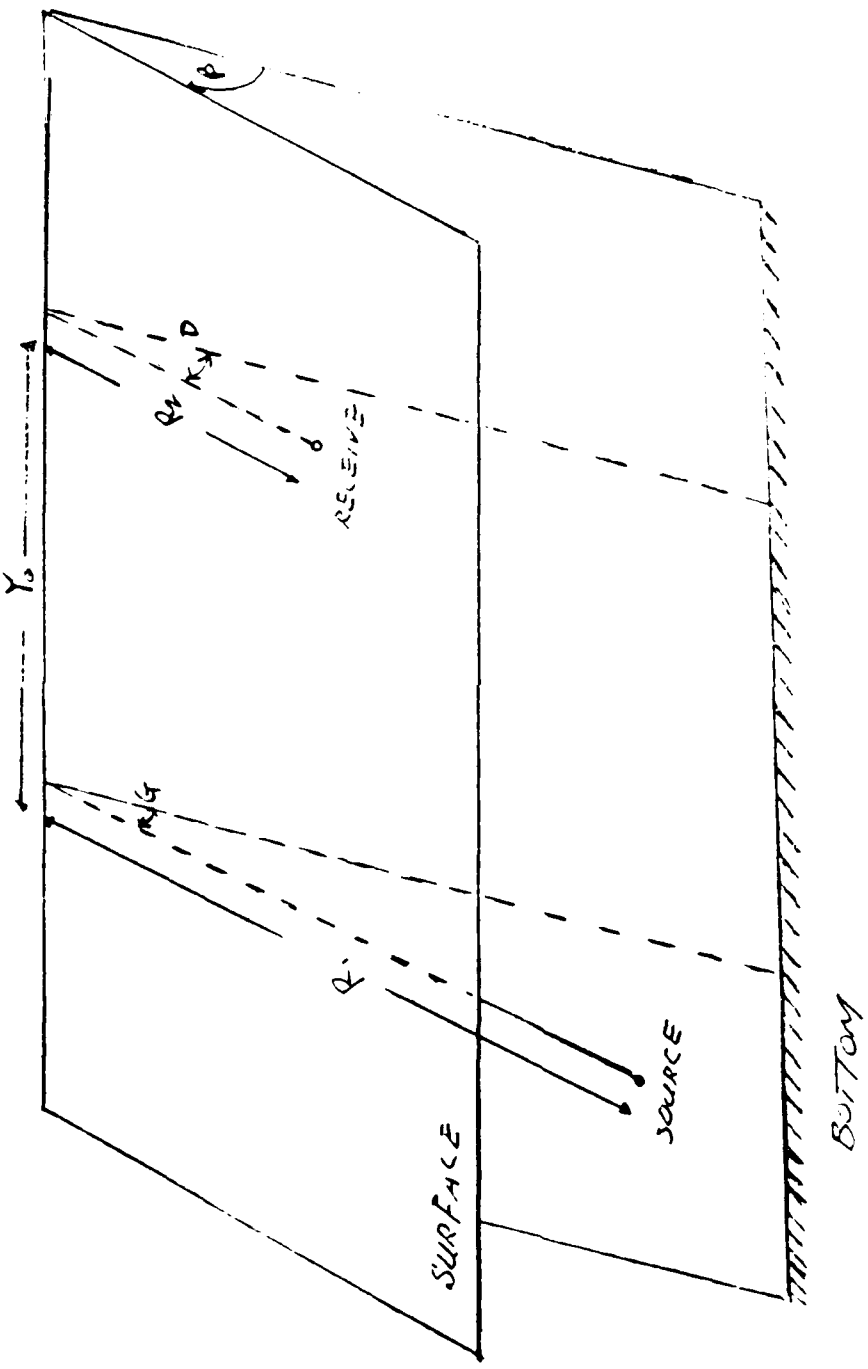

Figure 1

Three-Dimensional Wedge Geometry

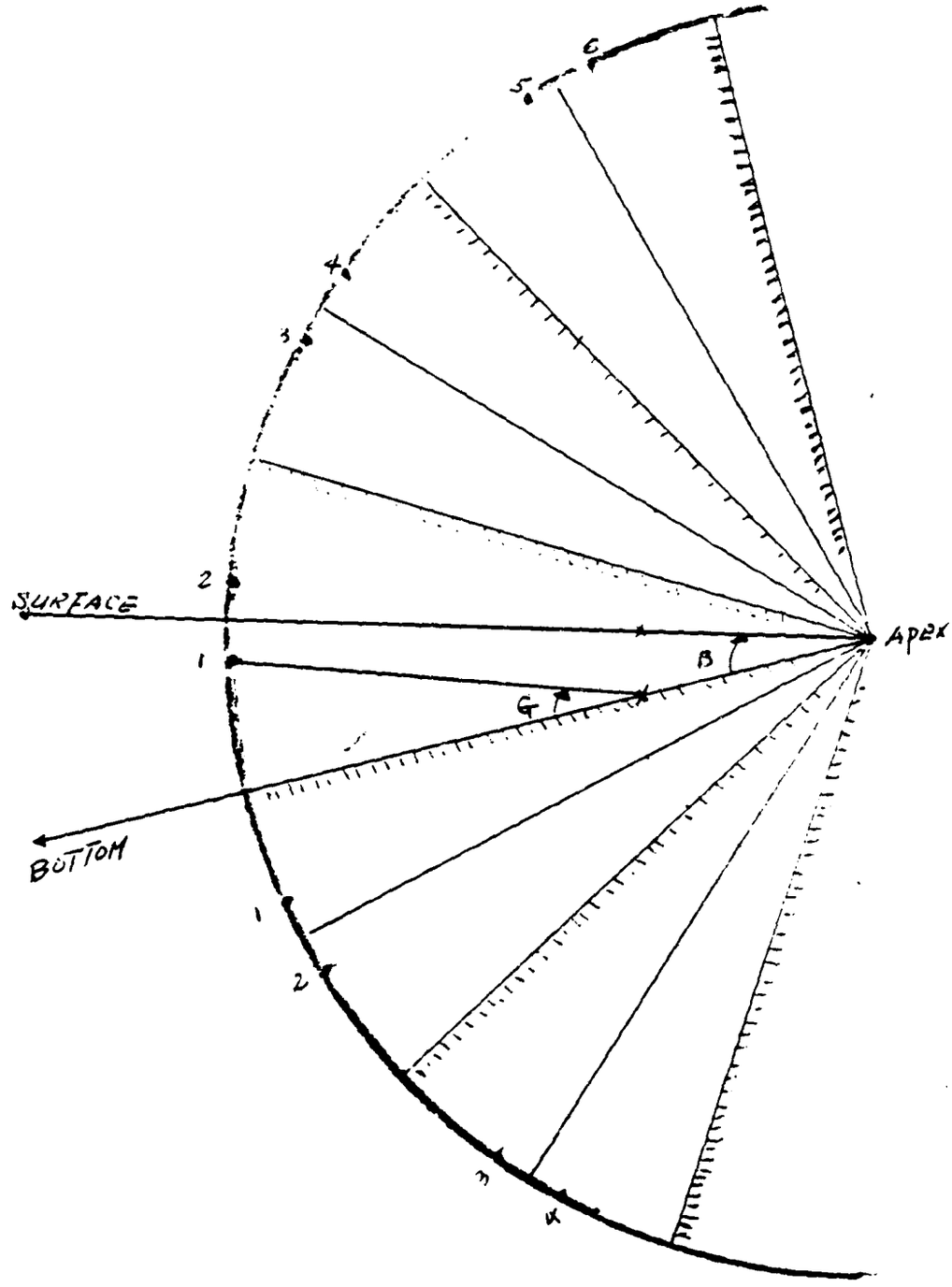

Figure 2

The Geometry of Image Solution

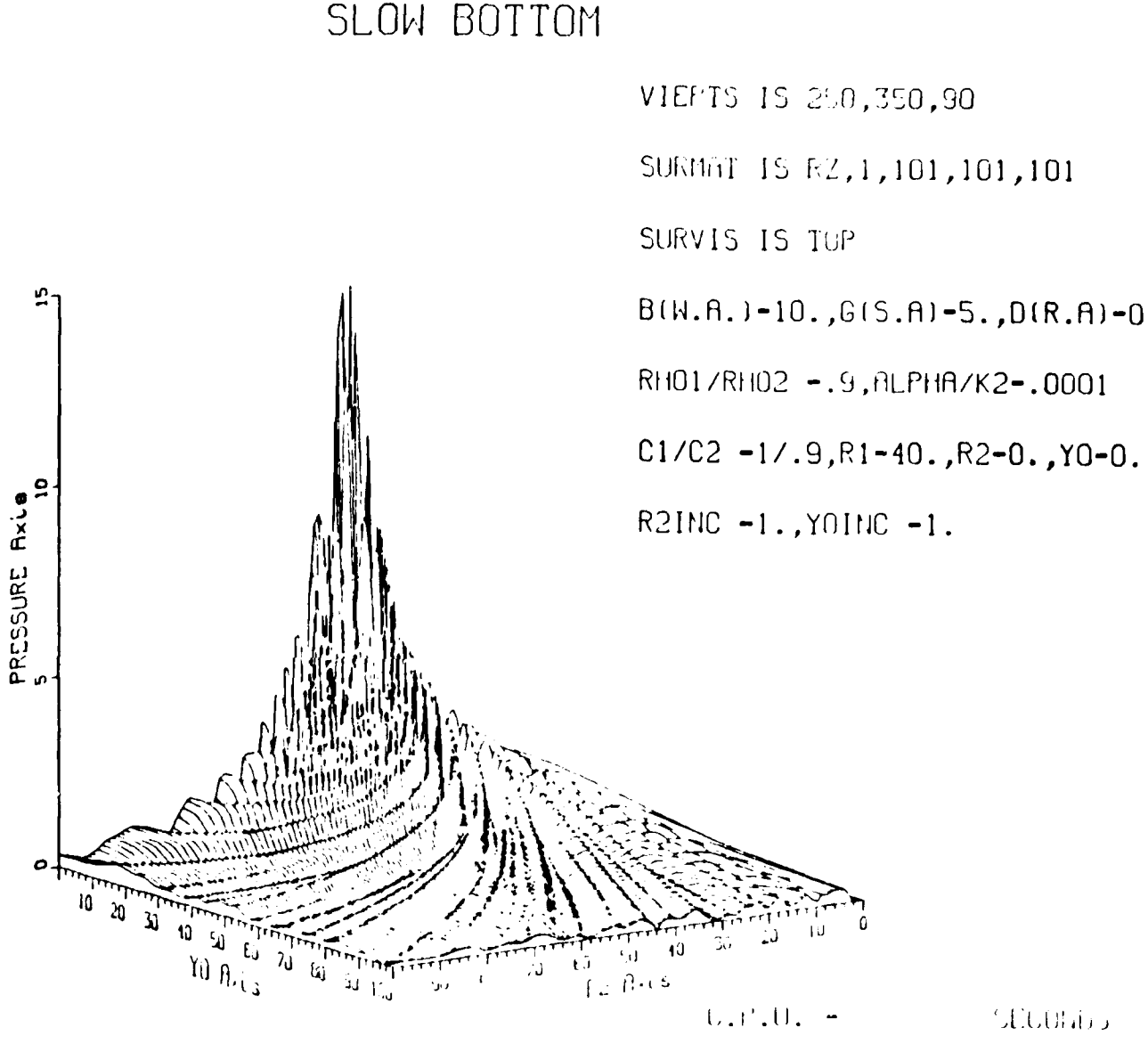

Figure 3-A

Pressure on the Bottom of the Wedge as Calculated by the Image Model for the Indicated Values of Parameters

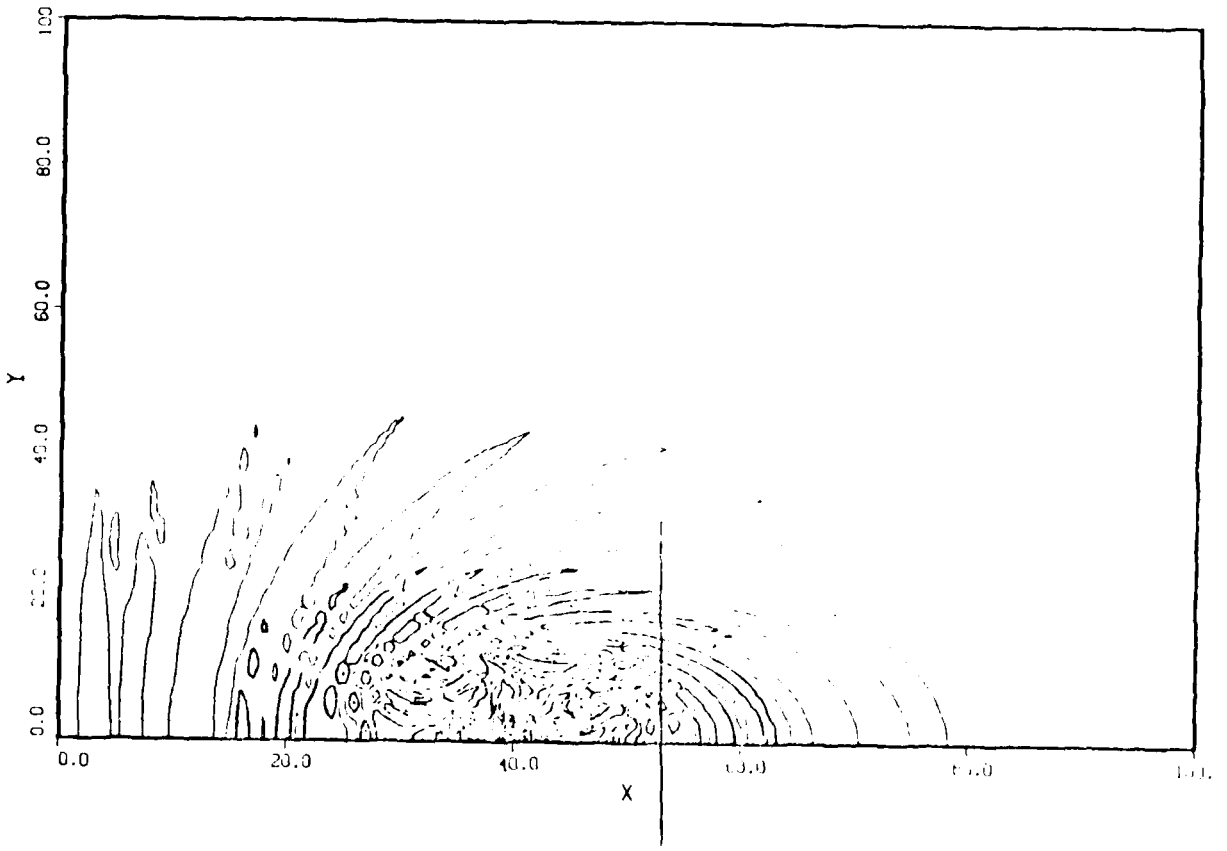

Figure 3-B

Equal-Pressure Contours on the Bottom of the Wedge for the Indicated Values of Parameters

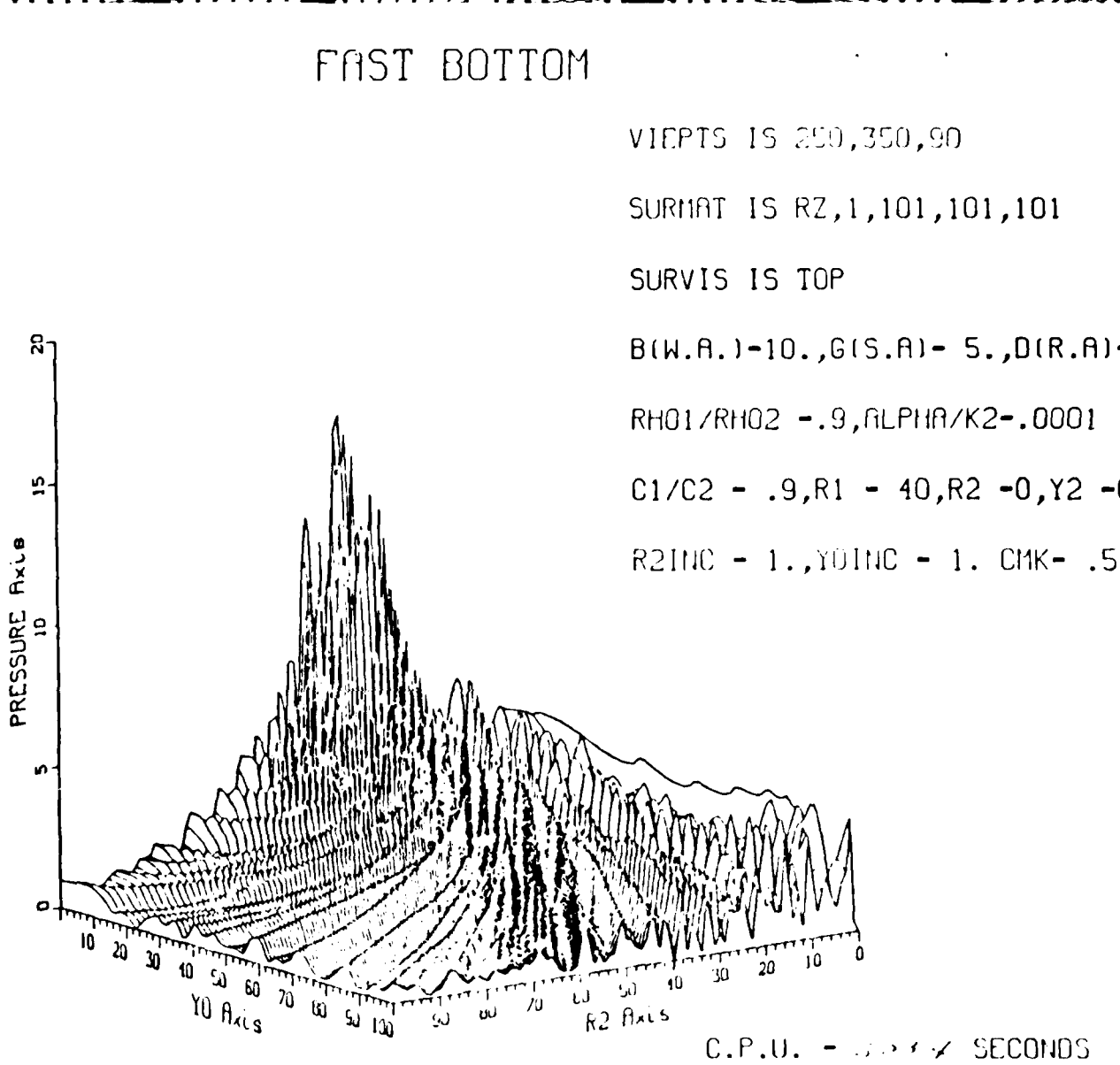

Figure 4-A

Pressure on the Bottom of the Wedge as Calculated by the Image Model for the Indicated Values of Parameters

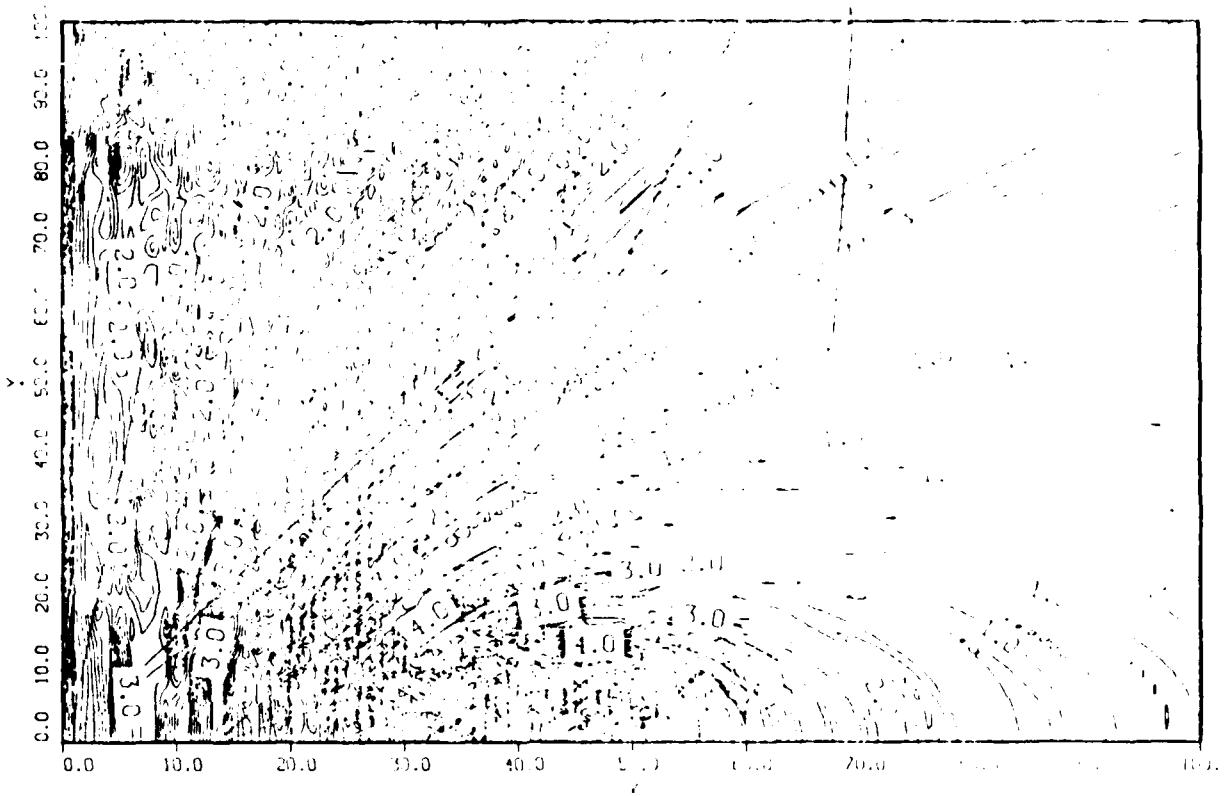

Figure 4-B

Equal-Pressure Contours on the Bottom of the Wedge for the Indicated Values of Parameters

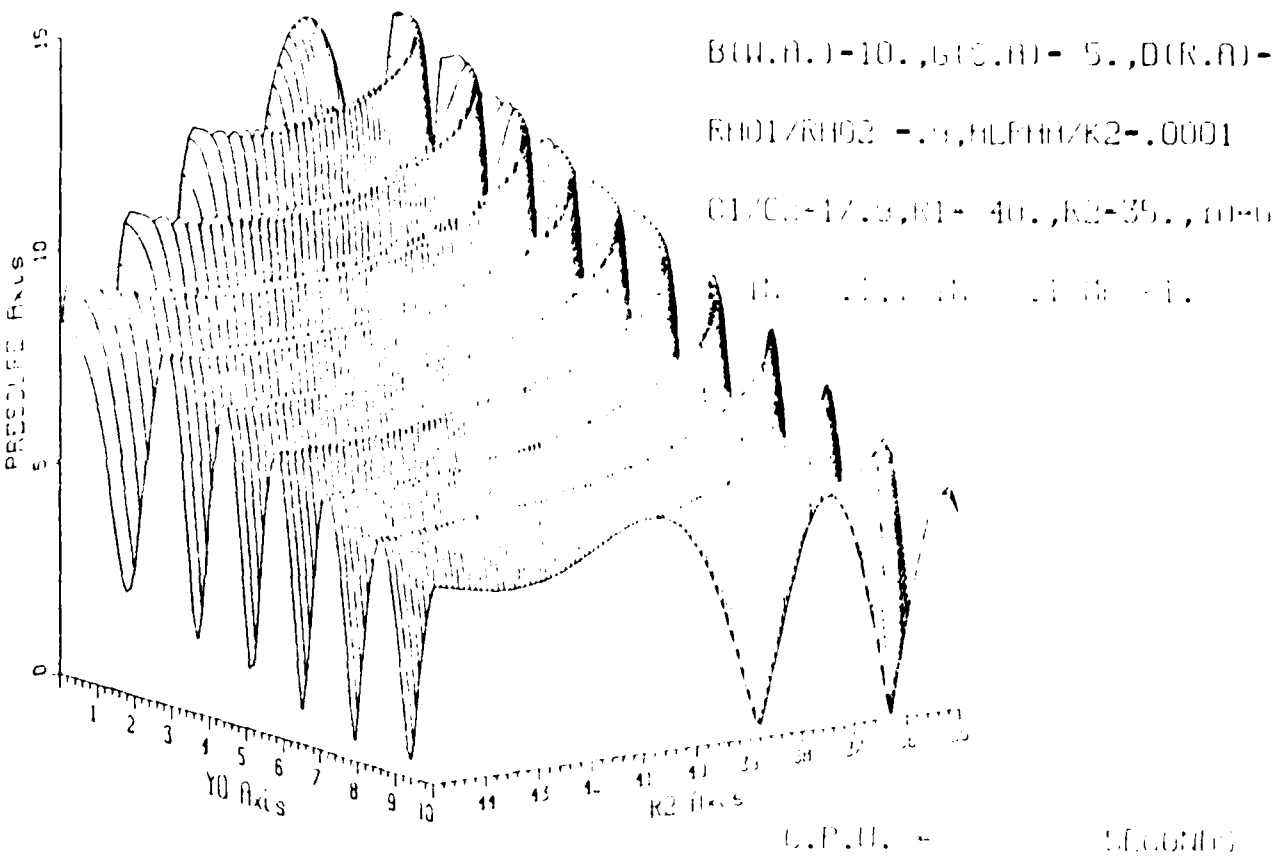

Figure 5-A

Pressure on the Bottom of the Wedge as Calculated by the Image Model for the Indicated Values of Parameters

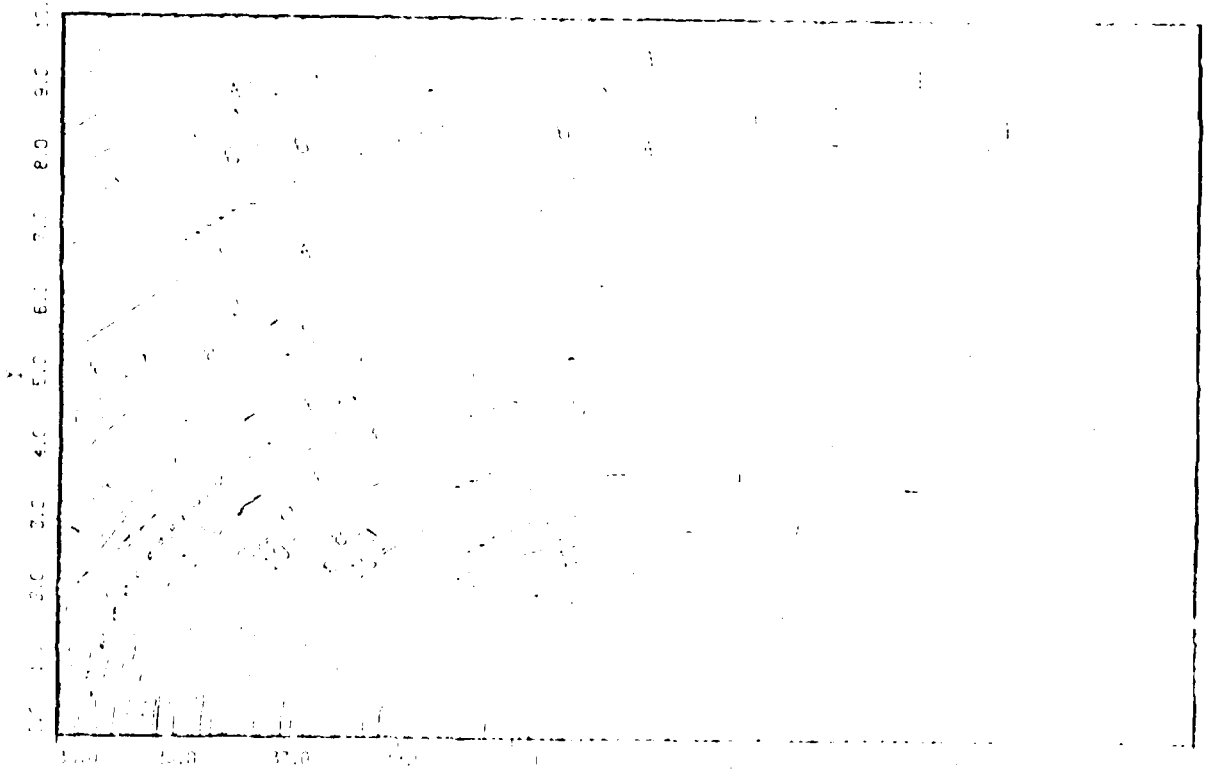

Figure 5 B

Equal-Pressure Contours on the Bottom of the Wedge for the Indicated Values of Parameters

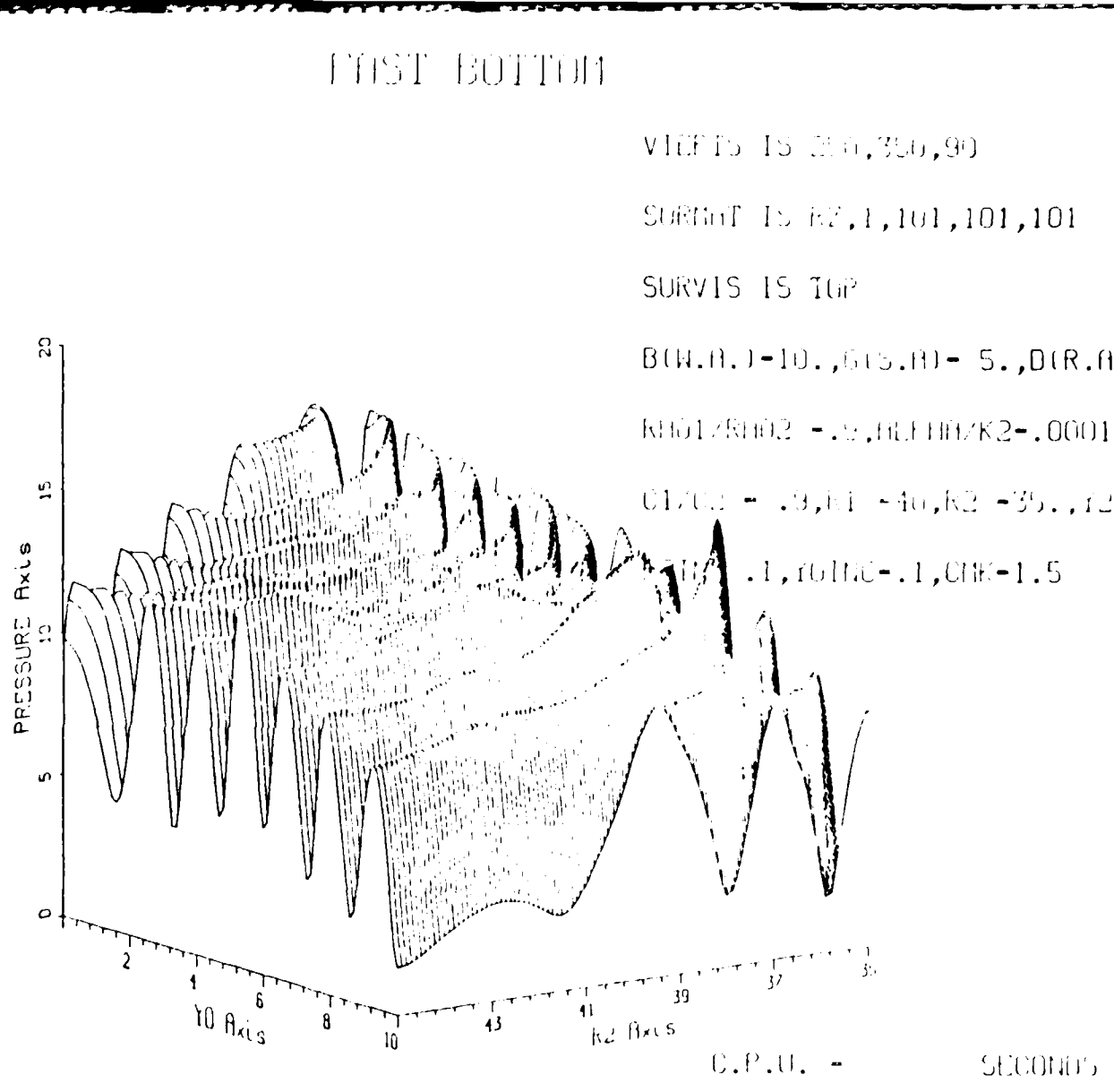

Figure 6-A

Pressure on the Bottom of the Wedge as Calculated by the Image Model for the Indicated Values of Parameters

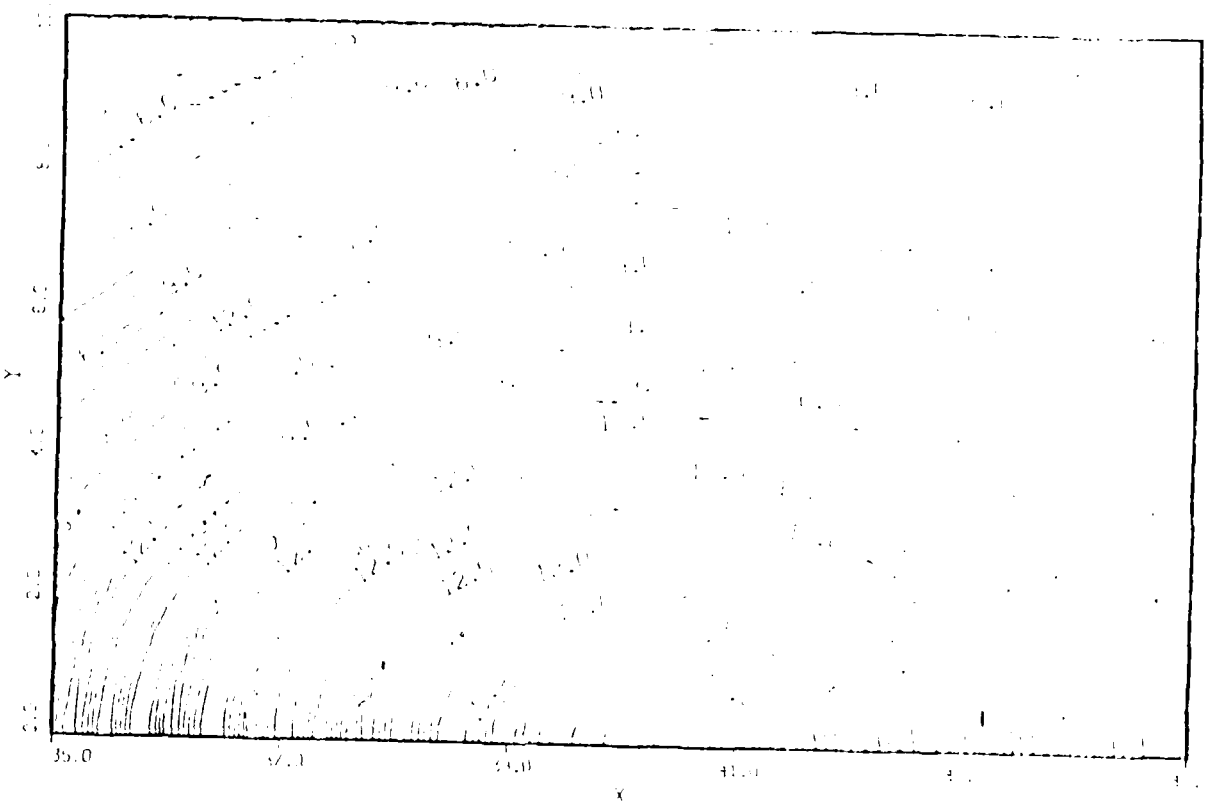

Figure 6-B

Equal-Pressure Contours on the Bottom of the Wedge for the Indicated Values of Parameters

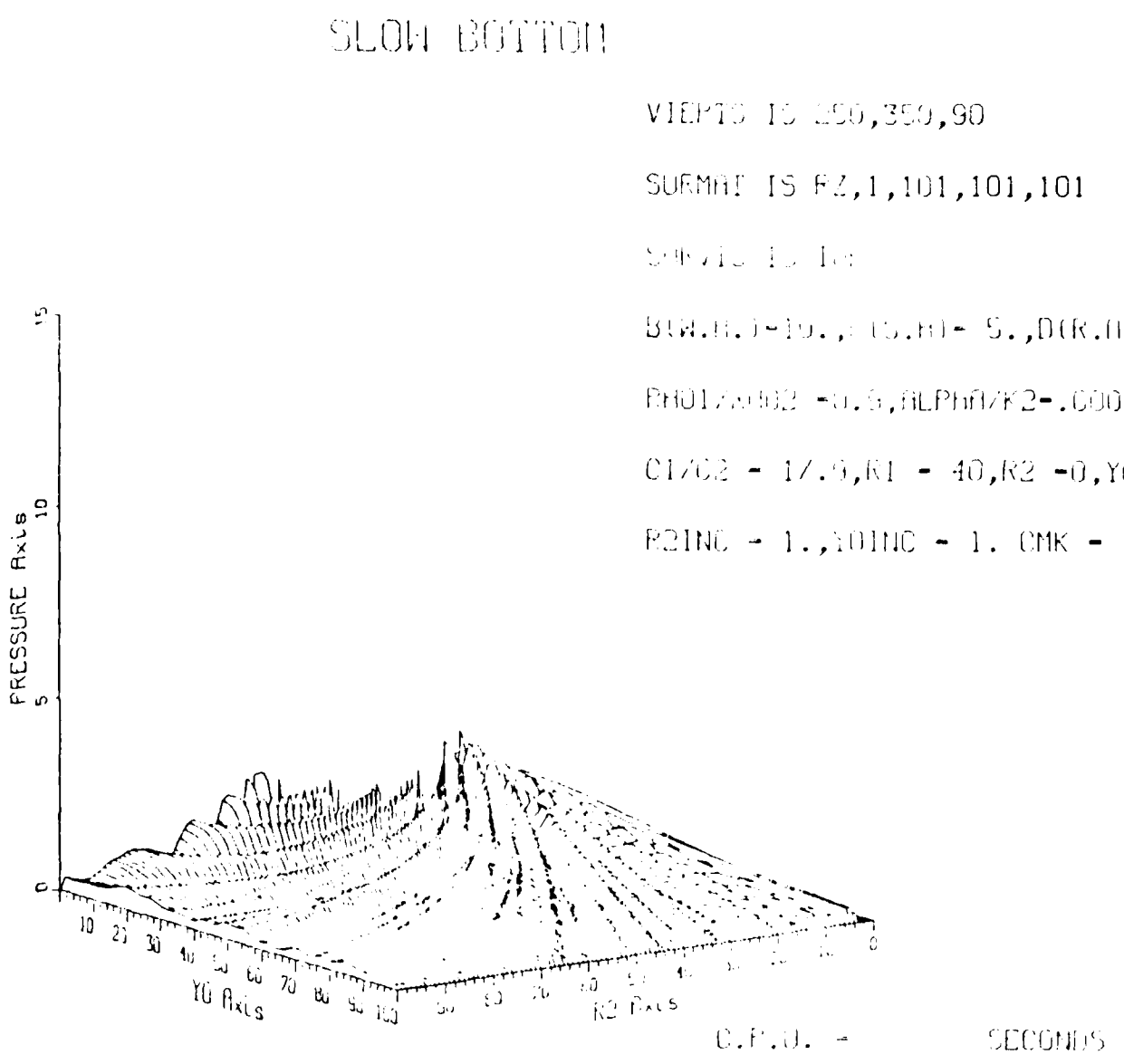

Figure 7-A

Pressure on the Bottom of the Wedge as Calculated by the Image Model for the Indicated Values of Parameters

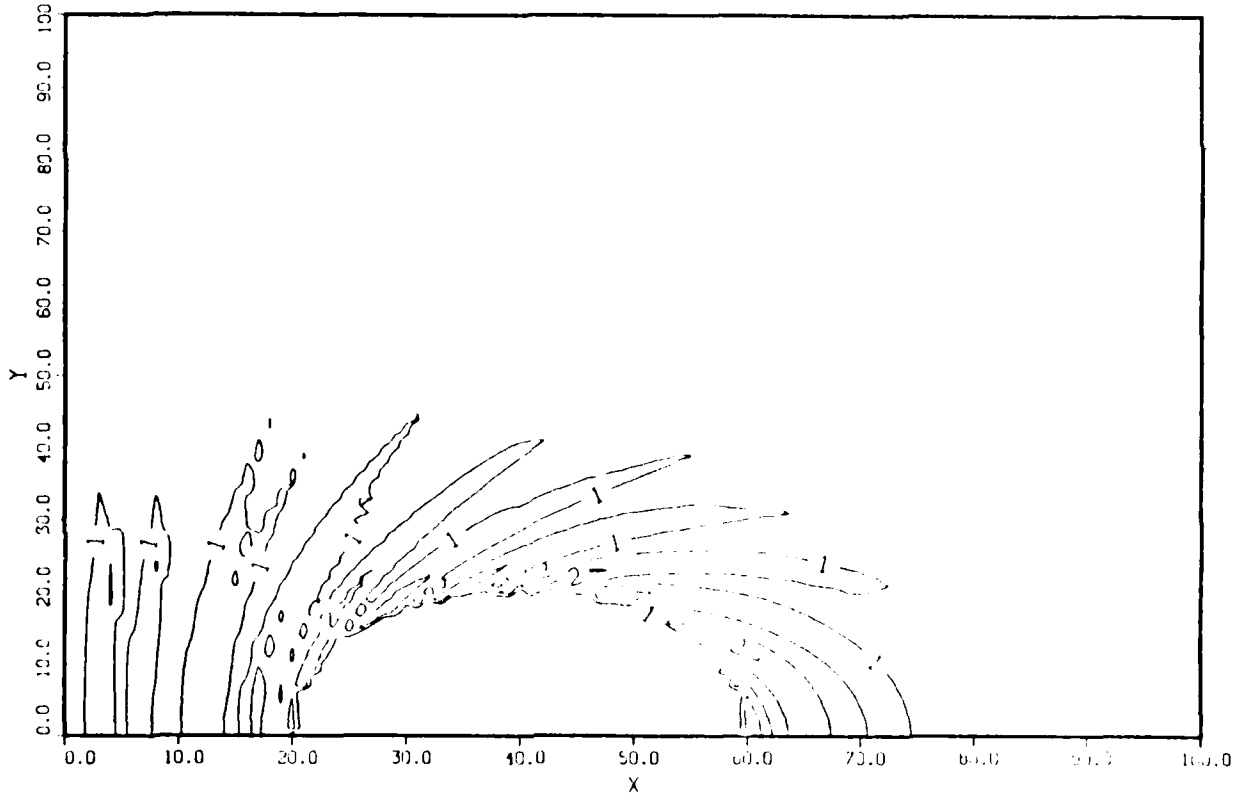

Figure 7-B

Equal-Pressure Contours on the Bottom of the Wedge for the Indicated Values of Parameters

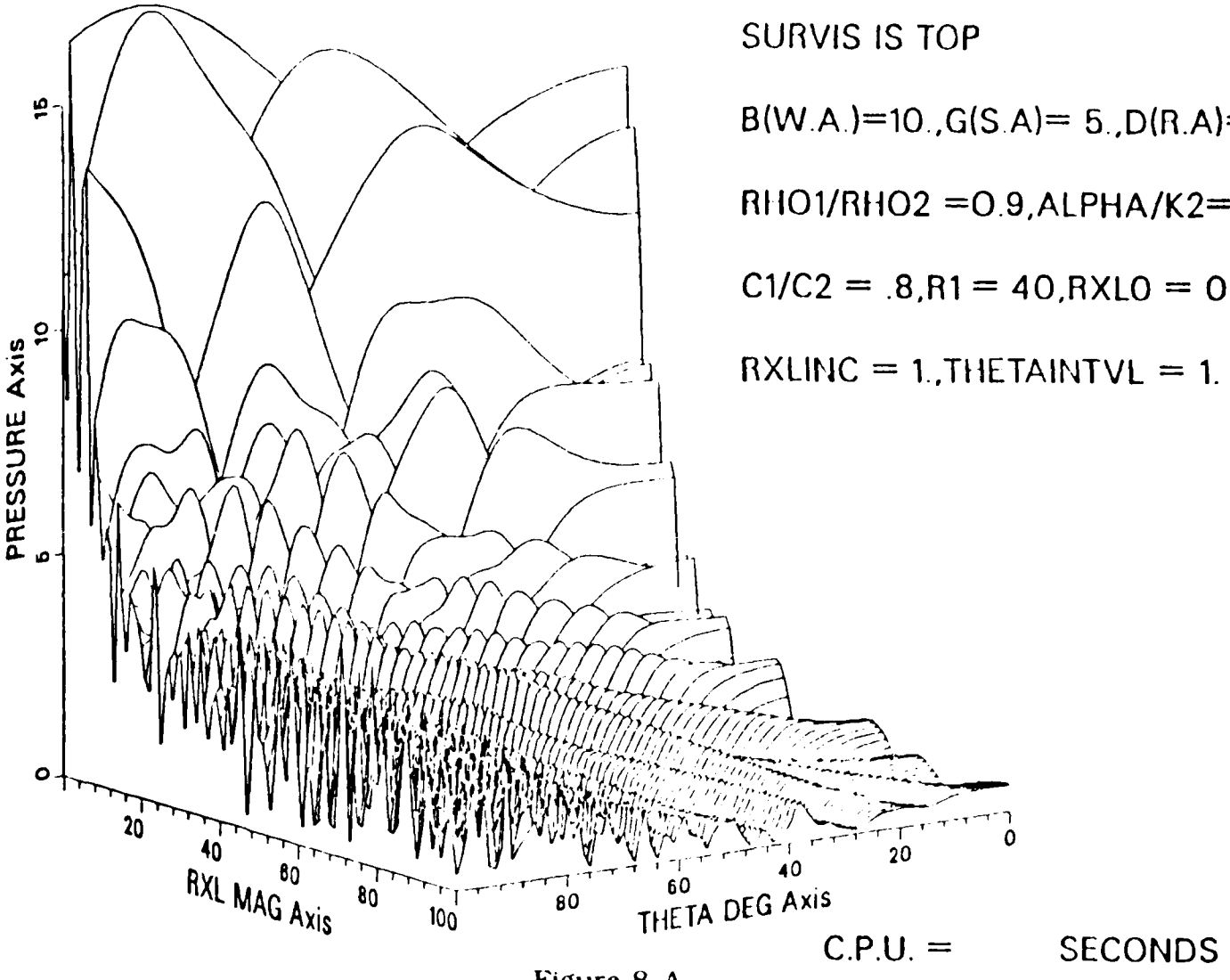

Figure 8-A

Pressure on the Bottom of the Wedge as Calculated by the Image Model for the Indicated Values of Parameters

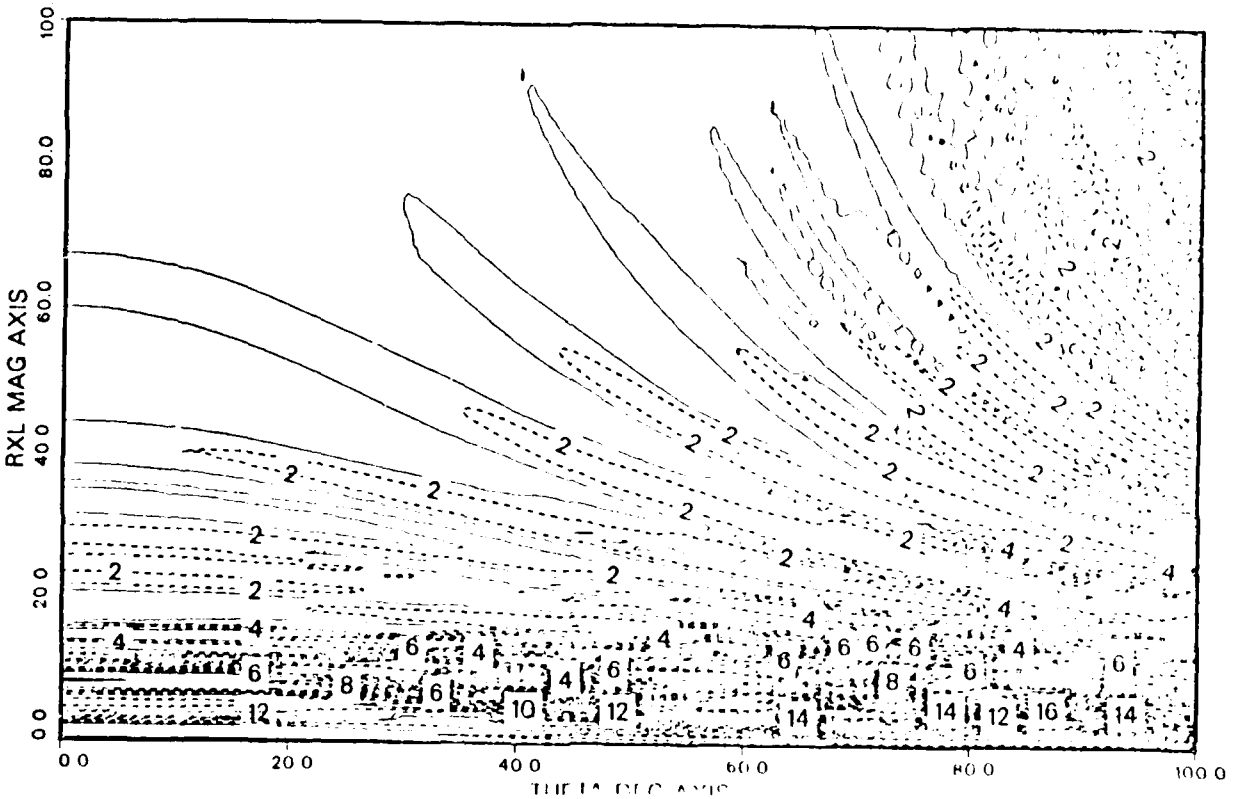

Figure 8-B

Equal-Pressure Contours on the Bottom of the Wedge for the Indicated Values of Parameters

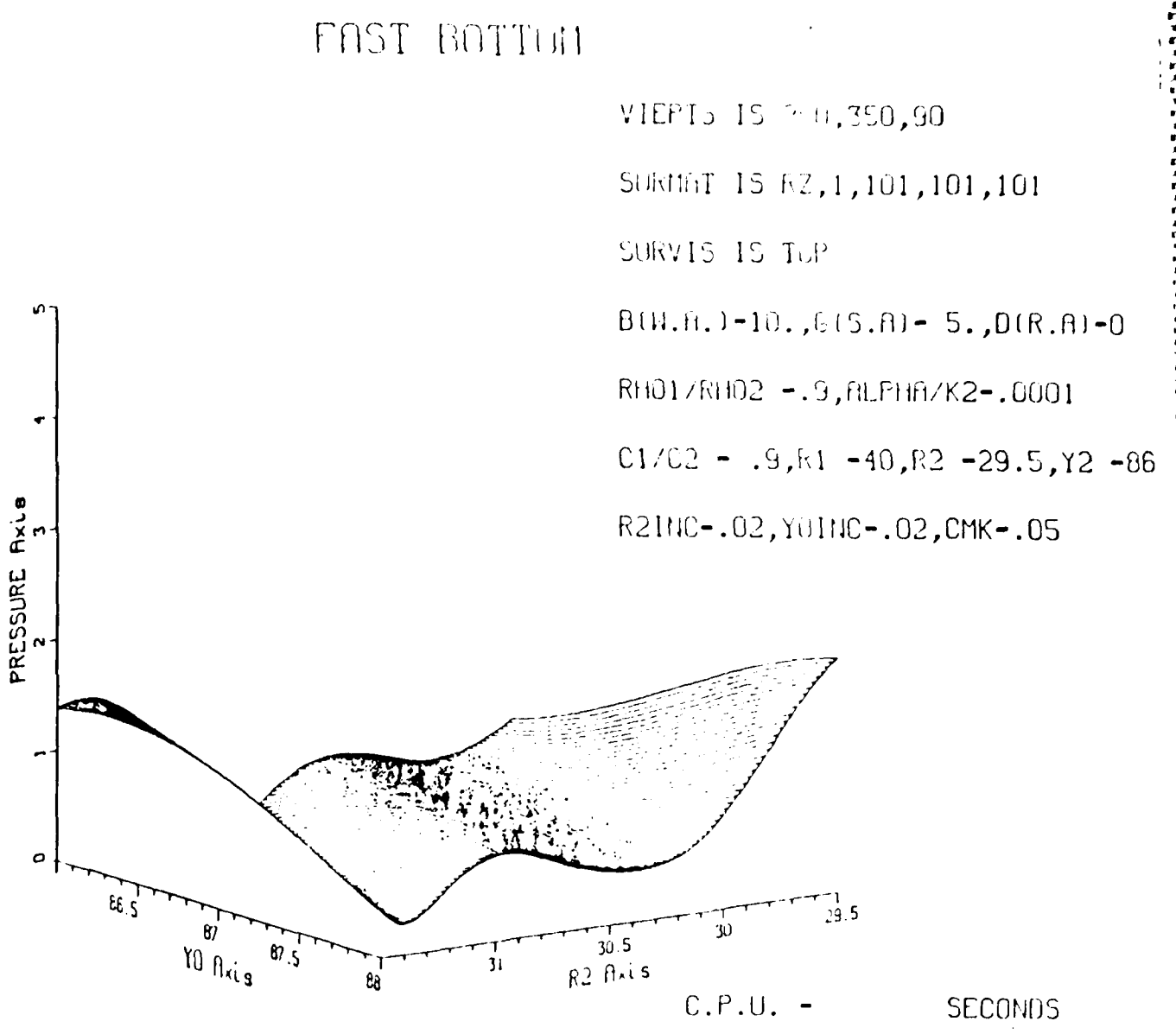

Figure 9-A

Pressure on the Bottom of the Wedge as Calculated by the Image Model for the Indicated Values of Parameters

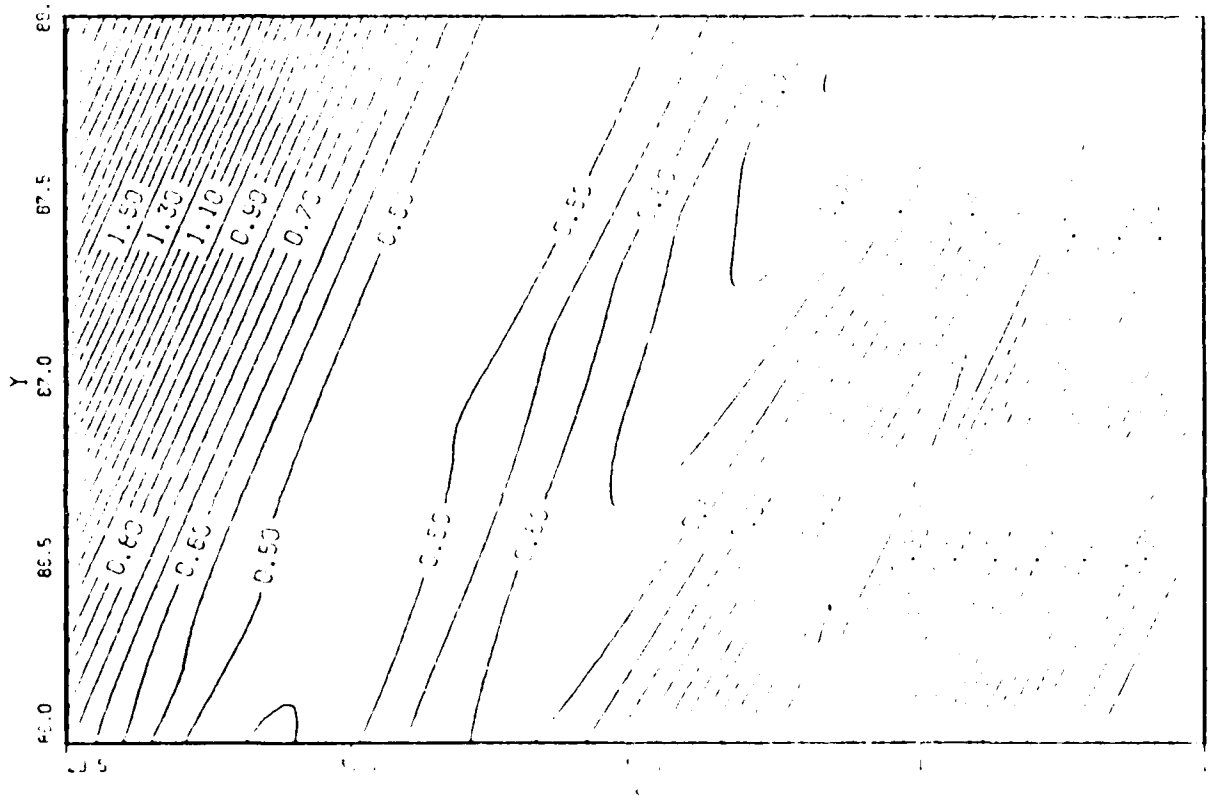

Figure 9.13

Equal-Pressure Contours on the Bottom of the Wedge for the Indicated Values of Parameters

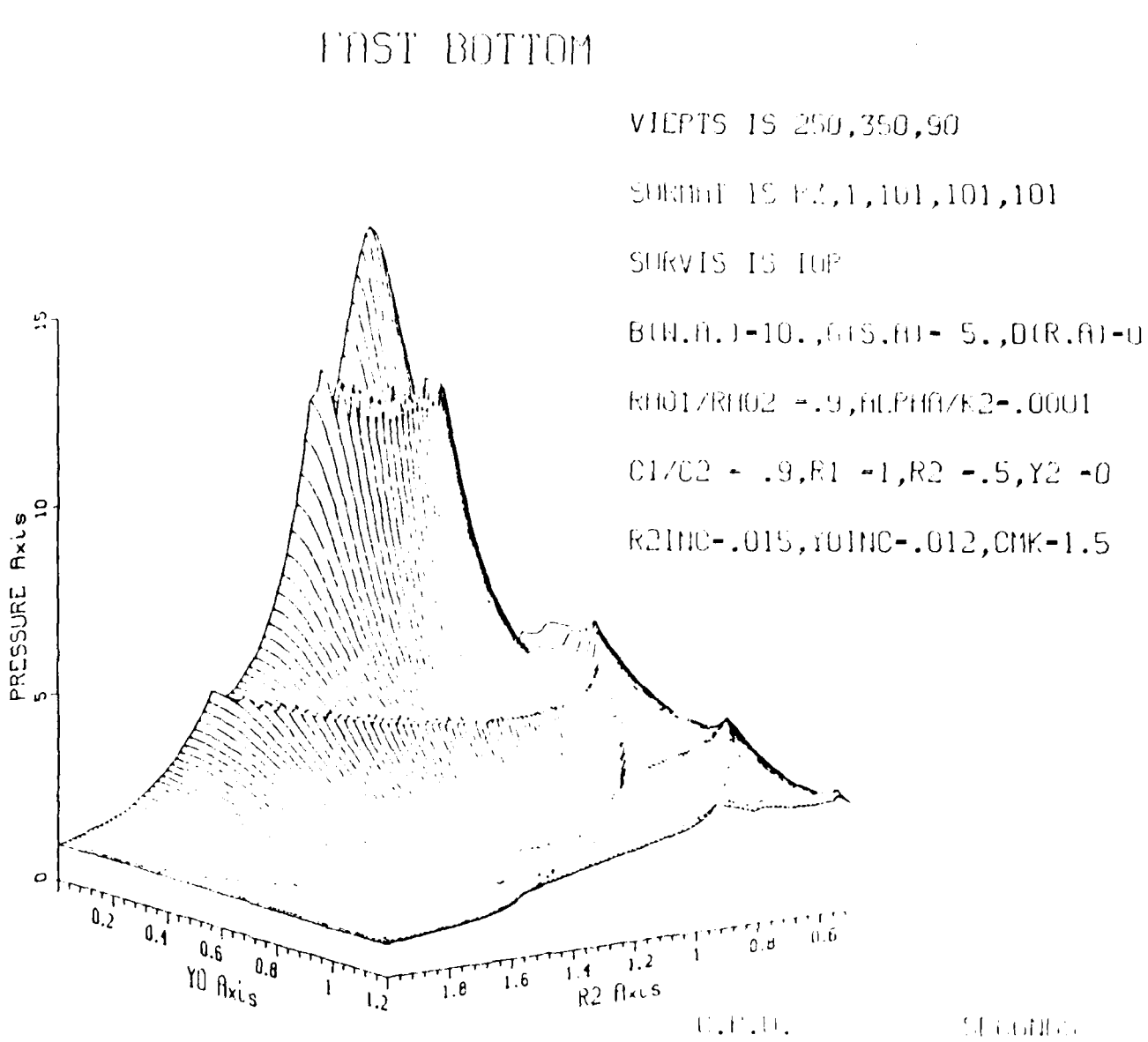

Figure 10-A

Pressure on the Bottom of the Wedge as Calculated by the Image Model for the Indicated Values of Parameters

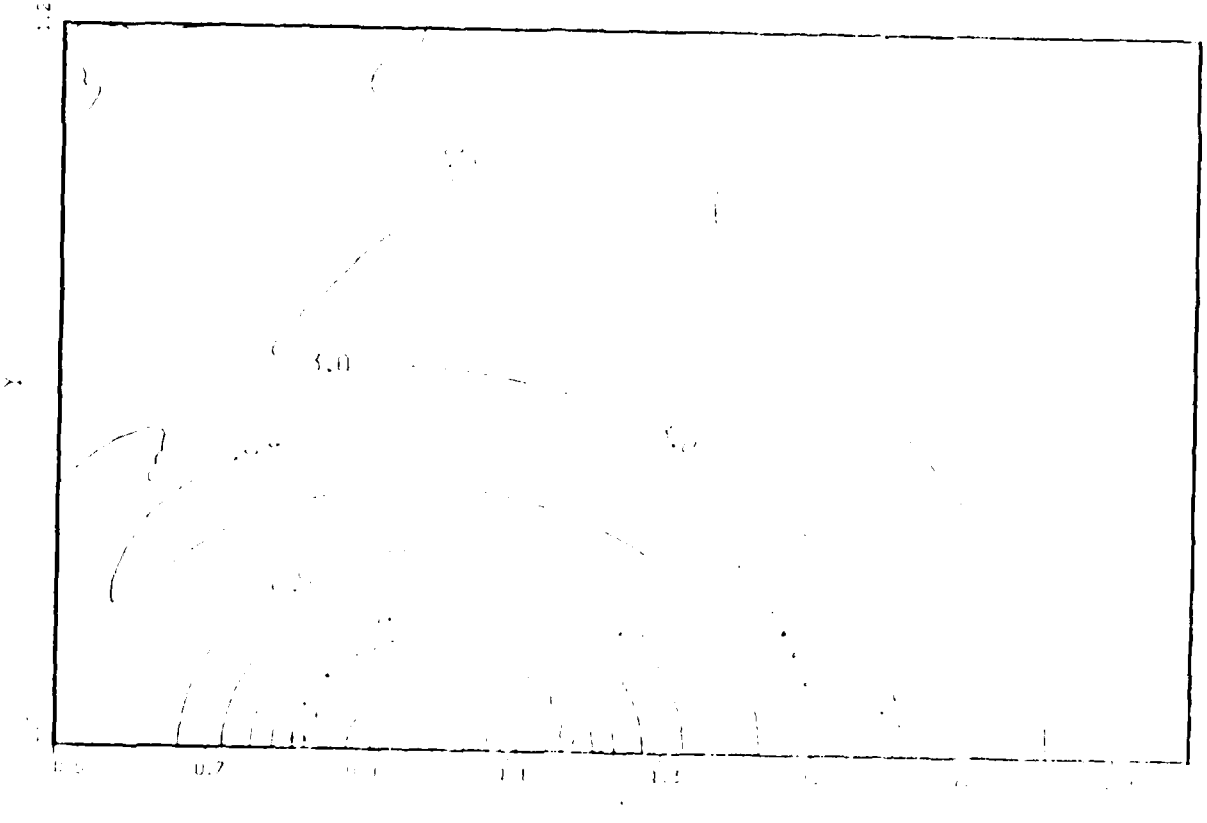

Figure 10-B

Equal-Pressure Contours on the Bottom of the Wedge for the Indicated Values of Parameters

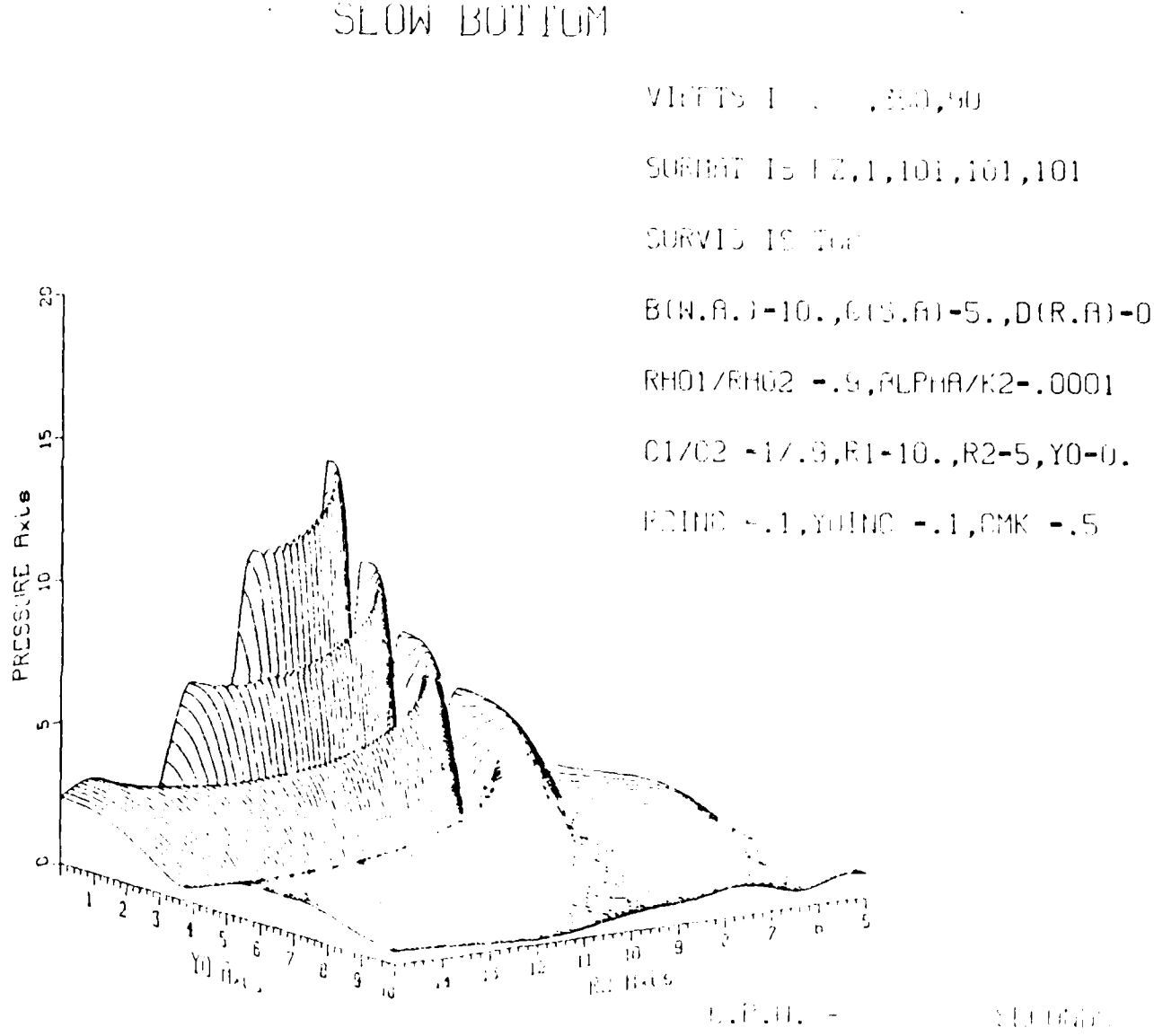

Figure 11-A

Pressure on the Bottom of the Wedge as Calculated by the Image Model for the Indicated Values of Parameters

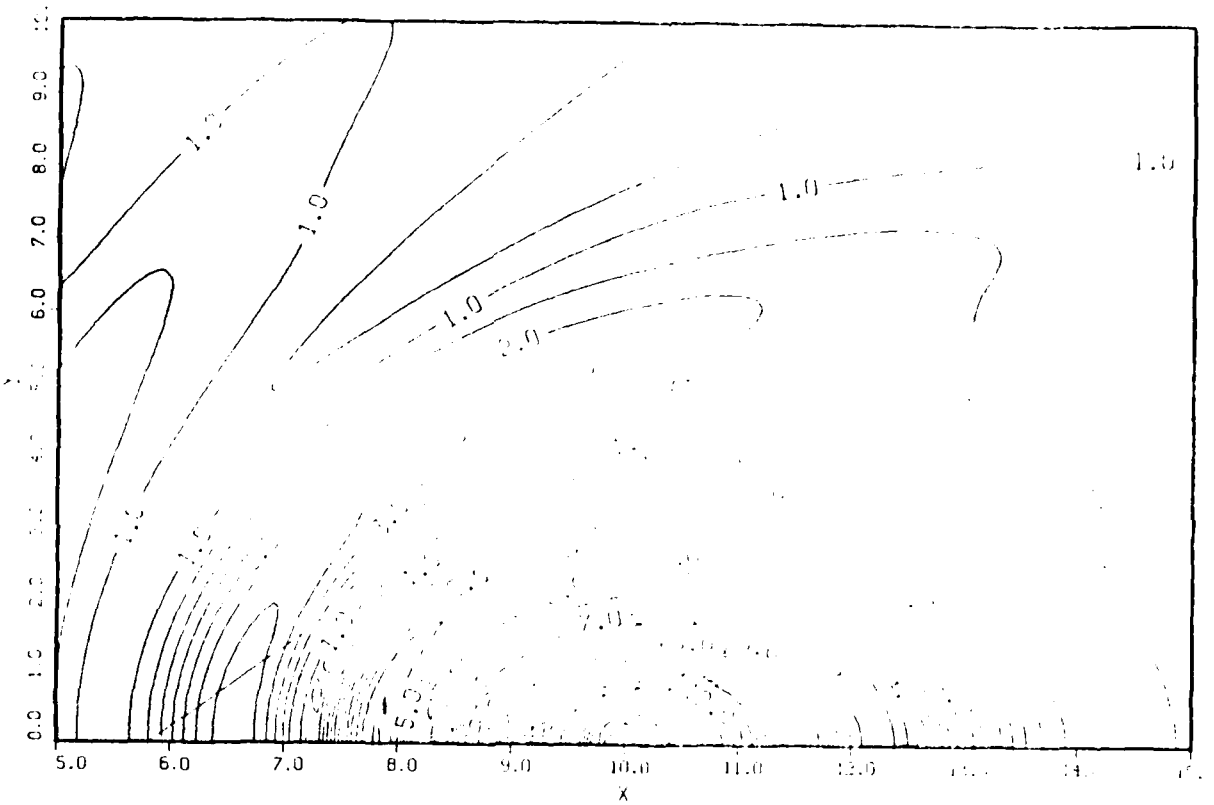

Figure 11-B

Equal-Pressure Contours on the Bottom of the Wedge for the Indicated Values of Parameters

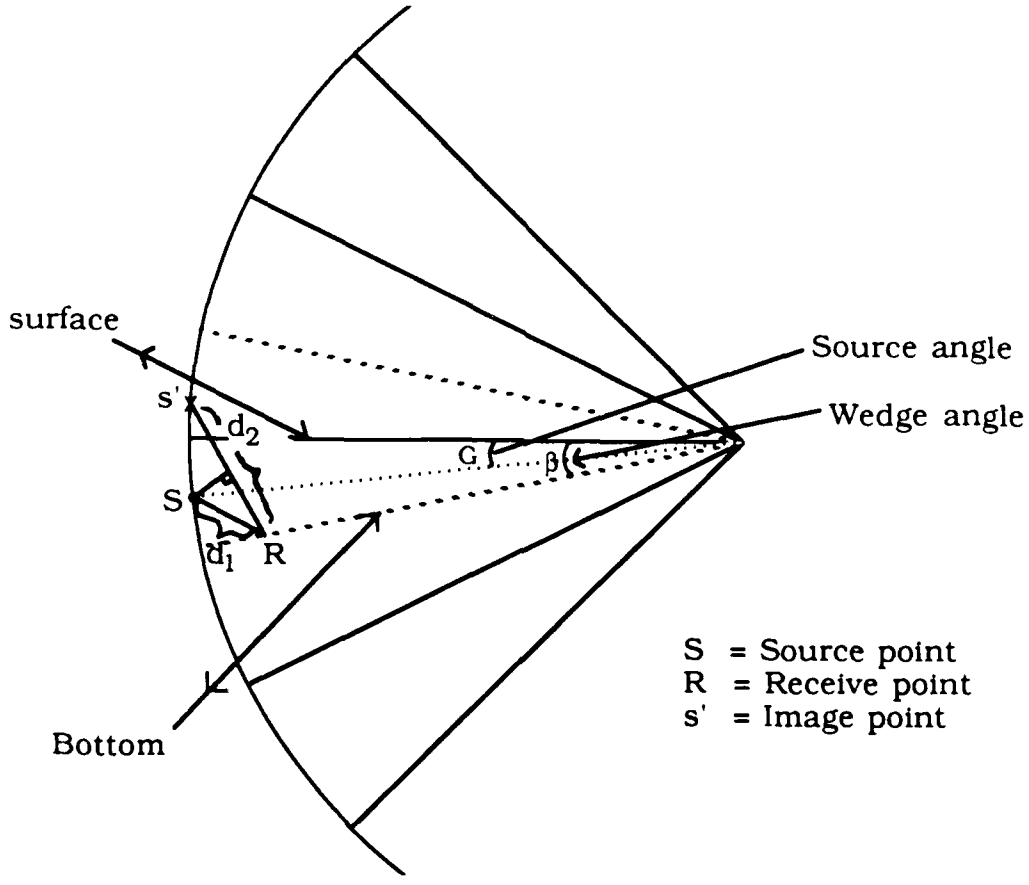

Figure 12

Interference Pattern from a Point Source and an Image Point

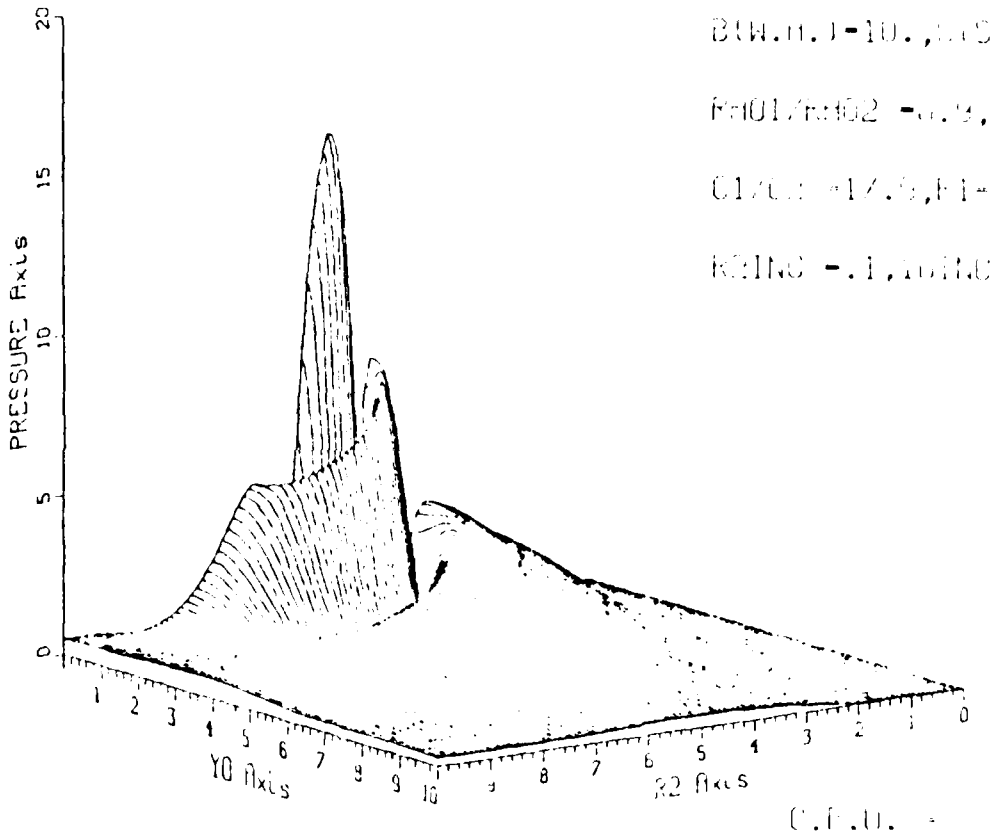

Figure 13 A

Pressure on the Bottom of the Wedge as Calculated by the Image Model for the Indicated Values of Parameters

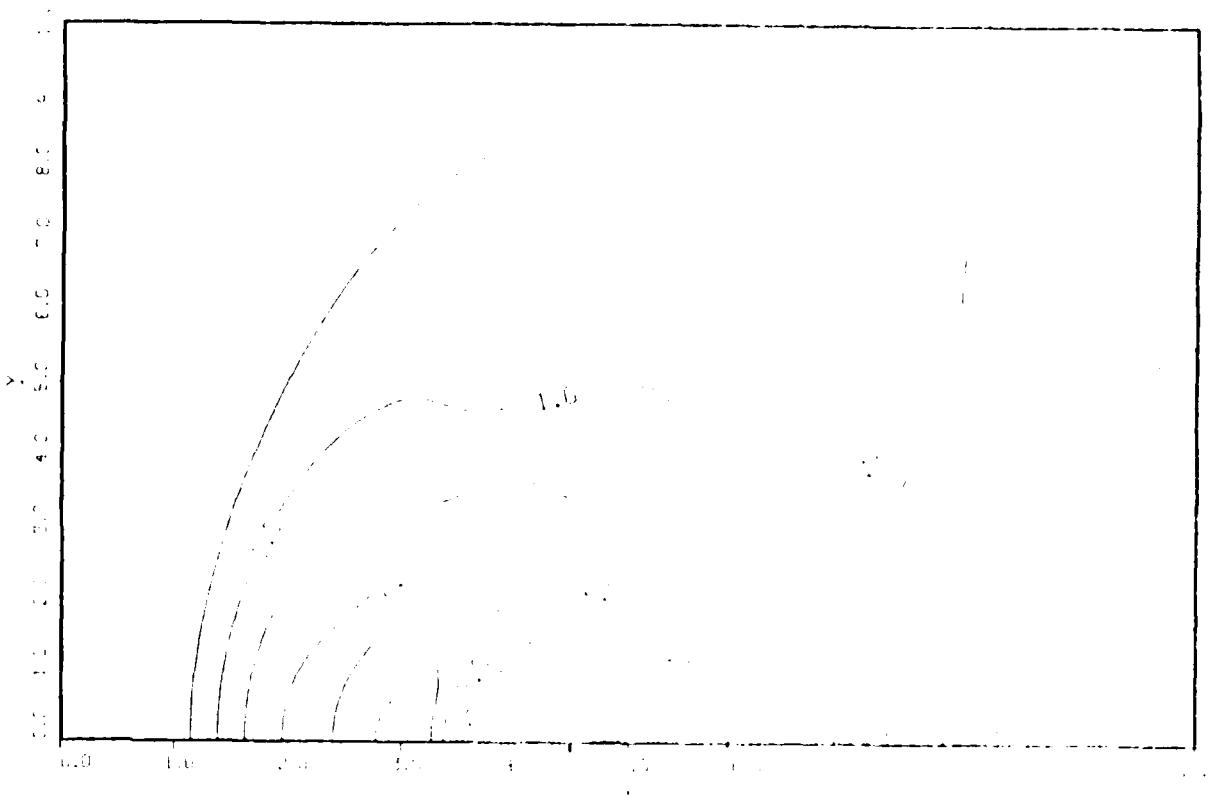

Figure 13-B

Equal-Pressure Contours on the Bottom of the Wedge for the Indicated Values of Parameters

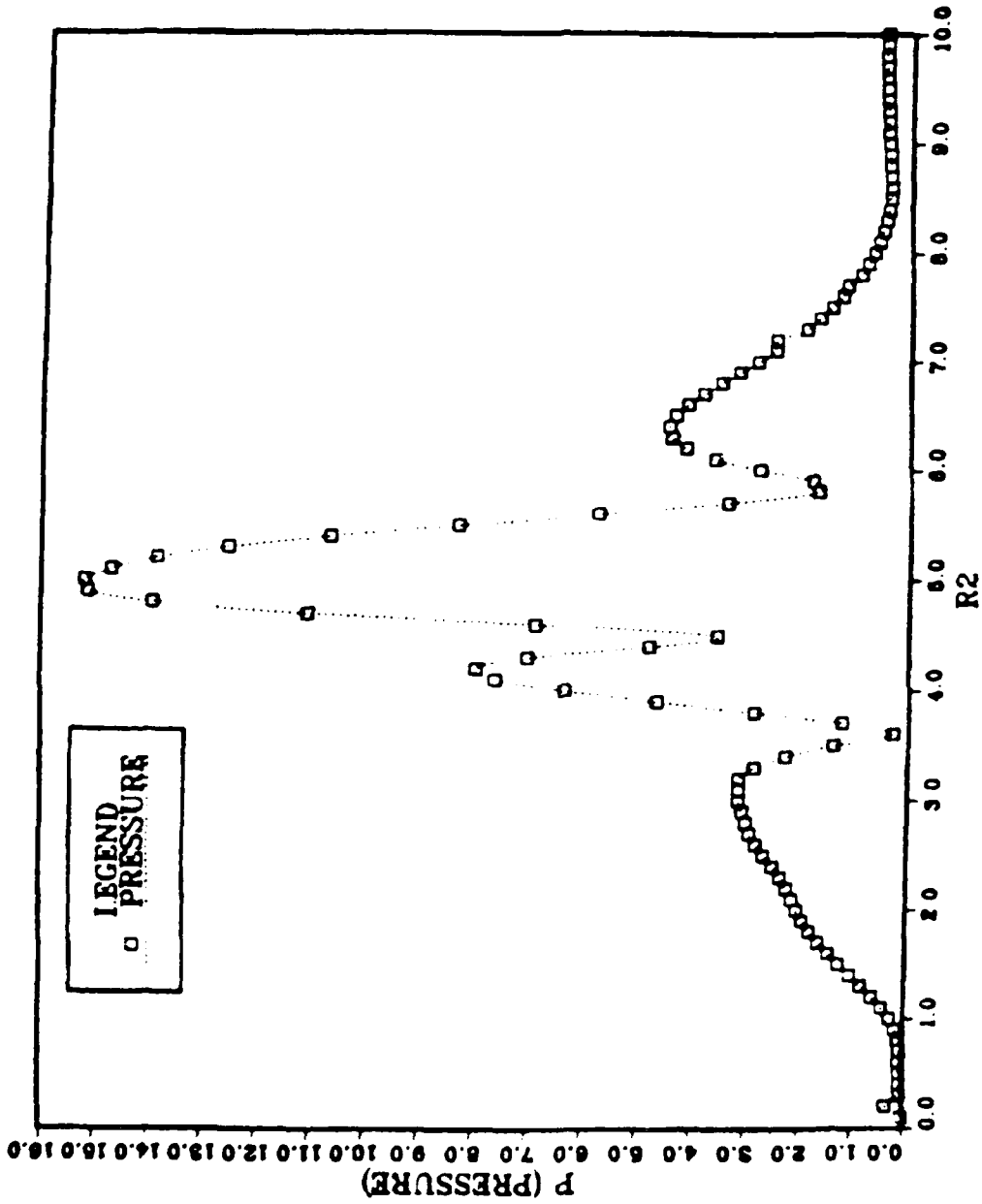

Figure 13-C

Pressure on Axis Response of Wedge

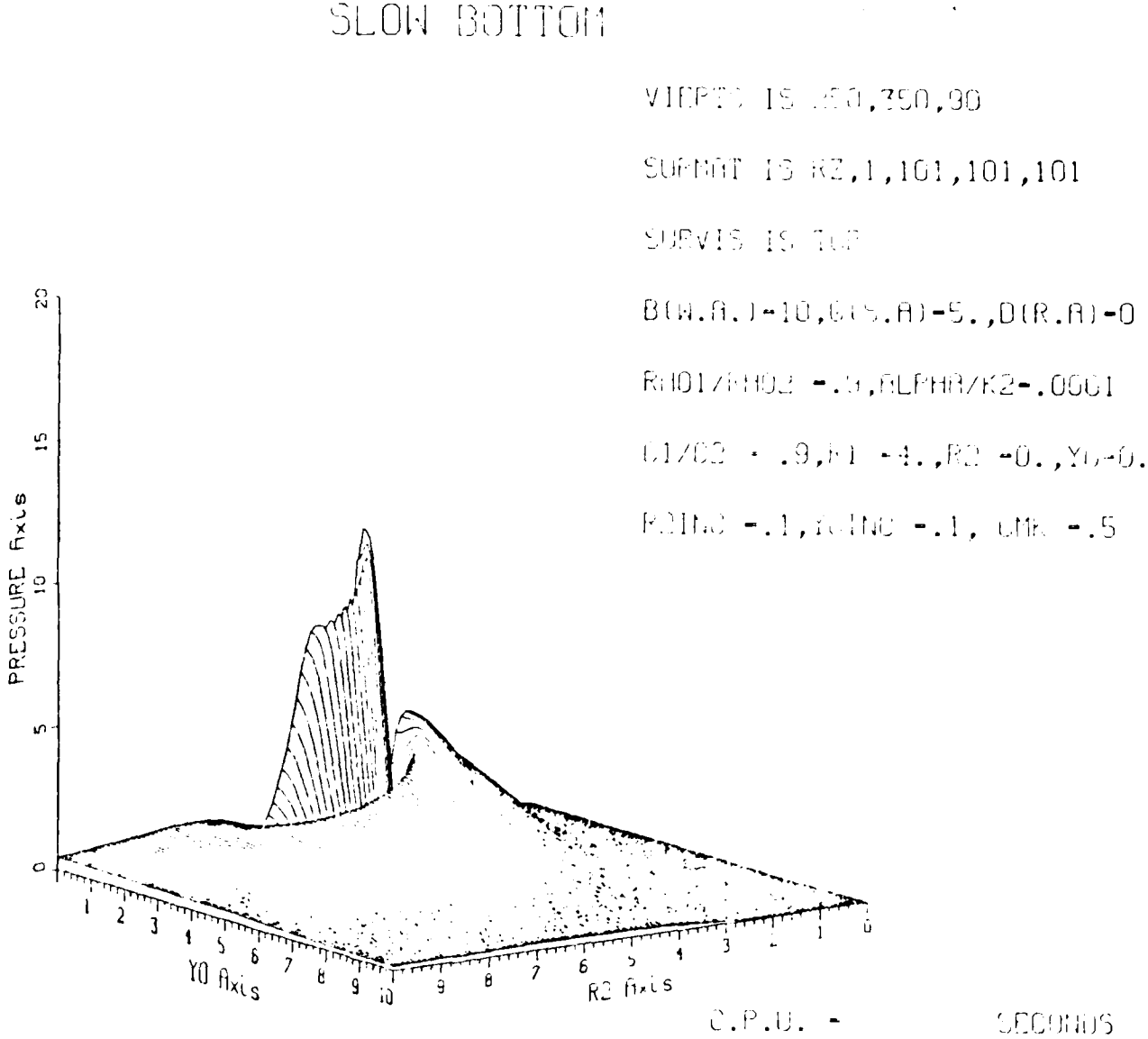

Figure 14-A

Pressure on the Bottom of the Wedge as Calculated by the Image Model for the Indicated Values of Parameters

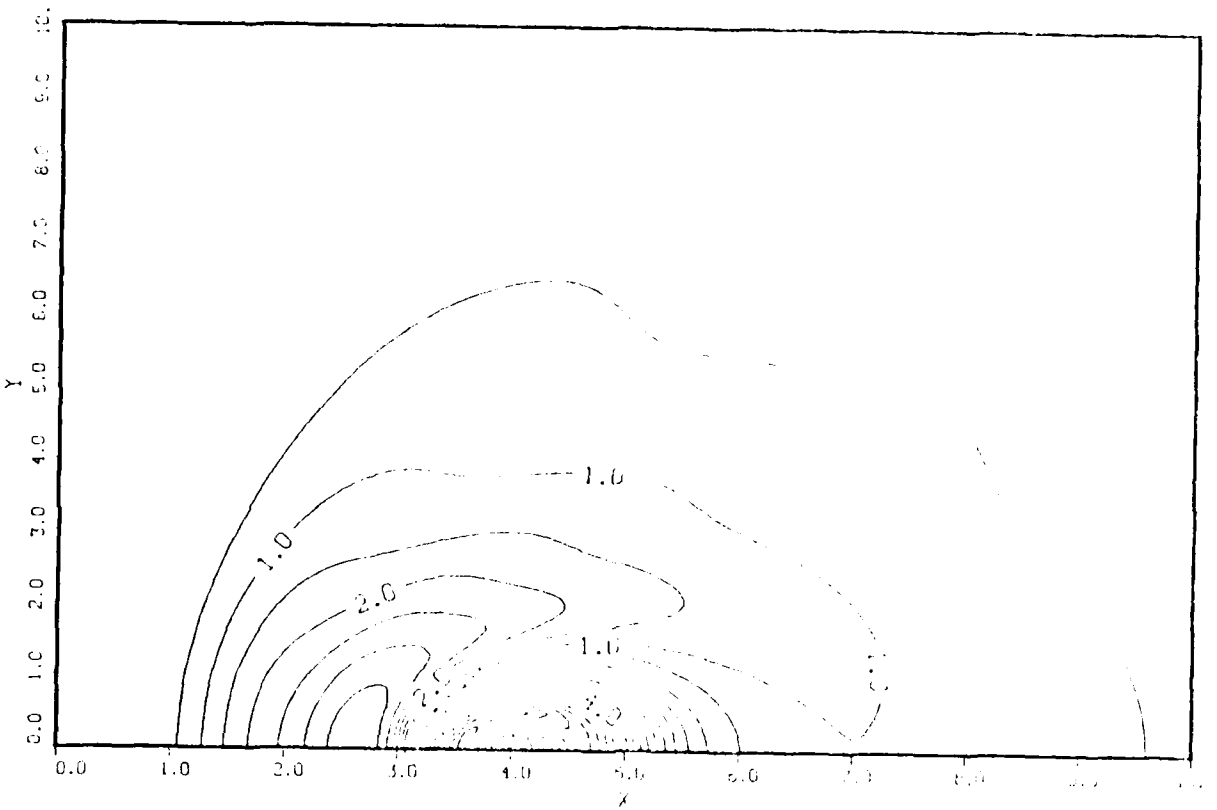

Figure 14-B

Equal-Pressure Contours on the Bottom of the Wedge for the Indicated Values of Parameters

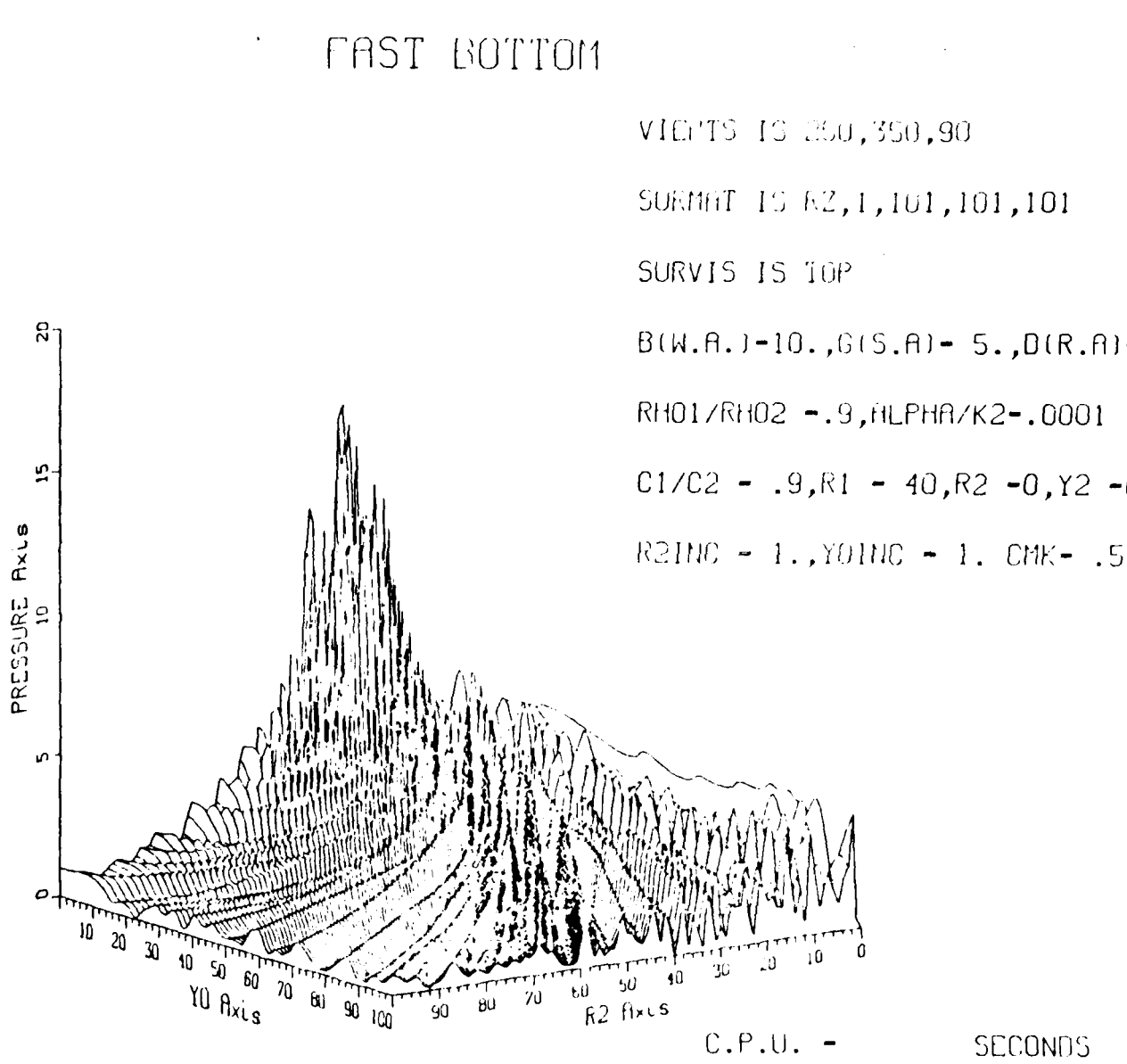

Figure 15-A

Pressure on the Bottom of the Wedge as Calculated by the Image Model for the Indicated Values of Parameters

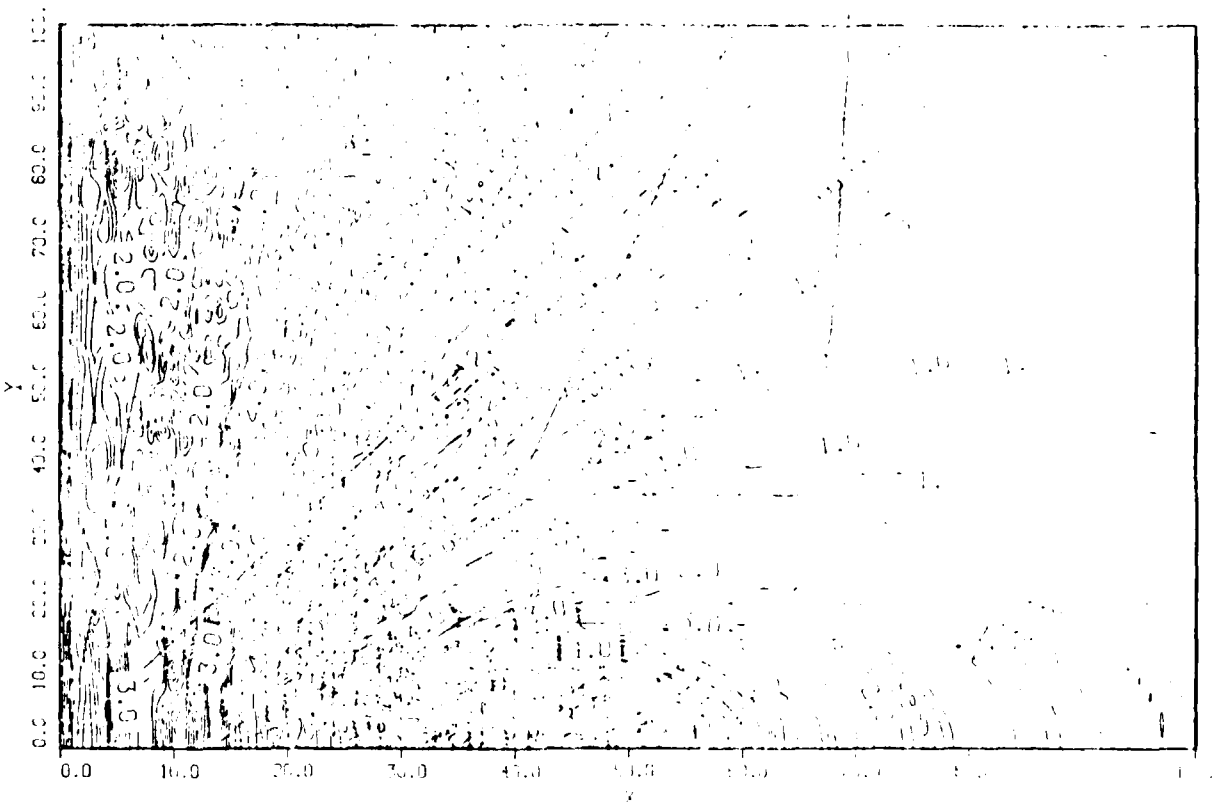

Figure 15-B

Equal-Pressure Contours on the Bottom of the Wedge for the Indicated Values of Parameters

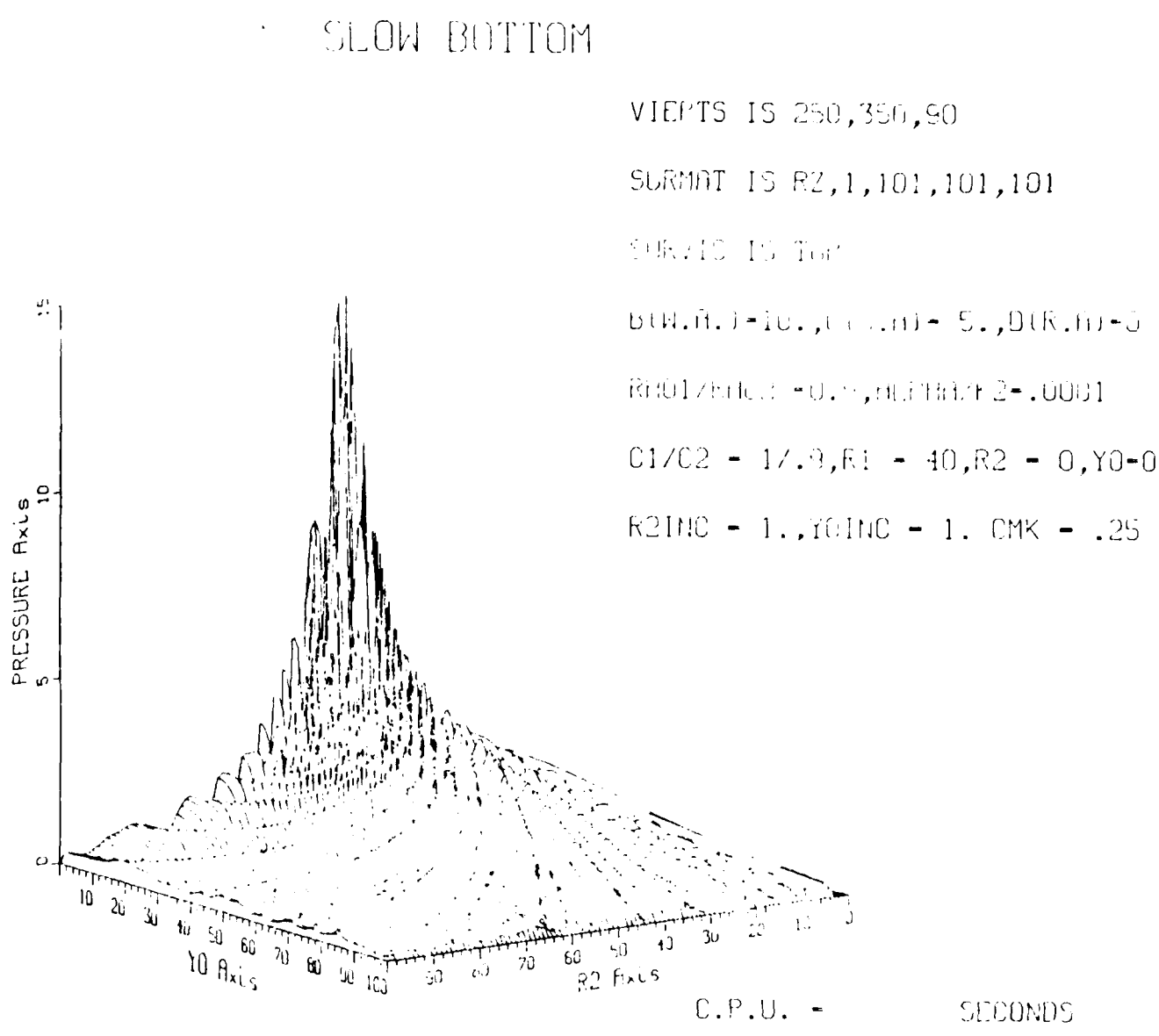

Figure 16-A

Pressure on the Bottom of the Wedge as Calculated by the Image Model for the Indicated Values of Parameters

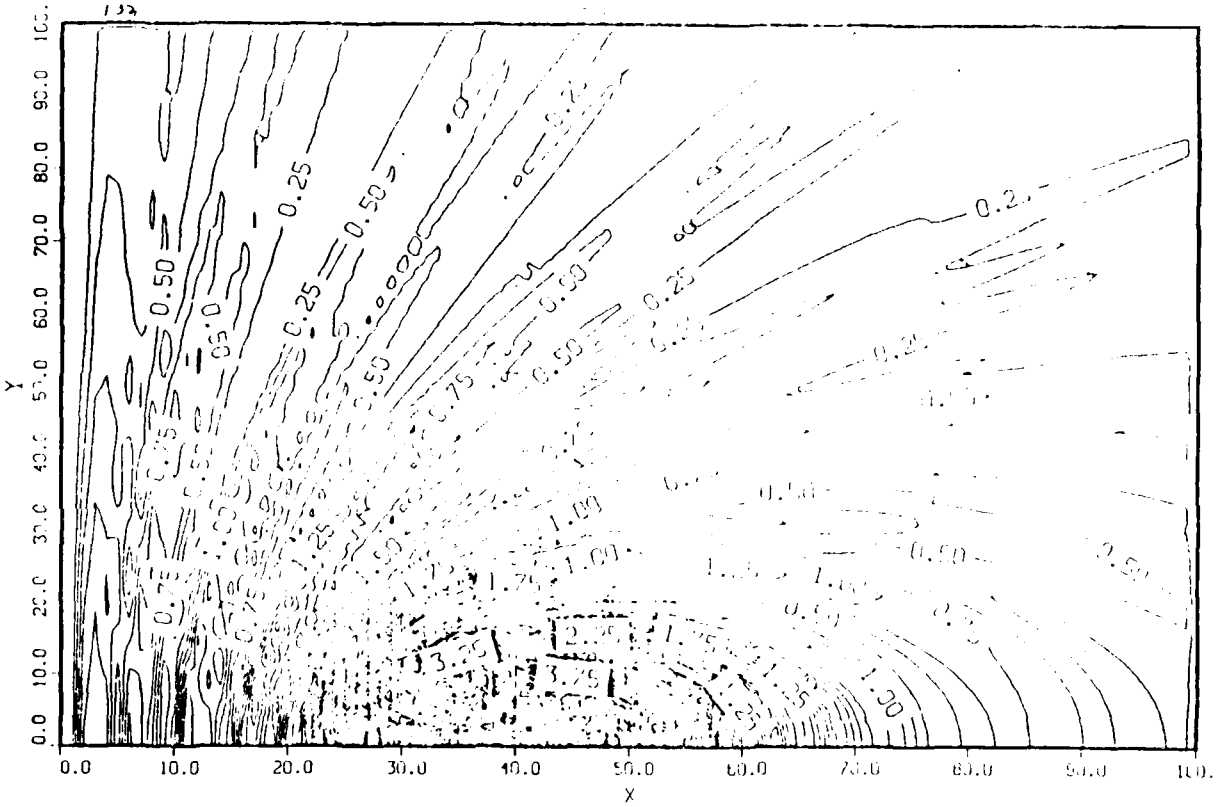

Figure 16-B

Equal-Pressure Contours on the Bottom of the Wedge for the Indicated Values of Parameters

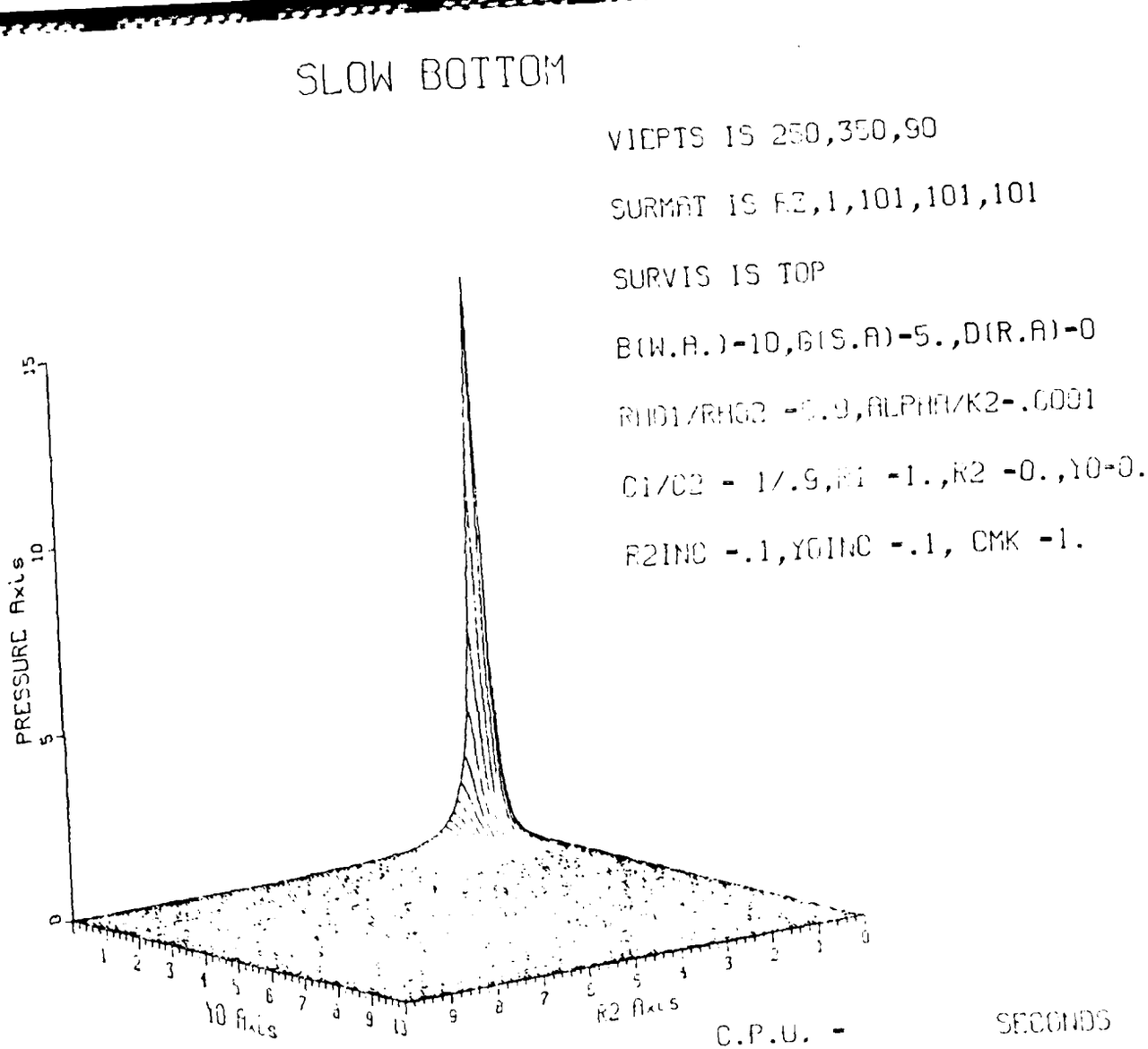

Figure 17-A

Pressure on the Bottom of the Wedge as Calculated by the Image Model for the Indicated Values of Parameters

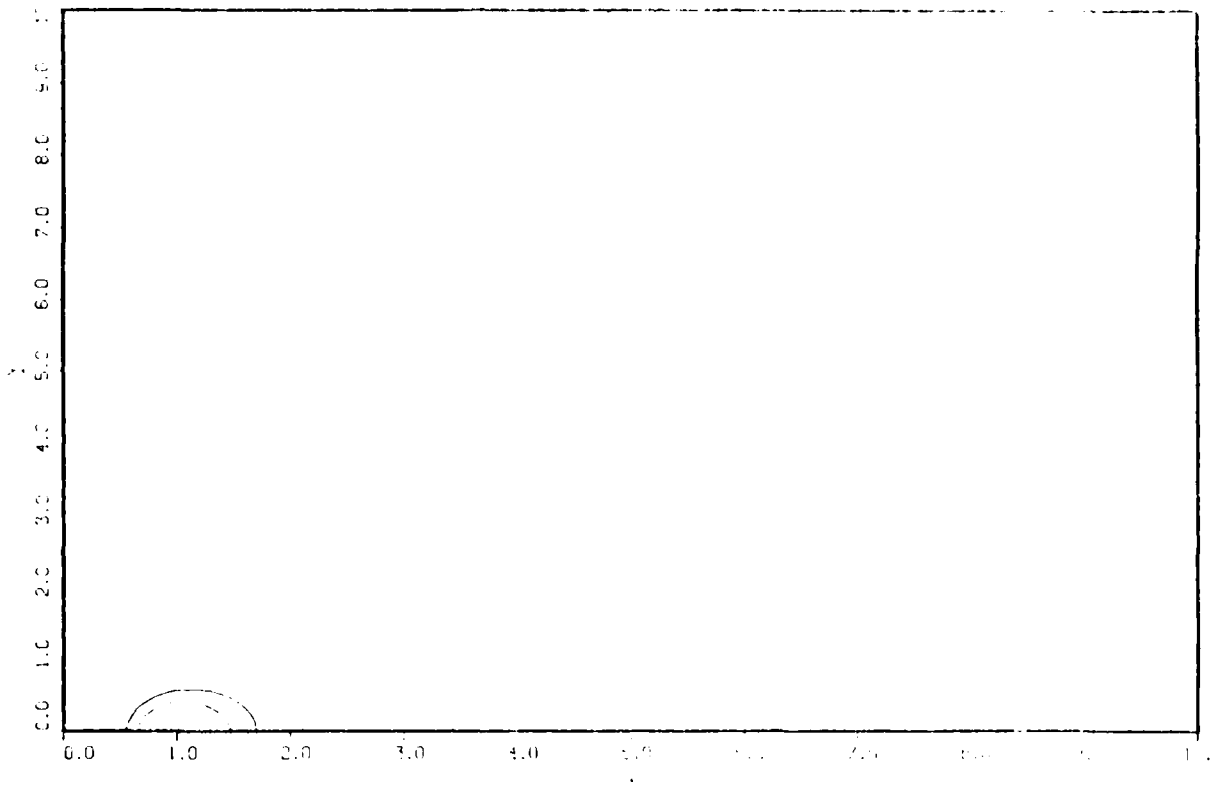

Figure 17-B

Equal-Pressure Contours on the Bottom of the Wedge for the Indicated Values of Parameters

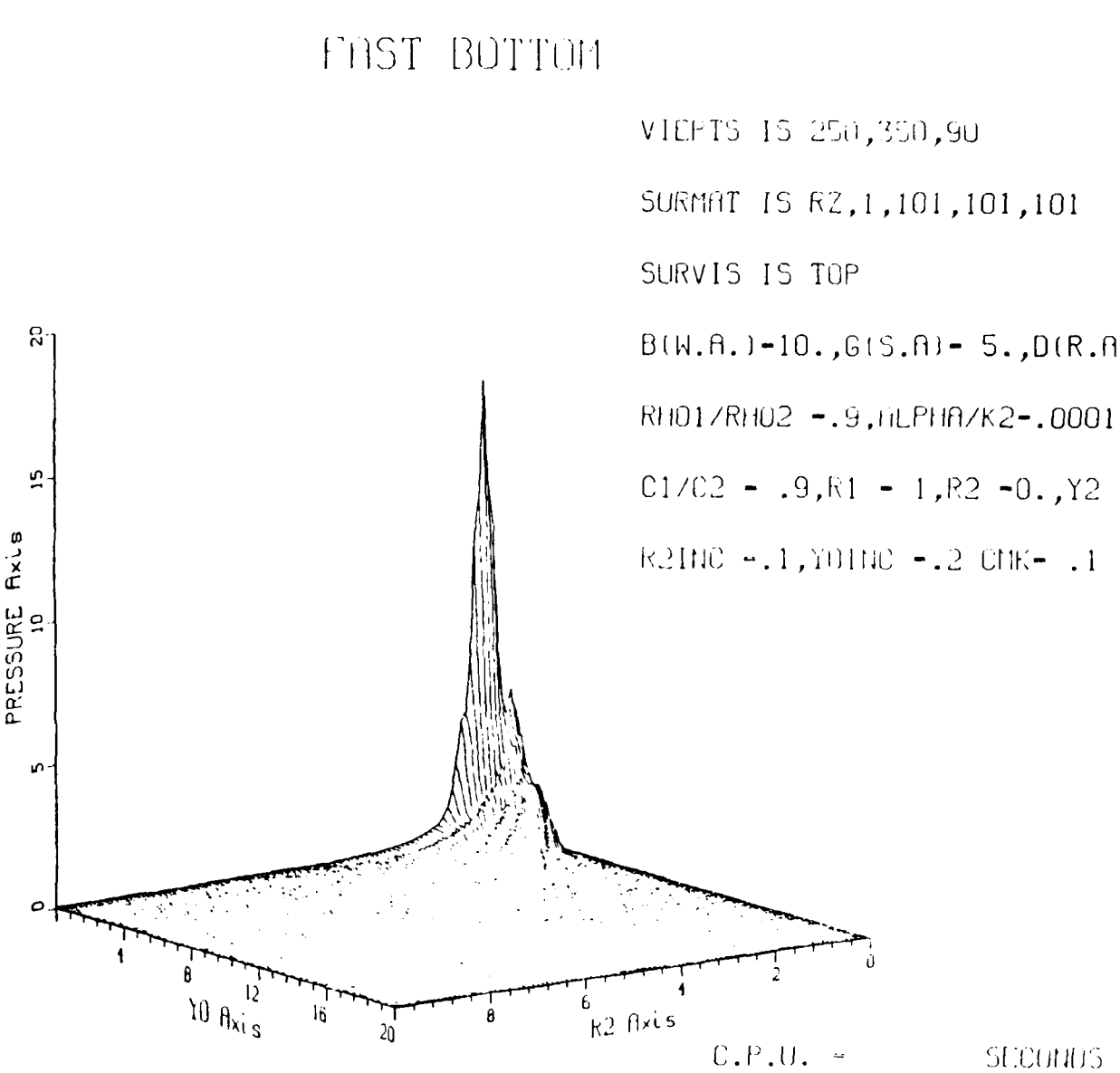

Figure 18-A

Pressure on the Bottom of the Wedge as Calculated by the Image Model for the Indicated Values of Parameters

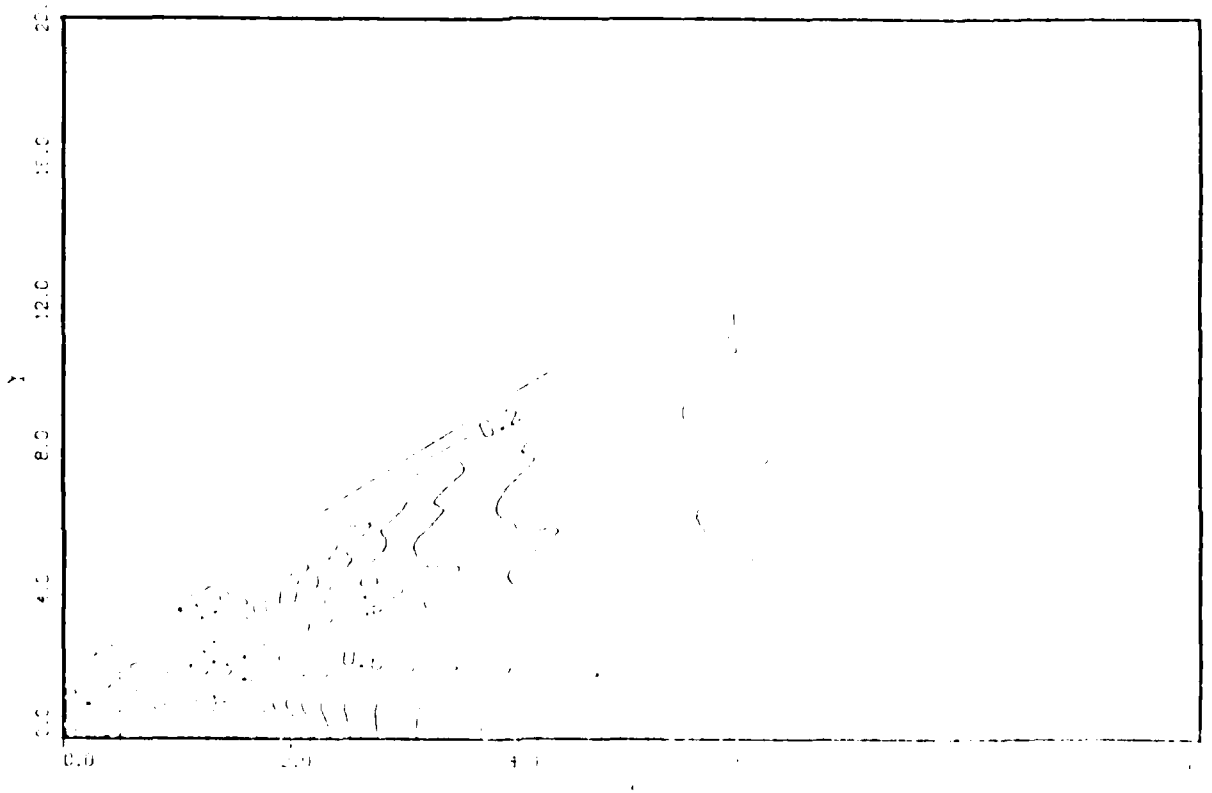

Figure 18-B

Equal-Pressure Contours on the Bottom of the Wedge for the Indicated Values of Parameters

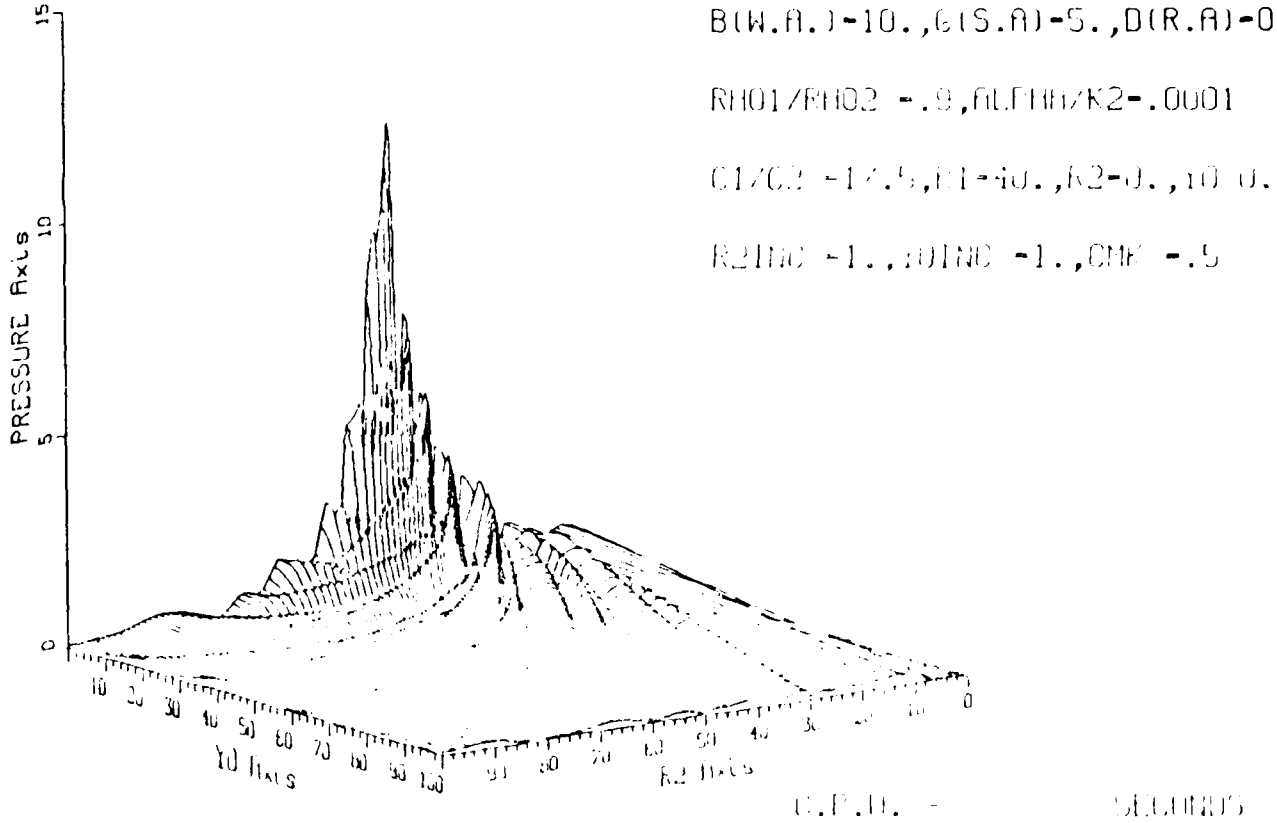

Figure 19-A

Pressure on the Bottom of the Wedge as Calculated by the Image Model for the Indicated Values of Parameters

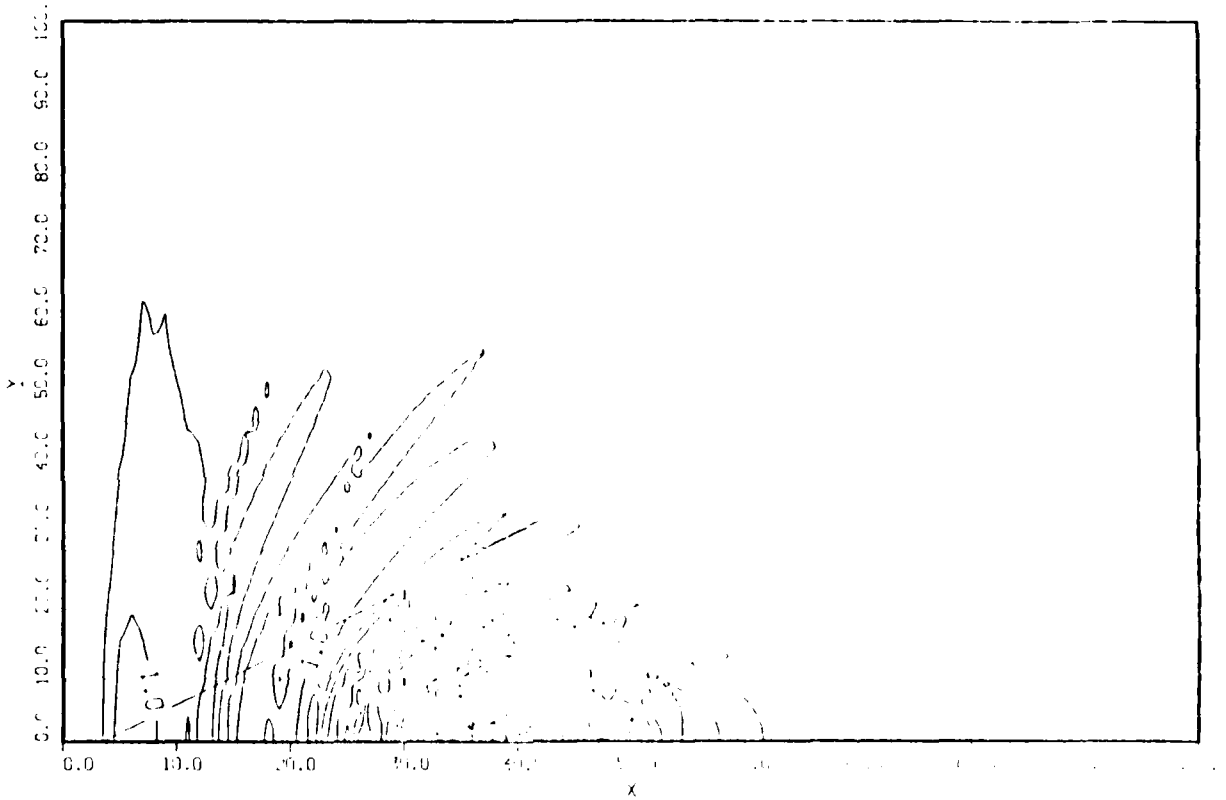

Figure 19-B

Equal-Pressure Contours on the Bottom of the Wedge for the Indicated Values of Parameters

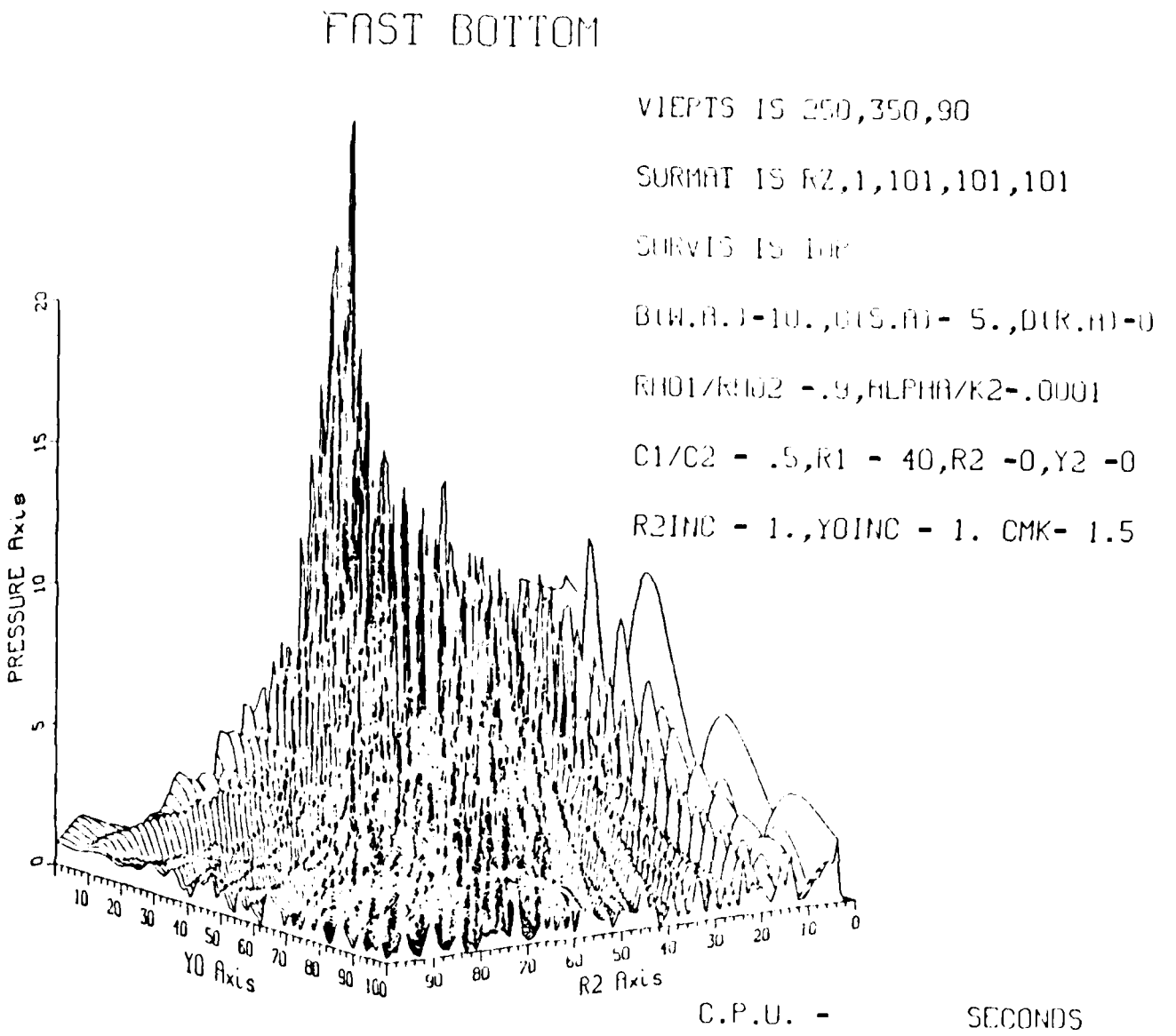

Figure 20-A

Pressure on the Bottom of the Wedge as Calculated by the Image Model for the Indicated Values of Parameters

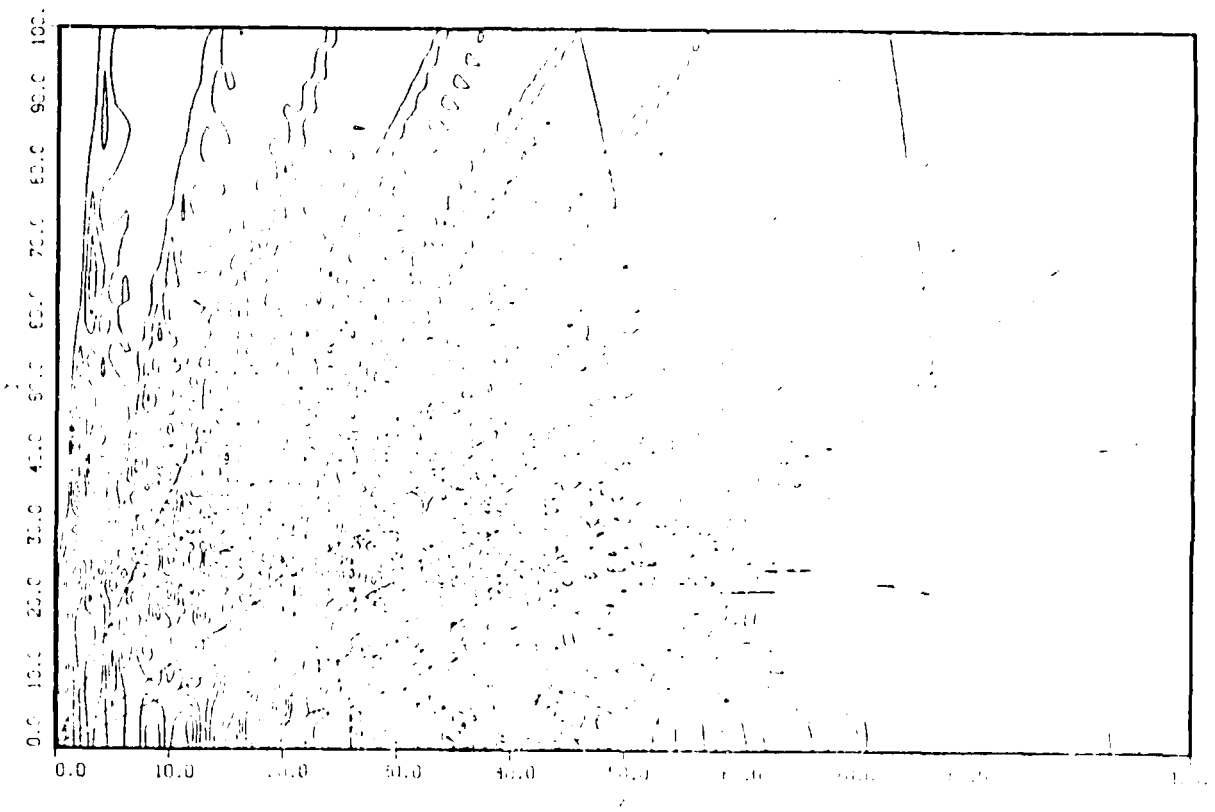

Figure 20-B

Equal-Pressure Contours on the Bottom of the Wedge for the Indicated Values of Parameters

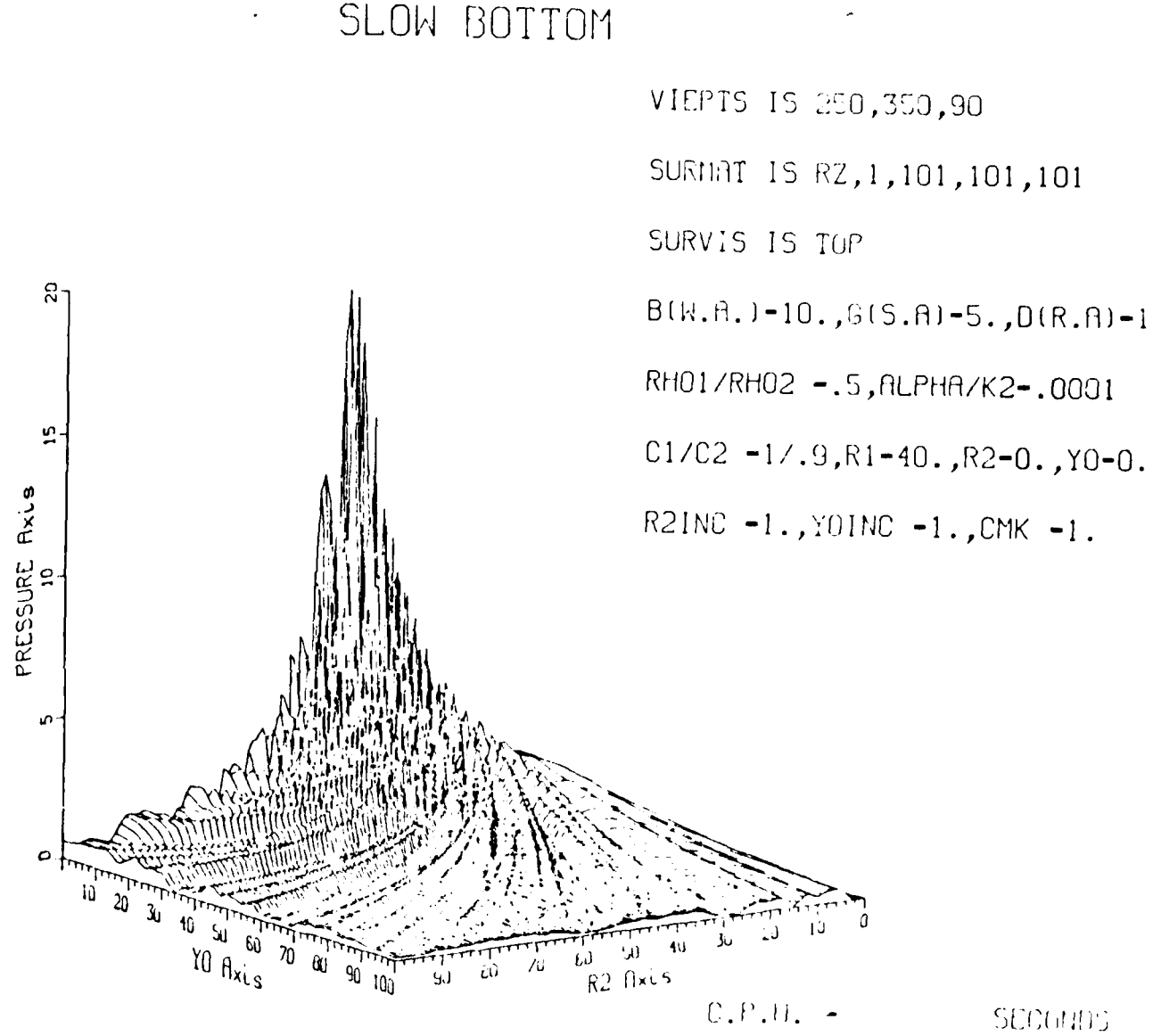

Figure 21-A

Pressure on the Bottom of the Wedge as Calculated by the Image Model for the Indicated Values of Parameters

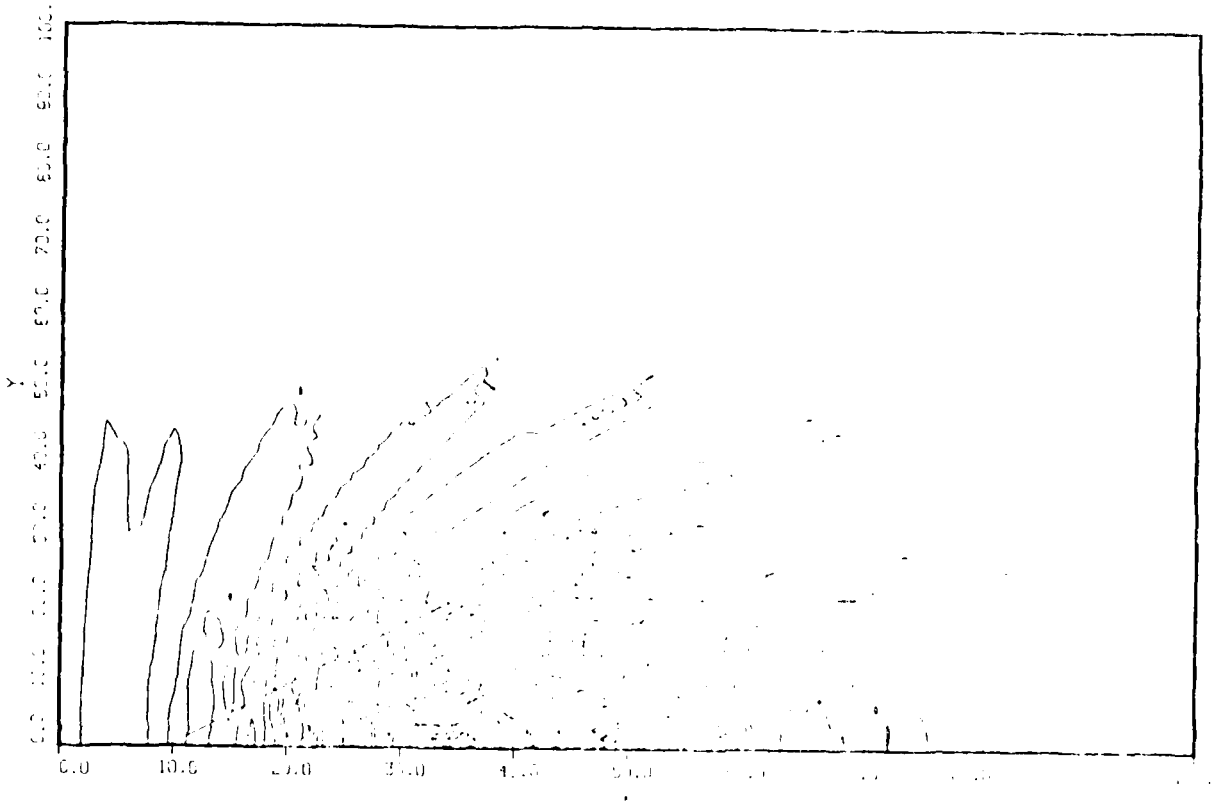

Figure 21-B

Equal-Pressure Contours on the Bottom of the Wedge for the Indicated Values of Parameters

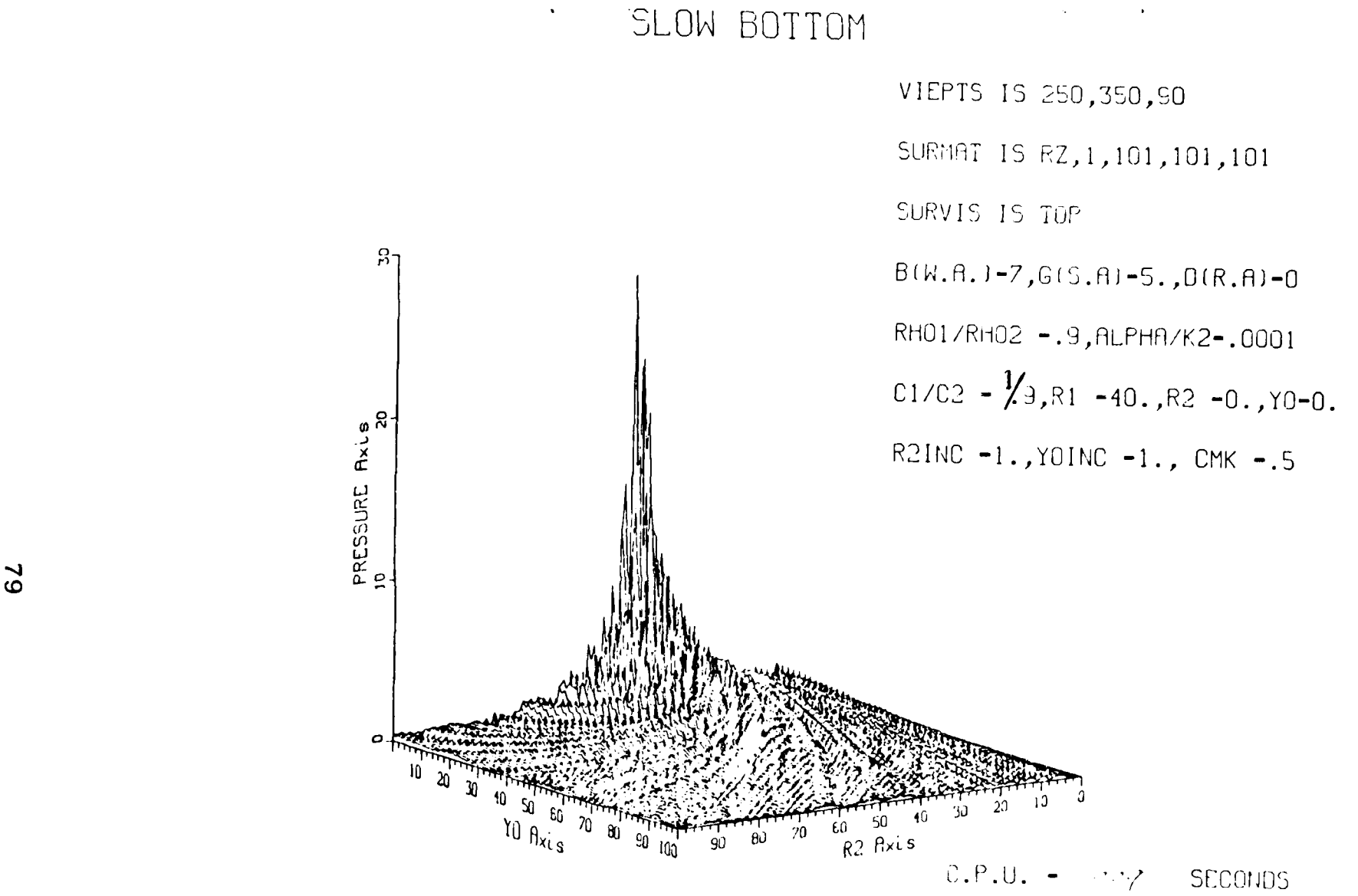

Figure 22-A

Pressure on the Bottom of the Wedge as Calculated by the Image Model for the Indicated Values of Parameters

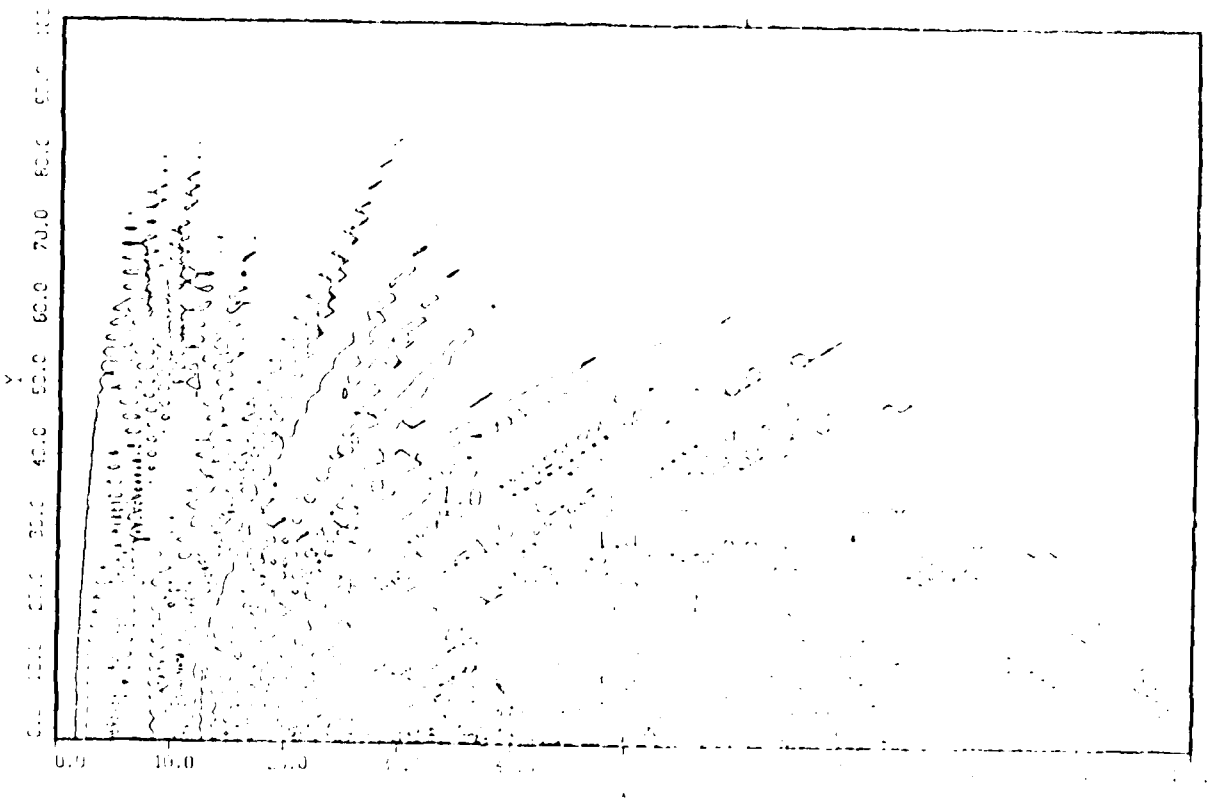

Figure 22-B

Equal-Pressure Contours on the Bottom of the Wedge for the Indicated Values of Parameters

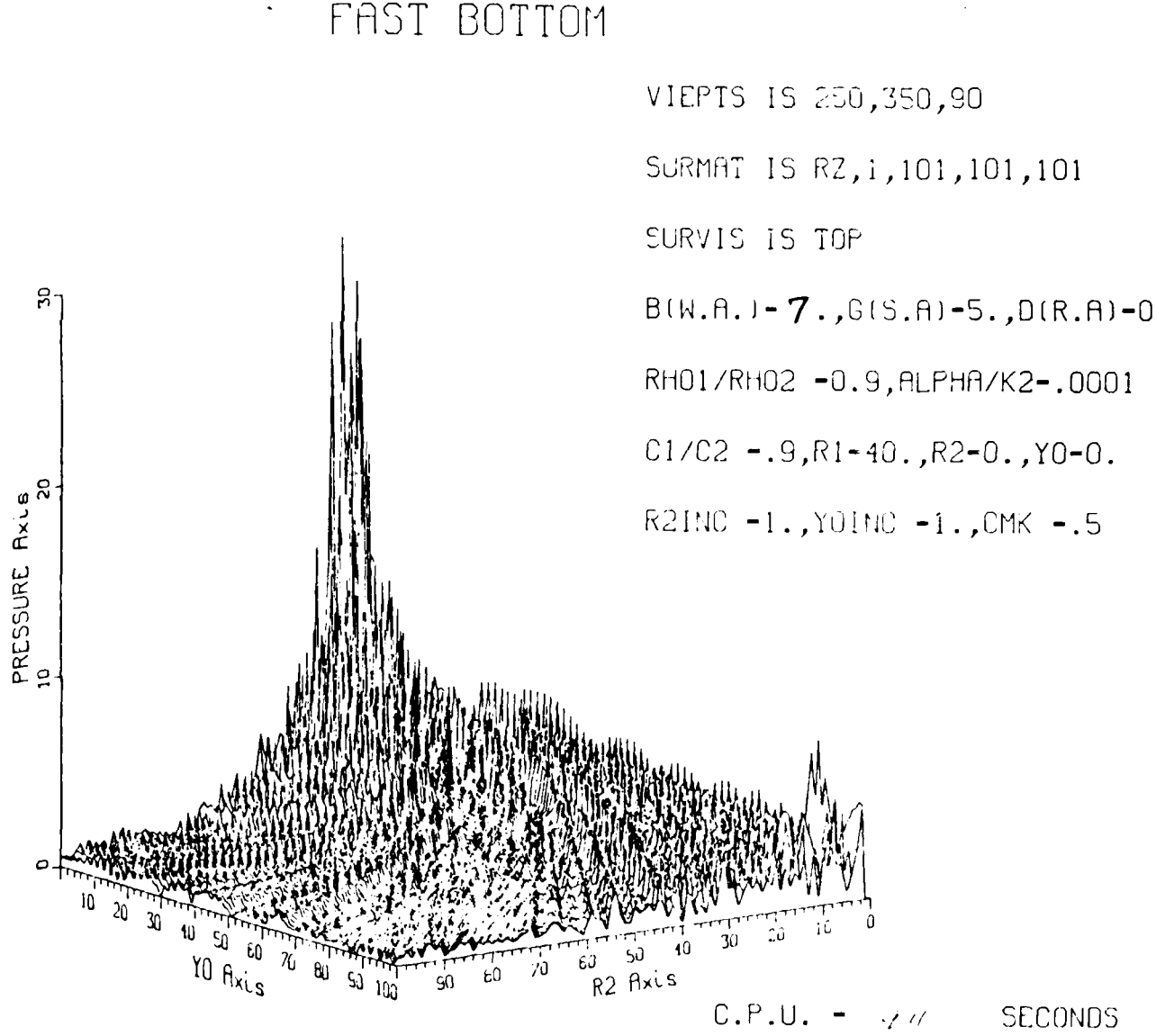

Figure 23-A

Pressure on the Bottom of the Wedge as Calculated by the Image Model for the Indicated Values of Parameters

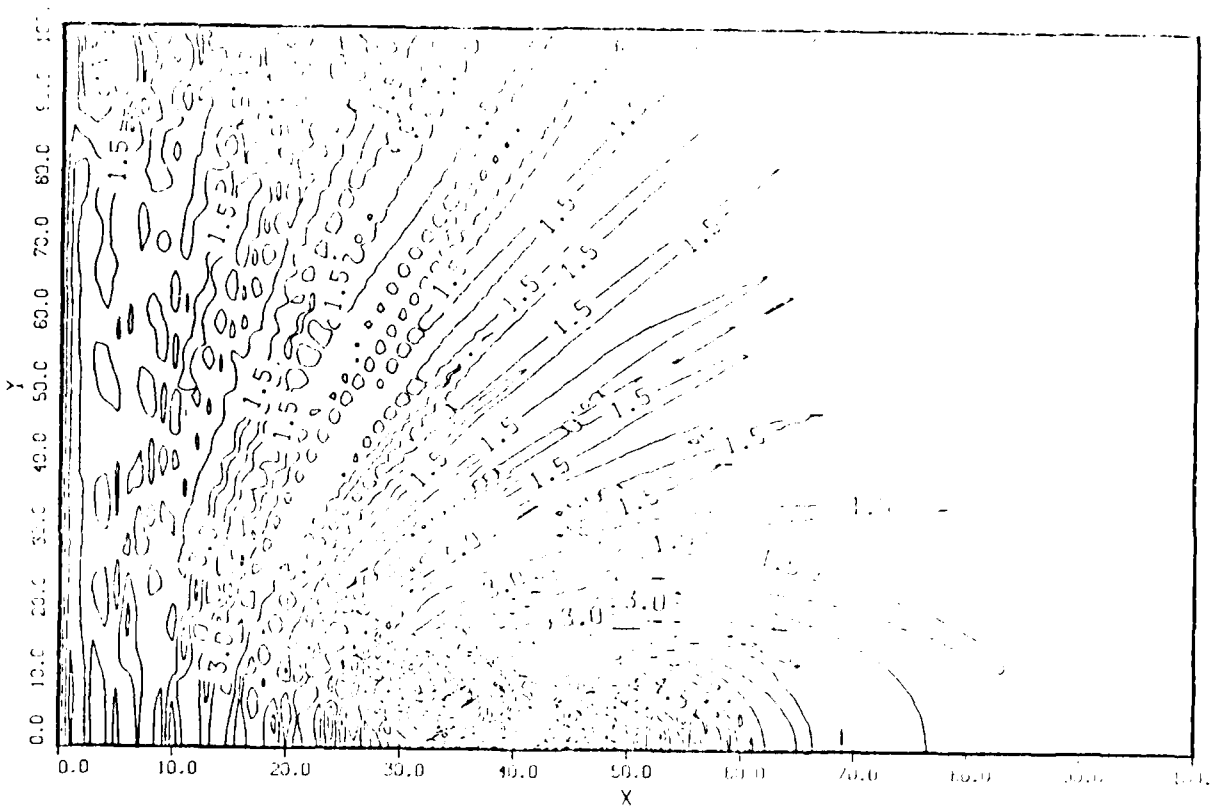

Figure 23-B

Equal-Pressure Contours on the Bottom of the Wedge for the Indicated Values of Parameters

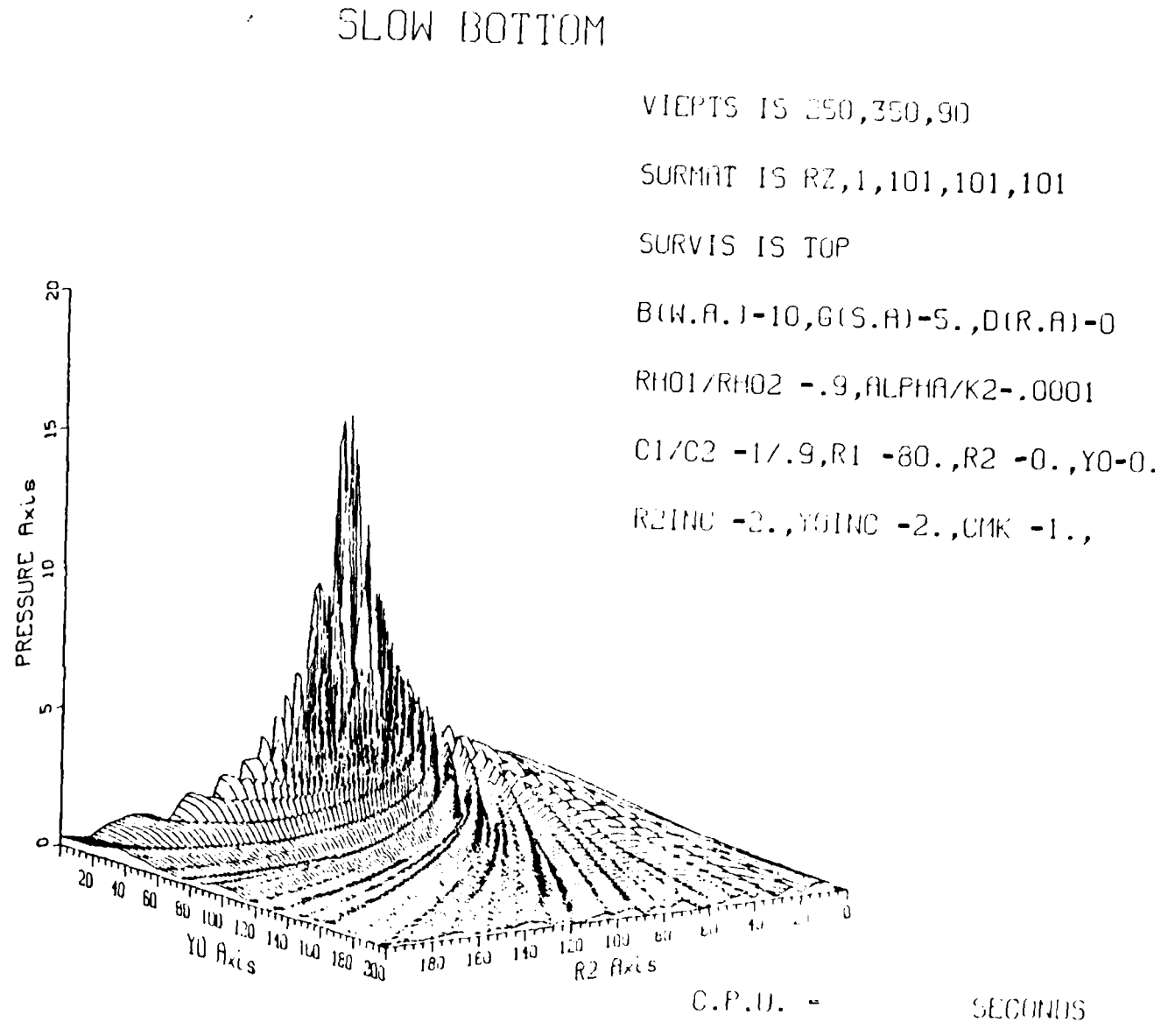

Figure 24-A

Pressure on the Bottom of the Wedge as Calculated by the Image Model for the Indicated Values of Parameters

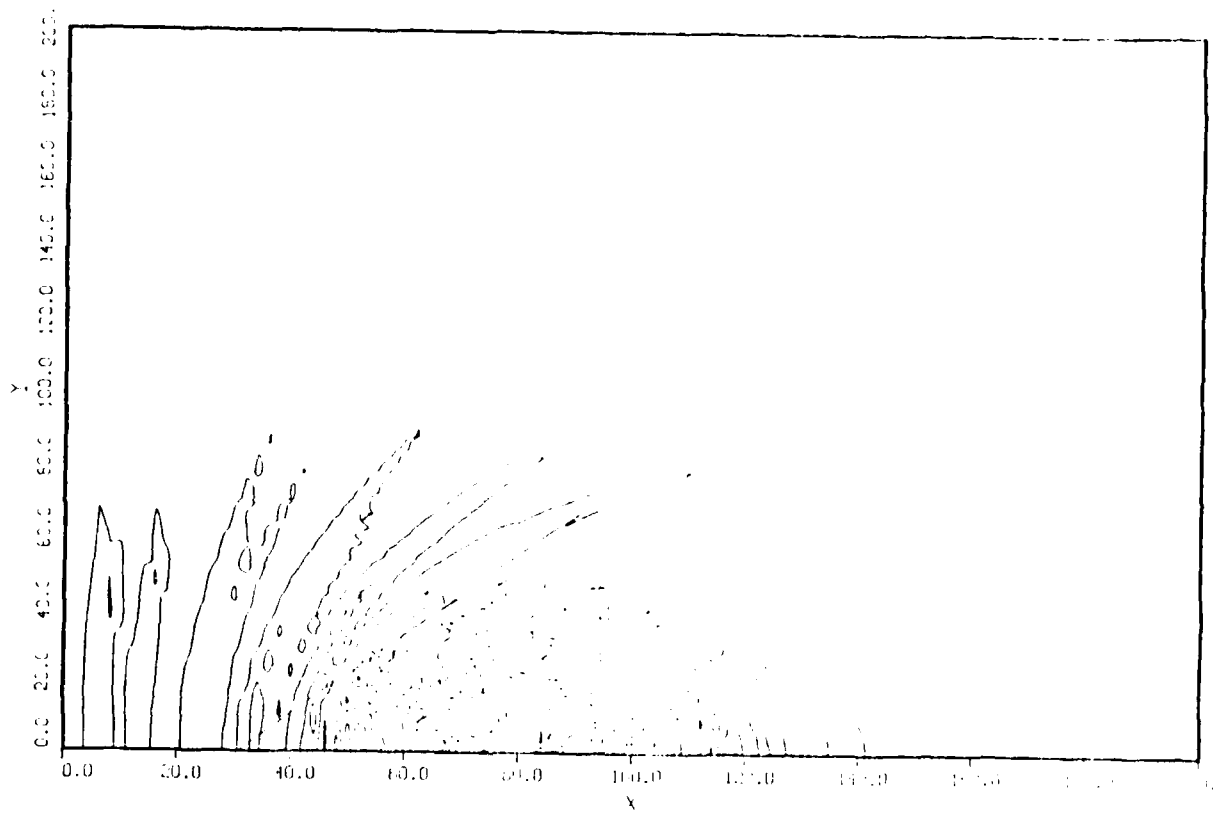

Figure 24-B

Equal-Pressure Contours on the Bottom of the Wedge for the Indicated Values of Parameters

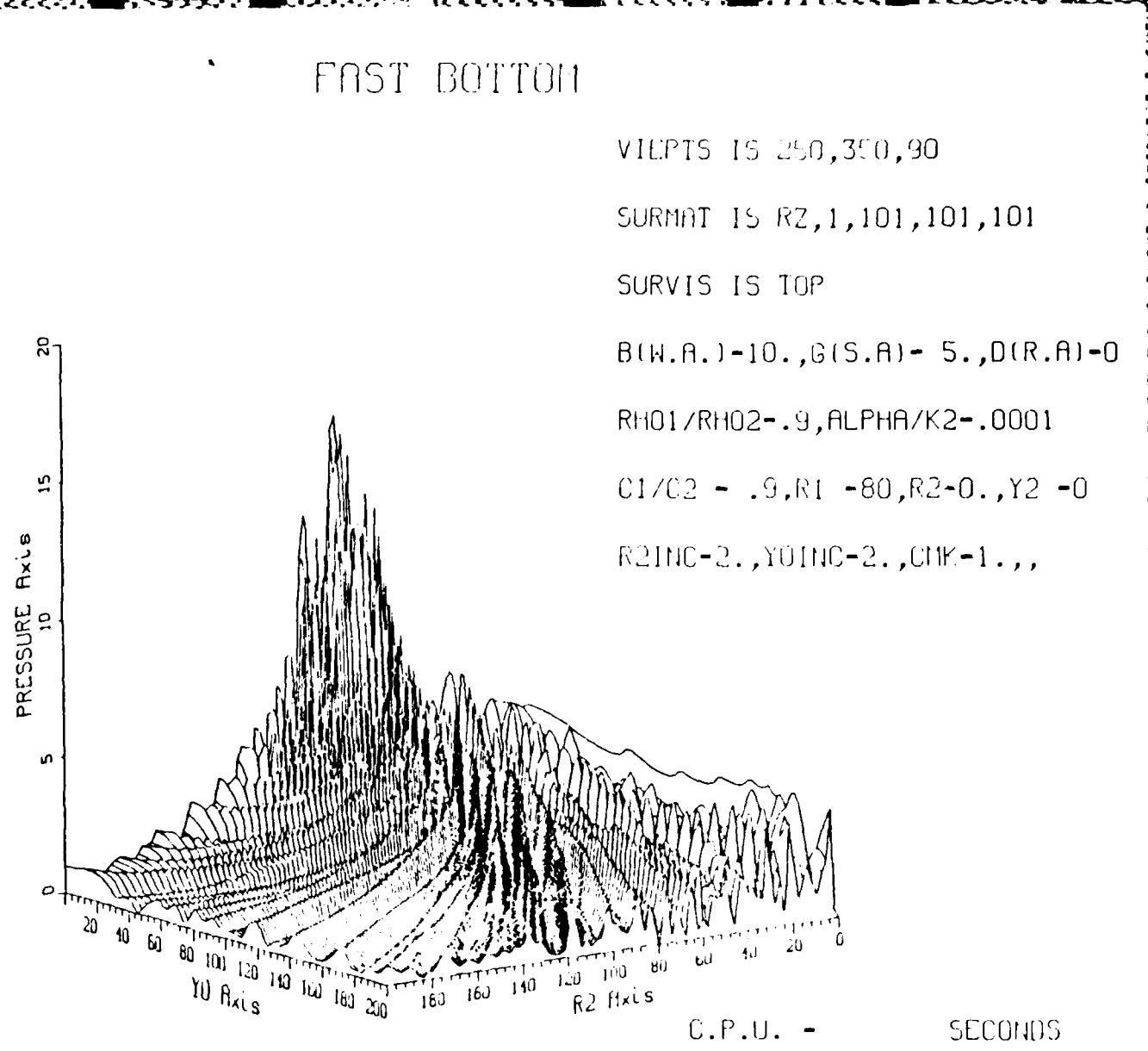

Figure 25-A

Pressure on the Bottom of the Wedge as Calculated by the Image Model for the Indicated Values of Parameters

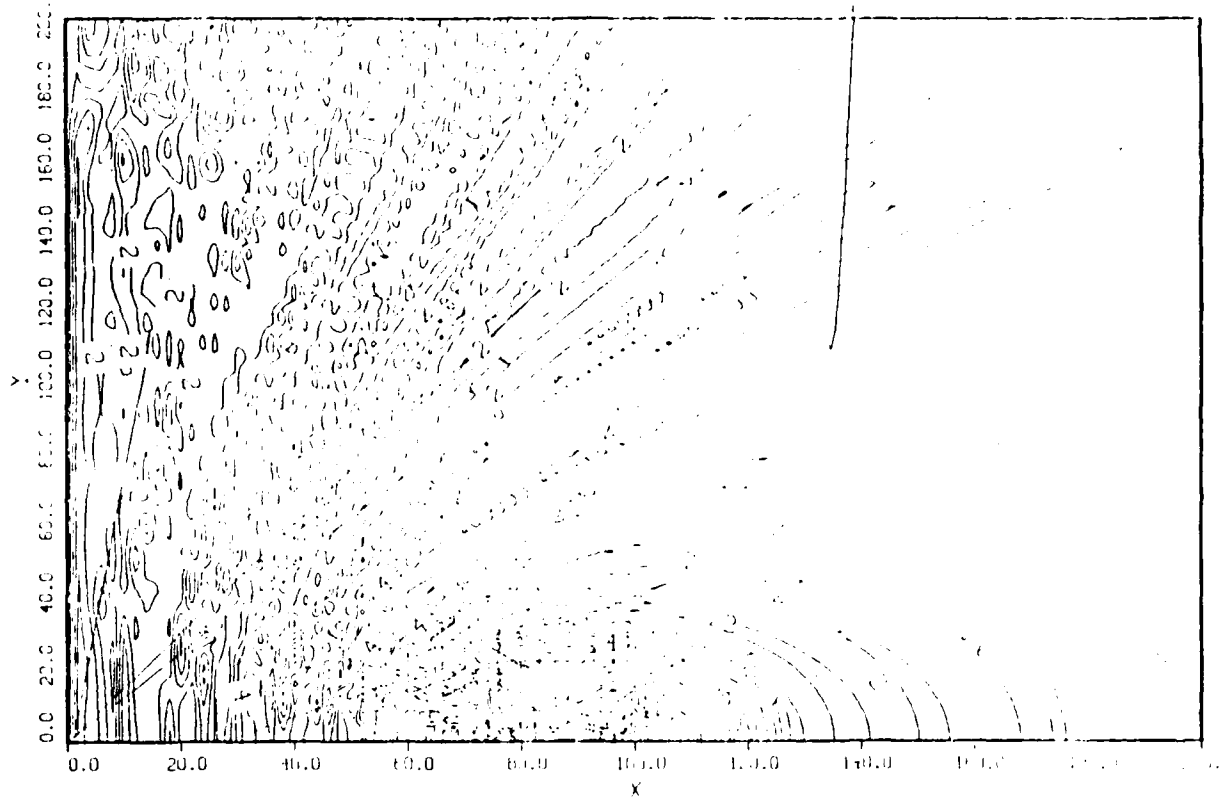

Figure 25-B

Equal-Pressure Contours on the Bottom of the Wedge for the Indicated Values of Parameters

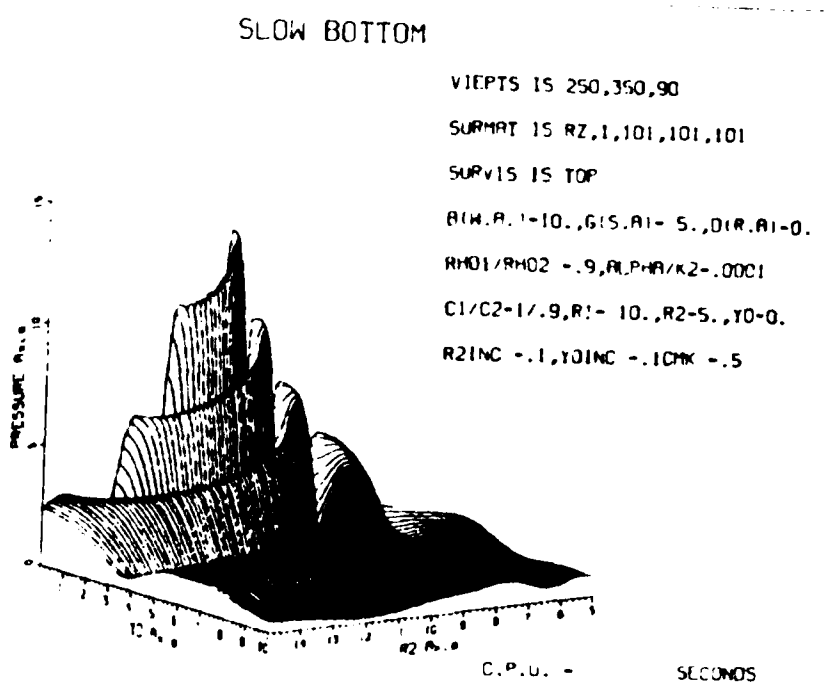

Figure 26-A

Pressure on the Bottom of the Wedge as Calculated by the Image Model for the Indicated Values of Parameters

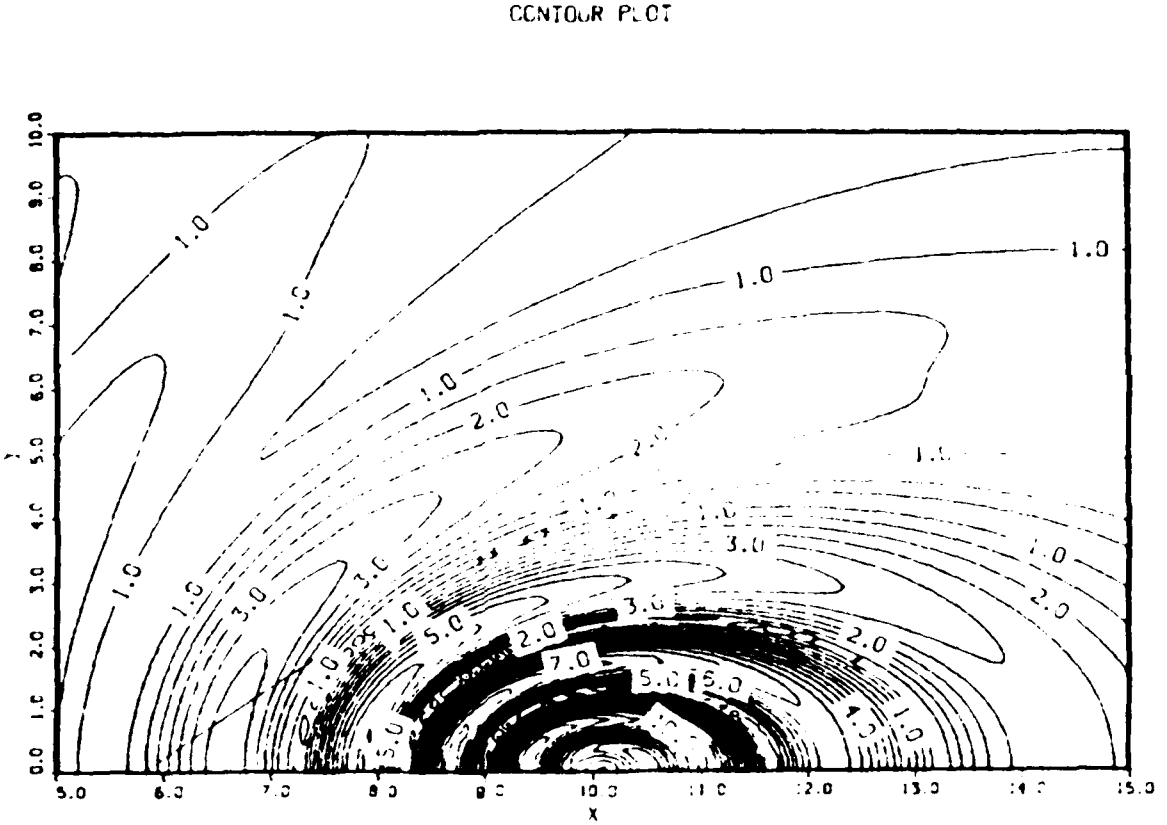

Figure 26-B

Equal-Pressure Contours on the Bottom of the Wedge for the Indicated Values of Parameters

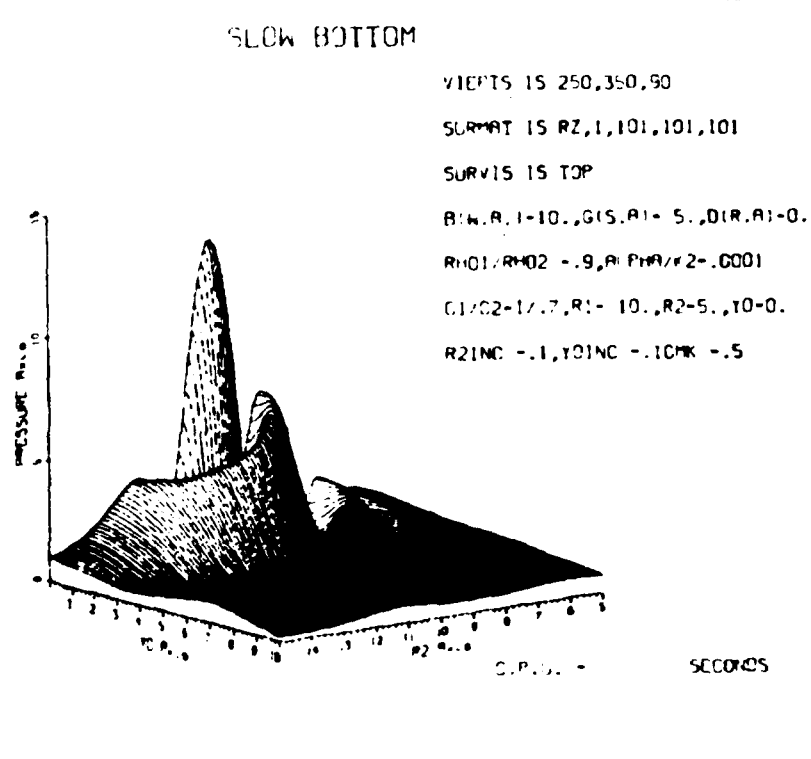

Figure 27-A

Pressure on the Bottom of the Wedge as Calculated by the Image Model for the Indicated Values of Parameters

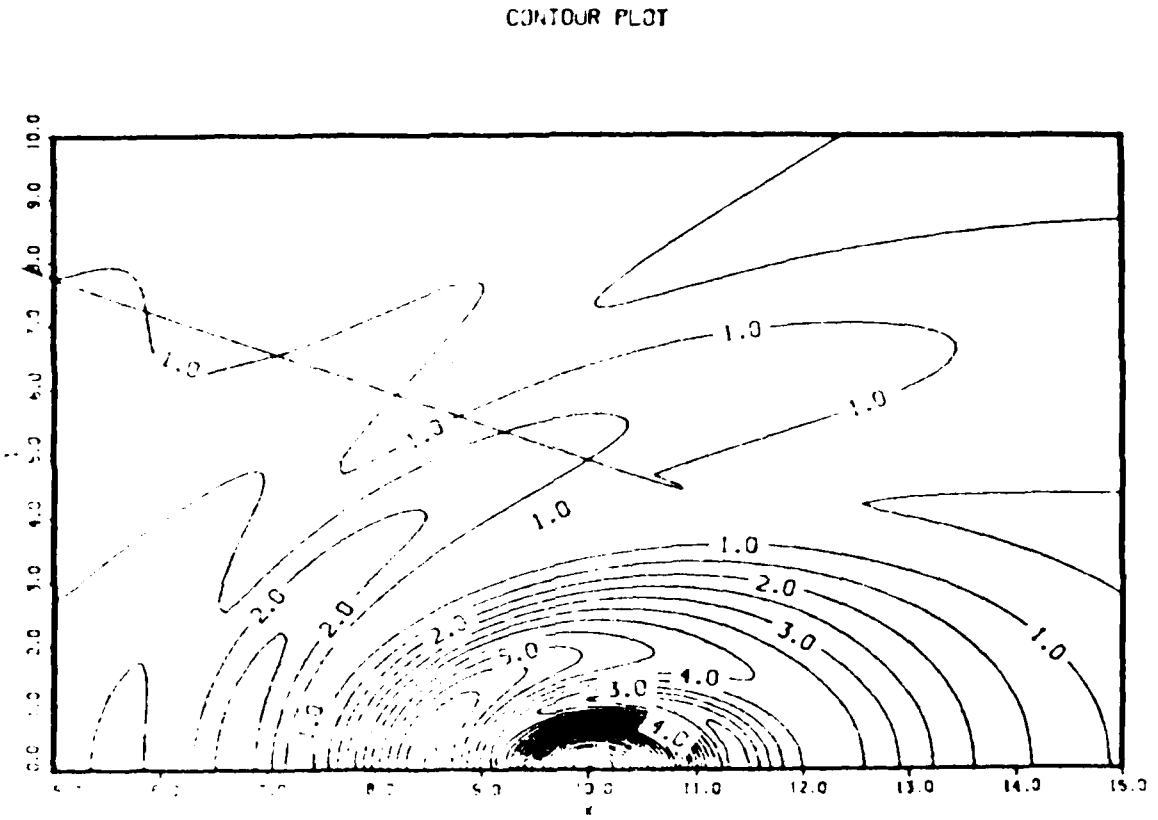

Figure 27-B

Equal-Pressure Contours on the Bottom of the Wedge for the Indicated Values of Parameters

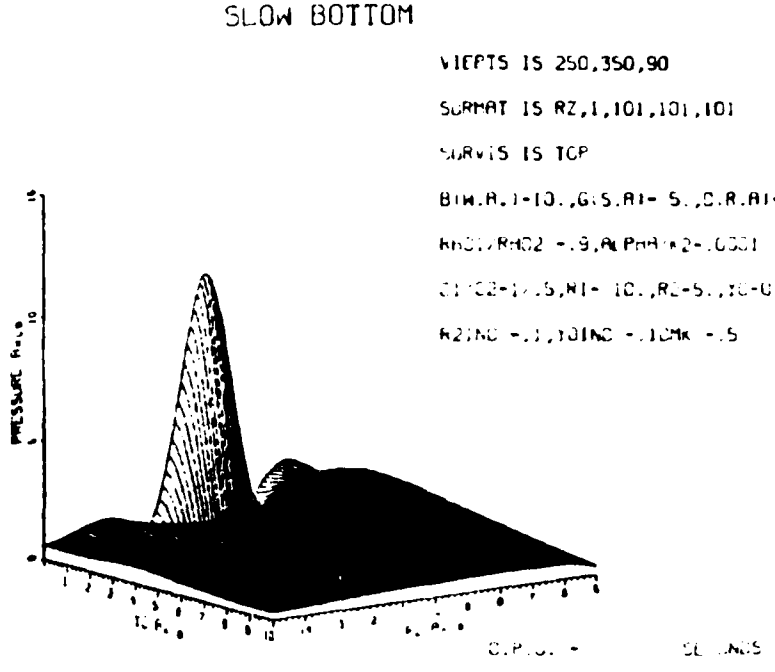

Figure 28-A

Pressure on the Bottom of the Wedge as Calculated by the Image Model for the Indicated Values of Parameters

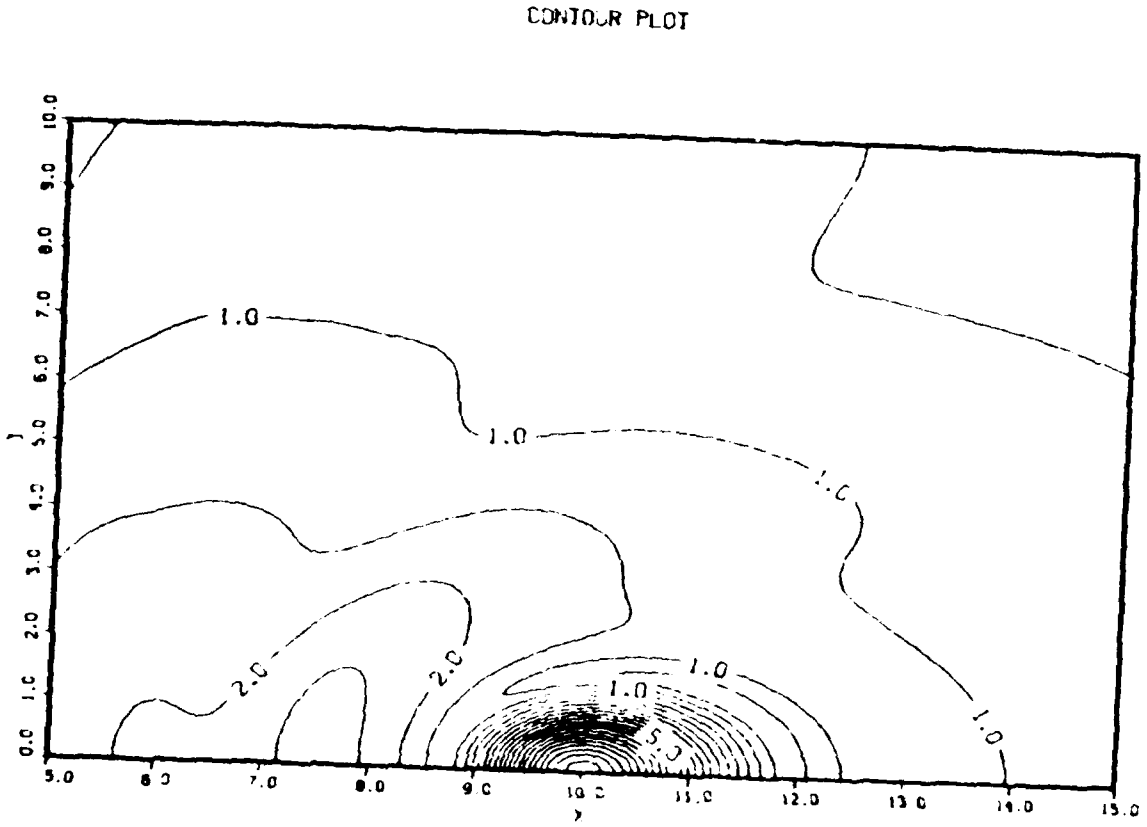

Figure 28-B

Equal-Pressure Contours on the Bottom of the Wedge for the Indicated Values of Parameters

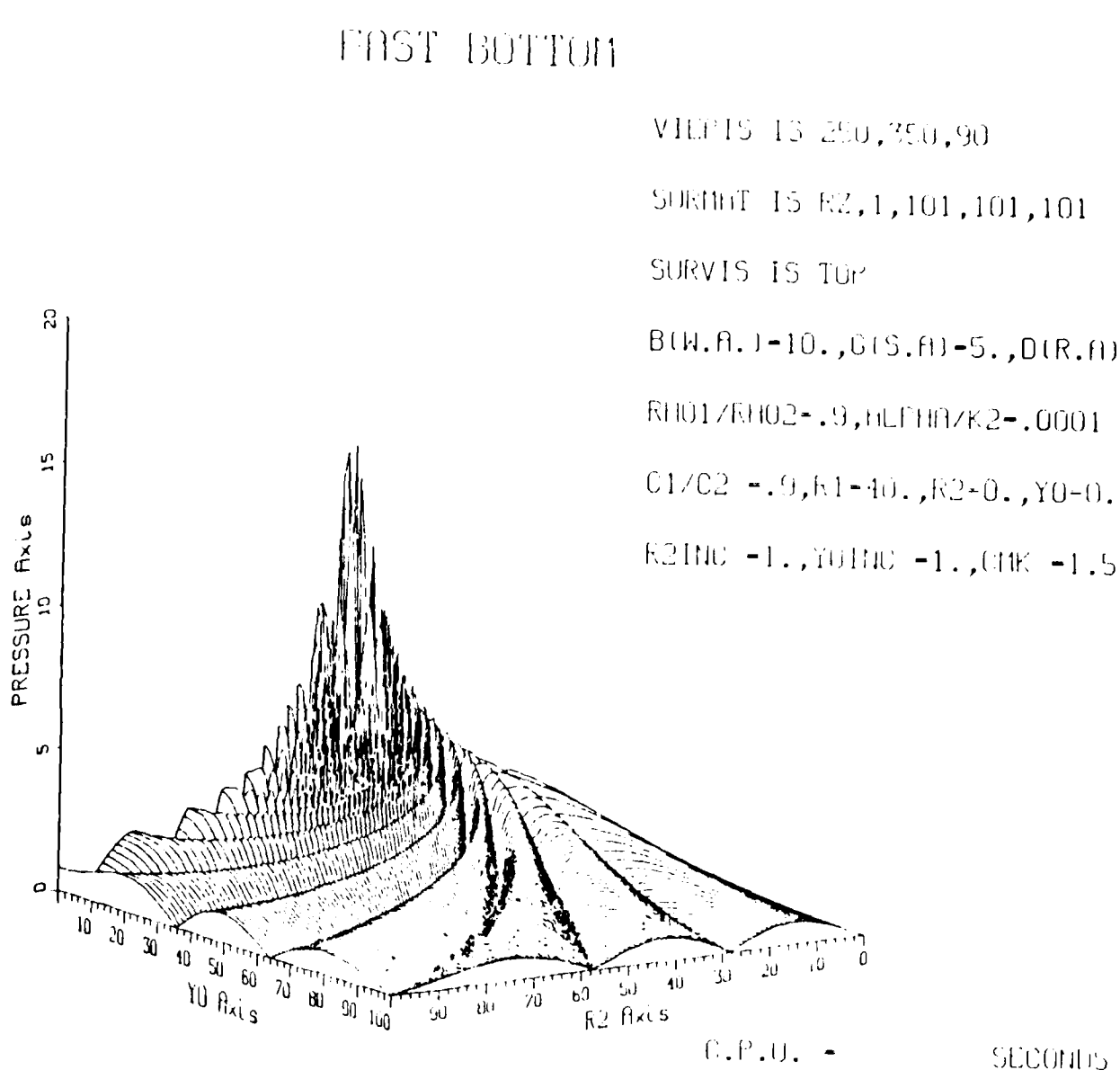

Figure 29-A

Pressure on the Bottom of the Wedge as Calculated by the Image Model for the Indicated Values of Parameters

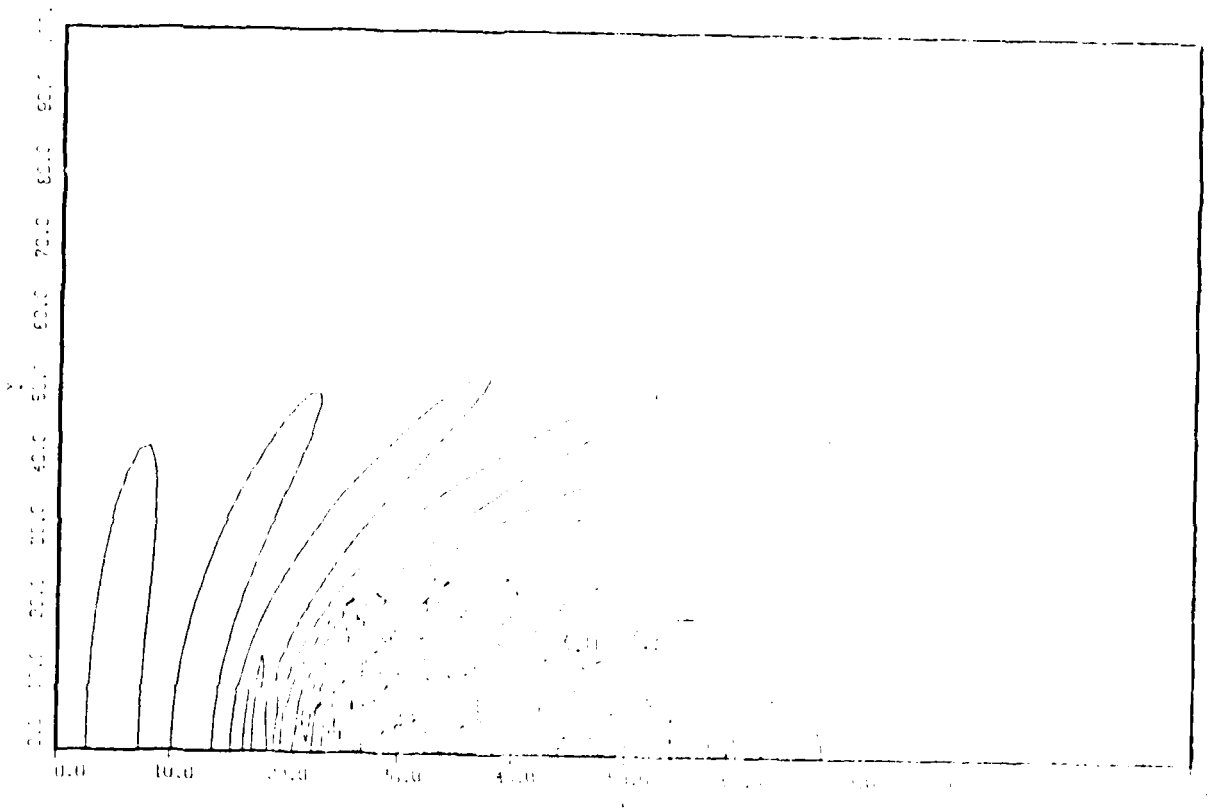

Figure 29-B

Equal-Pressure Contours on the Bottom of the Wedge for the Indicated Values of Parameters

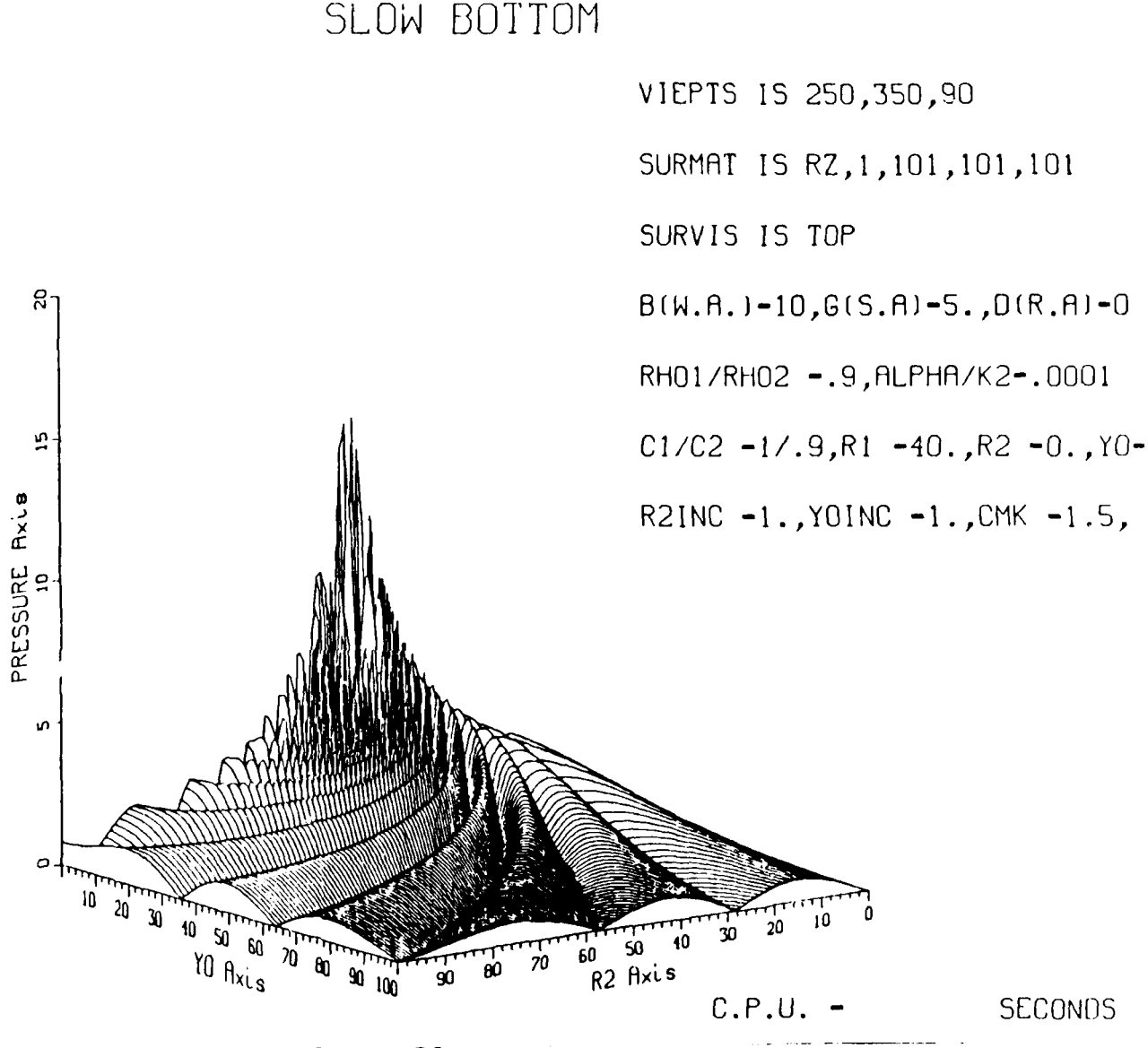

Figure 30-A

Pressure on the Bottom of the Wedge as Calculated by the Image Model for the Indicated Values of Parameters

AD-A193 961 ACOUSTIC PRESSURE DISTRIBUTION ON THE BOTTOM OF A WEDGE-SHAPED OCEAN(U) NAVAL POSTGRADUATE SCHOOL MONTEREY CA Y LI DEC 87 2/2

UNCLASSIFIED F/G 20/1 NL

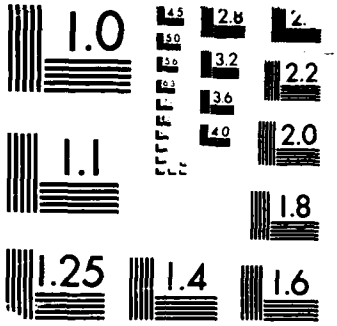

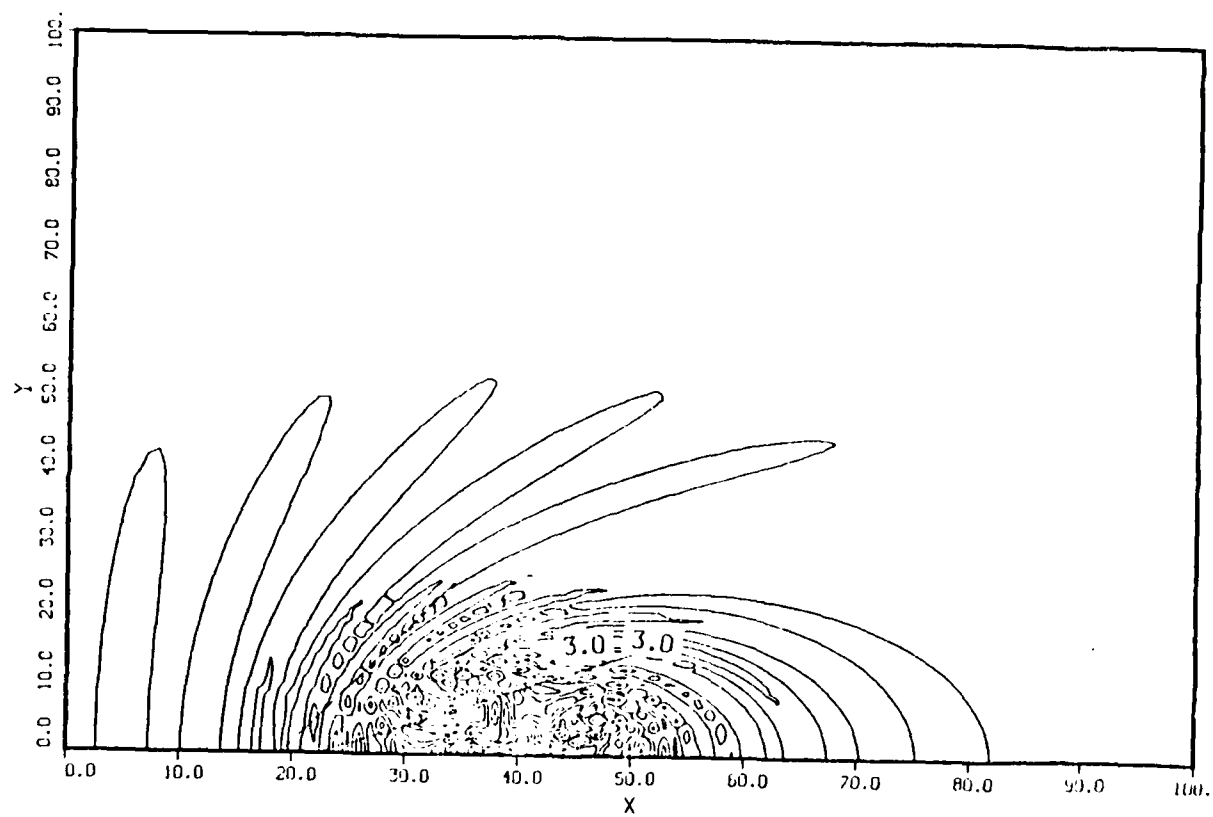

Figure 30-B

Equal-Pressure Contours on the Bottom of the Wedge for the Indicated Values of Parameters

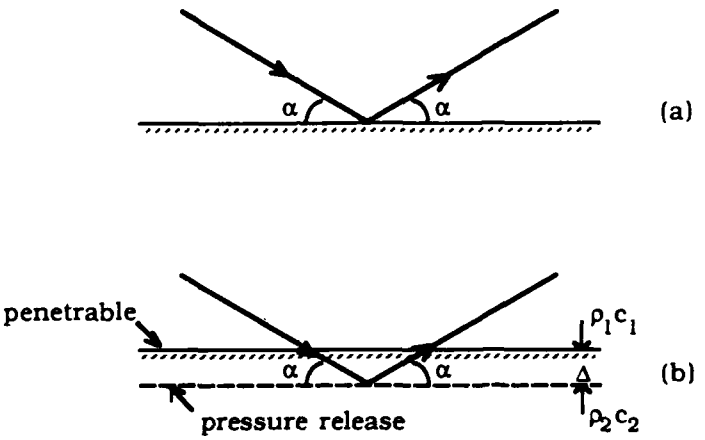

(a) Total internal reflection of a ray and
(b) a reflection with the same phase shift from an effective-release surface

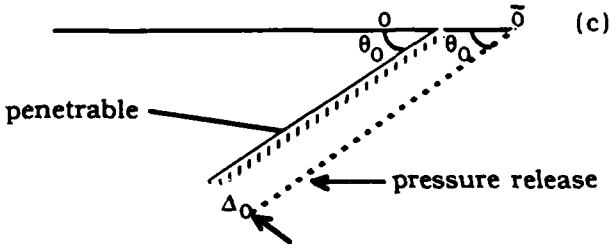

(a) Wedge with penetrable bottom and apex 0 and "effective" wedge wth pressure-release bottom and apex $\bar{0}$.

Figure 31

Effective Pressure-Release Bottom

LIST OF REFERENCES

1. Bradley, D., and A. A. Hudimac, The Propagation of Sound in a Wedge Slow Duct, pp. 4-6, The Catholic University of America, 1970.

2. Buckingham, M. J., Acoustic Propagation in Wedge-Shaped Ocean, The A. B. Wood Memorial Lecture, pp. 251-259, Naval Research Lab, 1967.

3. Evans, R. B., "A Coupled Mode Solution for Acoustic Propagation in a Wave Guide With Stepwise Depth Variation of a Penetrable Bottom," J.A.S.A. 74, No. 1 (1983), pp. 188-195.

4. Jensen, F. B., and W. A. Kuperman, "Sound Propagation in a Wedge-Shaped Ocean With a Penetrable Bottom," J.A.S.A. Vol. 65, No. 5 (1980), pp. 1564-1566.

5. Jensen, F. B., and C. T. Tindle, "Numerical Modeling Results for Mode Propagation in a Wedge," J.A.S.A. Vol. 82, No. 1 (1987), pp. 11-216.

6. Pierce, Allan D., "Guided Mode Disappearance During Up-Slope Propagation in Variable Depth Shallow Water Overlying a Fluid Bottom," J.A.S.A. 72, No. 2 (1982), pp. 523-531.

7. Kuznetsov, V. K., "Emergence of Normal Modes Propagating in a Wedge on a Half-Space From the Former into the Latter," Soviet Phys. Acoust. Vol. 19, No. 3 (1973), pp. 241-245.

8. Coppens, A. B., M. Humphries, and J. V. Sanders, "Propagation of Sound Out of a Fluid Wedge into an Underlying Fluid Substrate of Greater Sound Speed," J.A.S.A. Vol. 76, No. 5 (1984), pp. 1456-1465.

9. Lesesne, P. K., Development of Computer Program Using the Method of Images to Predict the Sound Field in a Wedge Overlying a Fast Fluid Bottom, M. S. Thesis, Naval Postgraduate School, Monterey, California, 1984.

10. Coppens, A. B., the theory "Transmission of Acoustic Wave into a Fast Fluid Bottom from a Converging Fluid Wedge," O.N.R./N.R.L., workshop in Seismic Wave Propagation in a Shallow Water, 1978.

11. Coppens, A. B.,, J. V. Sanders, Ionnou, and Kawamura. Two Computer Programs for the Evaluation of the Acoustic Pressure Amplitude and Phase over Overlying a Fast Fluid Half-Space. NPS Report 61-79-002, 1978.

12. Baek, C. K., The Acoustic Pressure in a Wedge-Shaped Water Layer Overlying a Fast-Fluid Bottom, M. S. Thesis, Naval Postgraduate School, Monterey, California, 1984.

13. Sommerfeld, A., "Mathematische Theorie der Diffraktion," Math. Ann. Vol. 47, 1896, pp. 317-341.

14. Tolstoy ,I., and M. A. Biot, "Formulation of Wave Propagation in Infinite Media by Normal Coordinates with an Application to Diffraction," J.A.S.A. Vol. 29, No. 3 (1956), p. 3870.

15. Kuzentsov, V. K., "Method of Virtual Sources in the Underwater-Acoustical Description of High-Frequency Sound Fields in a Wedge," Soviet Phys. Acoust. Vol. 18, No. 2 (197_), pp. 223-228.

16. Tien, D. K., G. Smalinsky, and R. J. Martin, "Radiation Field of Trapered Film and a Novel Film to Fiber Coupler," I.E.E.E., MIT-23 7P-79 (1975).

17. Coppens, A. B., and J. V. Sanders, "Propagation of Sound from a Fluid Wedge Into a Fast Fluid Bottom," from Bottom Interacting Ocean Acoustics, W. A. Kuperman and F. B. Jensen, eds., Plenum Press, New York, 1980.

18. Buckingham, M. J., Acoustic Propagation in a Wedge-Shaped Ocean with Perfectly Reflecting Boundaries, NATO Advanced Research Workshop on Hybrid Formulation of Wave Propagation and Scattering, 1983.

19. Weston, D. E., "Horizontal Refraction in a Three-Dimensional Medium of Variable Stratification," Proc. Phys. Soc. LXXVII, No. 1 (1960), pp. 46-52.

20. Disspla Pocket Guide and Disspla User Manual, Integrated Software System Corporation, 1981.

INITIAL DISTRIBUTION LIST

		No. Copies
1.	Defense Technical Information Center Cameron Station Alexandria, VA 22304-6145	2
2.	Library, Code 0142 Naval Postgraduate School Monterey, CA 93943-5002	2
3.	Department Library, Code 61 Department of Physics and Chemistry Naval Postgraduate School Monterey, CA 93943-5002	2
4.	Dr. A. B. Coppens, Code 61Cz Department of Physics and Chemistry Naval Postgraduate School Monterey, CA 93943-5002	5
5.	Dr. J. V. Sanders, Code 61Sd Department of Physics and Chemistry Naval Postgraduate School Monterey, CA 93943-5002	2
6.	Dr. S. L. Garret, Code 61Gx Engineering Acoustic Academic Committee Chairman Naval Postgraduate School Monterey, CA 93943-5002	1
7.	LT Li Yu-Ming #584 Section 1 Hsin-chu Taiwan Republic of China	9
8.	LT R. D. Middleton, Jr. 141 John Street Hauppauge, NY 11787	1
9.	LT Wang Ming-hua SMC 2267 Naval Postgraduate School Monterey, CA 93943-5002	1

10. F. Bohr 1
SMC 2340
Naval Postgraduate School
Monterey, CA 93943-5002

11. C. Baek 1
971 McClellan Avenue
Monterey, CA 93940

12. Chief of Naval Operations 1
(Antisubmarine Warfare)
Code OP-02
Washington D.CC 20350-2000

END
DATE
FILMED
7-88
DTIC